Controlled degradation of low-fouling hydrogels for short- and long-term applications

By MUHAMMAD MUNEEB SHOAIB, B. Sc.

A Thesis Submitted to the School of Graduate Studies in Partial Fulfillment of the Requirements for the Degree Master of Science

McMaster University MASTER OF SCIENCE (2019) Hamilton, Ontario (Chemistry)

TITLE: Controlled degradation of low-fouling hydrogels for short- and long-term applications

AUTHOR: Muhmmad Muneeb Shoaib, B.Sc. (McMaster University) SUPERVISOR; Dr. Ryan G. Wylie. NUMBER OF PAGES: xiii, 77

Lay Abstract: The delivery of drugs and cells to disease sites is hindered by transport barriers, which can be overcome through local delivery. Injectable hydrogels can serve as local depots that release drugs or cells to improve therapeutic benefit. Currently, however, hydrogels suffer from uncontrolled degradation in the body, degrading at unpredictable rates dependent on the local environment; hydrogels with predictable and tunable degradation rates are therefore required. Herein, we report a method to produce a library of polymers that in situ crosslink to form hydrogels with a range of degradation rates only influenced by the local environments pH, a known quantity. Moreover, the polymers are low-fouling and therefore have minimal non-specific interactions with biomolecules and cells, which improves biocompatibility.

Abstract: Degradable low-fouling hydrogels are ideal vehicles for drug and cell delivery. For each application, hydrogel degradation rate must be re-optimized for maximum therapeutic benefit. We developed a method to rapidly tune degradation rates of low-fouling poly(oligo(ethylene glycol) methyl ether methacrylate) ($P(EG)_xMA$) hydrogels by modifying two interdependent variables: (1) base-catalyzed crosslink degradation kinetics, dependent on crosslinker electronics (electron withdrawing groups (EWGs)); and (2) polymer hydration, dependent on the molecular weight (MW) of poly(ethylene glycol) (PEG) pendant groups. By controlling EWG strength and PEG pendant group MW, $P(EG)_xMA$ hydrogels were tuned to degrade over 6 to 52 d. A six-member $P(EG)_xMA$ copolymer library yielded slow and fast degrading low-fouling hydrogels for short- and long-term delivery applications. The degradation mechanism was also applied to RGD-functionalized poly(carboxybetaine methacrylamide) (PCBMAA) hydrogels to achieve slow (52 d) and fast (13 d) degrading low-fouling, bioactive hydrogels.

Acknowledgements: I would like to thank Ryan for always being available and providing critical feedback to help streamline my project, by avoiding potential issues. Your patience, tact, and honesty helped me grow a lot as a graduate student. To Vince, your staunch work ethic and industriousness were incredibly motivating and pushed me to work harder. To Alex, your constructive and critical counsel helped focus my efforts. To Yousuf, your assistance with and dedication to the project kept it on track and I learned a lot through mentoring you. To Devang, for offering thoughtful advice and perspective that helped to guide my efforts. To Drs. Boyang and Anthony for their being a part of my committee. To Ayodele, Kevin, and the Jose lab for your helpfulness and feedback. To Stu, for your critical insight that helped streamline polymer synthesis. To the NMR, Mass Spec, and BI facilities and Hoare lab for access to equipment. To the Adronov lab, for providing us with DBCO.

A special thanks to my friends and family for their support through this endeavor. To Brandon, you provided feedback so often and so quickly; I really appreciate all your assistance. To my wife, for your support, sacrifice, and diligent editing throughout this endeavor. To my parents, for your countless prayers, encouragement, and sacrifice that are the seed for all my successes. Finally, to my sister, for being there for me at my lowest and helping me keep a level head. I am incredibly grateful and privileged to have such unwavering support from all my friends and family.

Table of Contents

List of figures and schemes

List of tables

List of abbreviations

$(EG)_xMA$: (ethylene glycol)$_x$ methyl ether methacrylate
^1H NMR: proton nuclear magnetic resonance
3T3: fibroblast cell line
APMA: aminopropyl methacrylamide
AZ: Azide
BSA: bovine serum albumin
Calcein AM: Calcein acetoxymethyl ester
CBMAA: carboxybetaine methacrylamide
CBS: calf bovine serum
CGGGGGGGGRGDSG: cysteine-(glycine)$_8$- arginine-glycine-aspartic acid-serine-glycine
CGRGDS: cysteine-glycine-arginine-glycine-aspartic acid-serine
CTP: 4-cyano-4-(phenylcarbonothioylthio)pentanoic acid
DBCO: dibenzocyclooctyne
DCM: dichloromethane
DMAPMA: N-[3-(dimethylamino)propyl]- methacrylamide
DMEM-F12: Dulbecco's Modified Eagle Medium: Nutrient Mixture F-12
DMSO: dimethyl sulfoxide
EDC: 1-Ethyl-3-(3-dimethylaminopropyl)carbodiimide
ESI: electrospray ionization
EWG: electron withdrawing group
FBGC: foreign body giant cell
FBR: foreign body response
GPC: gel permeation chromatography
hMSC: human mesenchymal stem cells
HUVEC: human umbilical vein endothelial cells
IKVAV: isoleucine-lysine-valine-alanine-valine
kDa: kilodalton
LCST: lower critical solution temperature
MC: methylcellulose
MMP: matrix metalloproteinase
M_n: number average molecular weight
MS: mass spectrometry
MW: molecular weight
MWCO: molecular weight cut-off
ND: non-degradable
NHS: N-hydroxysuccinimide
NHS-AZ: succinimidyl carbonate azides
NHS-DBCO: succinimidyl carbonate dibenzocyclooctyne
$P(EG)_xMA$: poly (ethylene glycol)$_x$ methyl ether methacrylate
$P(EG)_xMA$-AZ-R#: poly (ethylene glycol)$_x$ methyl ether methacrylate-azide modified polymer
$P(EG)_xMA$-R#: poly (ethylene glycol)$_x$ methyl ether methacrylate modified hydrogel
PBS: Phosphate buffered saline
PCB: poly (carboxybetaine)

PCBMA: poly (carboxybetaine) methacrylate
PCBMAA: poly (carboxybetaine) methacrylamide
PCBMAA-AZ-R#: poly (carboxybetaine) methacrylamide-azide modified polymer
PCBMAA-R#: poly (carboxybetaine) methacrylamide modified hydrogel
PEG: polyethylene glycol
PEO: polyethylene oxide
PGA: poly(glycolic acid)
PLA: poly(lactic acid)
PLGA: poly(lactic-*co*-glycolic acid)
R1: hydrogen (non-degrading)
R2: 4-methylphenyl sulfone (slow-degrading)
R3: 4-chlorophenyl sulfone (fast-degrading)
RAFT: reversible addition-fragmentation chain-transfer
RGD: arginine-glycine-aspartic acid
RGD-AZ: azide-cysteine-glycine-arginine-glycine-aspartic acid-serine
ROS: reactive oxygen species
RPU: repeat units
SDS: sodium dodecyl sulfate
SPAAC: strain-promoted azide-alkyne cycloaddition
TCI cryoprobe: triple resonance cryoprobe
TCP: tissue culture plate
TEMPO: 2,2,6,6-Tetramethyl-1-piperidinyloxy
THF: tetrahydrofuran
VA-044: 1,2-Bis(2-(4,5-dihydro-1H-imidazol-2-yl)propan-2-yl)diazene dihydrochloride
V-501: 4,4’-Azobis(4-cyanovaleric acid)

Declaration of Academic Achievement: Vincent Huynh synthesized PCBMAA-APMA, cultured cells, seeded cells on RGD-functionalized hydrogel surfaces, and conducted the cell encapsulation study. Yousuf Shad aided with degradation measurements and synthesis of PCBMAA derivatives. Alex Jesmer synthesized BSA-fluorescein. Rashik Ahmed conducted and analyzed NMR experiments to quantify $P(EG)_xMA$-AZ-R3 hydrolysis rate.

1 Introduction

1.1 Rationale

Hydrogels function as local delivery depots, providing sustained release of drugs, and surrogate extracellular matrices (ECM) for cells, improving cell survival and function. Localizing drug delivery with hydrogels increases drug accumulation at the disease site, reducing off-target effects and dosage.[1–4] For cell delivery applications, hydrogels retain cells at the disease site,[5–7] provide protection from both the shear force of injection[8,9] and the inflammatory environment,[10] and can provide sites for cell anchorage,[11] prolonging transplanted cell survival to enhance recovery of the damaged tissue.

To maximize therapeutic benefit, hydrogels should degrade at a rate appropriate for the intended application. Uncontrolled degradation of hydrogels leads to a large initial release of drug (i.e. burst release), which decreases therapeutic efficacy.[12] For cell delivery applications, hydrogel degradation can lead to large changes in mechanical properties, which affect cell fate[13,14] and release rates. Coordinating hydrogel degradation with tissue growth can improve tissue regeneration.[15,16] Therefore, degradation must be optimized for each application.

Hydrogels made from low-fouling polymers can help mitigate deleterious in vivo responses. Poly(ethylene glycol) (PEG) hydrogels immediately adsorb host proteins following implantation.[17] This leads to a cascade of events, known as the foreign body response (FBR), resulting in the formation of a collagenous capsule around the hydrogel, impeding drug and cell delivery.[18–20] To mitigate the FBR, polymers that tightly bind water molecules are used to make protein adsorption less energetically favorable. Polymers such as poly(oligo(ethylene glycol) methyl ether methacrylate) ($P(EG)_xMA$) and poly(carboxybetaine methacrylate) (PCBMA)

achieve this due to their strong hydration shell[21] with hydrogels made from P(EG)$_x$MA[22] and PCBMA[23] showing a reduced FBR in rodents.

Although low-fouling materials have been developed that mitigate the FBR, control of their degradation is limited, with most degrading quickly (<21d).[24–29] Enzymatic degradation of hydrogels depends on the implantation site,[30,31] making degradation unpredictable in vivo. As pH is relatively constant throughout the body, hydrolysis is a more predictable mechanism of degradation. Base-catalyzed hydrolysis, in particular, can be tuned by the strength of electron withdrawing groups (EWGs) adjacent to a degradable carbamate bond, which extended PEG hydrogel lifetime up to 105 d.[32] Combining this degradation mechanism with low-fouling materials, such as P(EG)$_x$MA and PCBMA, provides a simple method to form low-fouling hydrogels with precisely tunable degradation. Using different EWGs, a library of degradable polymers can be synthesized, which, when combined, can easily achieve different degradation rates for a broad range of applications.

1.2 Thesis objectives

This thesis aims to develop a library of in situ gelling polymers to achieve low-fouling hydrogels with a wide range of degradation rates, solely dependent on the pH of the local environment, that are suitable for drug or cell delivery applications. Specifically, we will synthesize P(EG)$_x$MA and poly(carboxybetaine methacrylamide) (PCBMAA) copolymers for in situ gelling hydrogels with:

1. Tunable degradation over short (<7 d) or long time (7 – 28 d) periods
2. Low-fouling properties toward proteins and cells
3. Tunable bioactivities (e.g. immobilization of RGD, a cell adhesive peptide)

1.3 Hydrogels: tunable delivery vehicles

Hydrogels have highly tunable chemical and physical properties and are used in a broad range of applications to deliver drugs and cells for cancer immunotherapy,[33,34] wound healing,[35] and pain management.[36,37] Their high water content mimics tissues, improves biocompatibility, and allows for the encapsulation of hydrophilic drugs. The crosslinked polymer network protects encapsulated biologics from premature degradation, by impeding the penetration of proteolytic enzymes and reducing drug immunogenicity.[10,38] By modifying the polymer network, the physical and chemical properties of hydrogels can be tuned. The rate of drug release from hydrogels can be controlled by diffusion, which is dependent on hydrogel mesh size (i.e. porosity). The mesh size depends on crosslink density and can be changed overtime through controlled degradation to tune drug release.[39,40] Additionally, affinity-based delivery systems can be used that utilize drug-hydrogel interactions to control drug release[41] through non-degradable covalent linkages,[42] cleavable linkages,[32] or non-covalent interactions.[43,44] Alternatively, nanoparticles can be incorporated into hydrogels to create a hybrid drug delivery system that leverages the drug delivery capabilities of both.[45] Thus, hydrogels are versatile delivery vehicles with various methods to control drug release.

The highly tunable properties of hydrogels give them several advantages to improve the efficacy of cell-based therapy as well, compared to simply delivering cells as suspensions. The increased viscosity of injectable hydrogels provides protection to cells against the shear force of injection[8,9] while also retaining cells near the target site by preventing mechanical washout.[5–7] The semi-permeable hydrogel network protects encapsulated cells from immune cells and large antibodies while permitting the diffusion of small molecules and nutrients.[10] As many cells are anchorage dependent, incorporating cell-adhesive moieties (e.g. RGD) can improve both survival

and function of transplanted cells.[11] Furthermore, hydrogel mechanical properties can be tuned over a wide range, with stiffness matching that of different tissues in the body,[46–49] affecting cell fate.[13,14] Moreover, coupling the degradation rate of hydrogels with the rate of tissue growth improves tissue regeneration.[15,16]

To maximize therapeutic efficacy, hydrogels must be formed using non-toxic crosslinking chemistries in situ. Once delivered, hydrogels must avoid recognition by the immune system, which abrogates therapeutic efficacy by fibrous encapsulation of the hydrogel. Hydrogels should degrade at a rate appropriate for the intended application and avoid uncontrolled degradation that leads to burst release and rapid changes in mechanical properties. When the drug is exhausted, the hydrogel should degrade into non-cytotoxic by-products to avoid surgical removal. For cell delivery, hydrogels should degrade at a rate coordinated with tissue regeneration and provide cell-hydrogel interactions that improve encapsulated cell survival and function.

1.4 Hydrogel administration

Drug- or cell-loaded hydrogel delivery via injection is less invasive than surgical implantation. Although both methods bypass tissue barriers and concentrate drug at the disease site, delivering hydrogels by injection avoids surgery, increasing patient comfort and recovery time. Moreover, for sites inaccessible with surgery or treatments requiring repeated administration, injectable hydrogels are a more suitable, minimally invasive alternative.[50]

Injectable hydrogels can be formed prior to or following injection in the body through physical or covalent crosslinking chemistries.[51] Shear-thinning hydrogels can be gelled outside the body and injected by application of shear force. These shear-thinning hydrogels can be

formed through reversible physical crosslinks (e.g. electrostatic interactions,[52] stereochemical interactions[53], or supramolecular chemistry[54]) or through dynamic covalent bonds (e.g. Diels-Alder cycloaddition[55–57] and hydrazone formation[58]). Alternatively, hydrogels can form in situ following injection. Thermoresponsive systems that undergo temperature-induced phase transition at body temperature have been explored (e.g. poly(N-isopropylacrylamide)[59] and block copolymers[60]). More recently, covalent crosslinking chemistries such as Michael addition[61,62] and strain-promoted alkyne-azide cycloaddition[63] (SPAAC; **Figure 1-1**) are being explored.

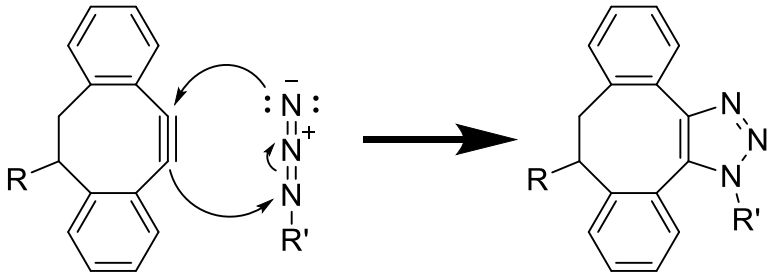

Figure 1-1. Strain promoted alkyne-azide cycloaddition (SPAAC).

1.5 Foreign body response to hydrogels

Once delivered, the immune system recognizes hydrogels, and other implanted biomaterials, as foreign objects and attempts to phagocytose them. Implants too large to phagocytose are, instead, encapsulated by a fibrous capsule, isolating them from the body.[18] This process is known as the foreign body response (FBR) and starts immediately after implantation (**Figure 1-2**); within seconds, blood proteins adsorb to biomaterial surfaces to reduce surface energy.[66] For example, after a 30-minute implantation in mice, PEG-based hydrogels adsorbed ~75 μg cm^{-2} of protein, the most abundant of which was albumin.[17] This blood protein deposition leads to the formation of a provisional matrix around the biomaterial, the composition of which affects subsequent events in the FBR.[67] Following this, neutrophils and mast cells are recruited to the implantation

site and release chemokines and other chemoattractants.[18] These alarm signals recruit macrophages to the implantation site, which are a necessary component of the FBR.[68] Unable to phagocytose the material due to its size, macrophages adhere to the material and fuse together to form a foreign body giant cell (FBGC). In a process known as frustrated phagocytosis, the adhered macrophages and FBGC release reactive oxygen species (ROS), acid, and degradative enzymes (e.g. matrix metalloproteinase) creating a unique local environment at the implant surface in an attempt to biodegrade the material.[69] Additionally, adhered macrophages also secrete factors that recruit and activate fibroblasts that release collagen resulting in a collagenous fibrous capsule that isolates the hydrogel from the host,[18] impeding drug release or cell egress from hydrogels.[20] Thus, there is a need to create hydrogels capable of resisting the FBR to improve the therapeutic efficacy of implanted hydrogels.

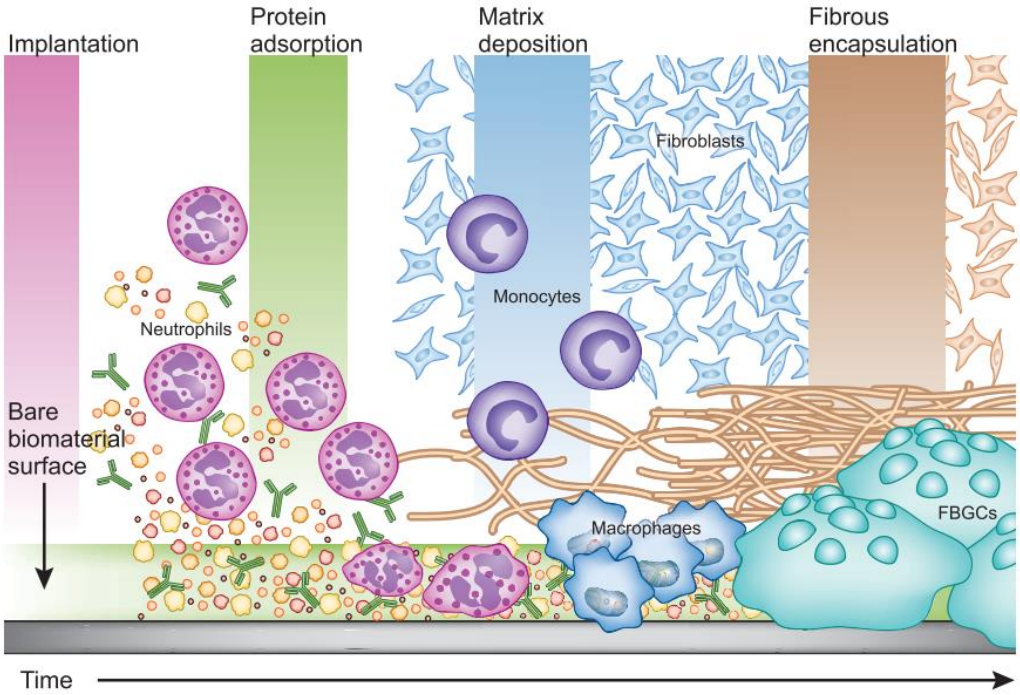

Figure 1-2. Foreign body response (FBR) to implanted biomaterials. Immediately after implantation blood proteins adsorb to the surface of the biomaterial forming a provisional matrix around the biomaterial that affects subsequent steps in the FBR. Neutrophils infiltrate the site and secrete alarm signals that recruit and activate local monocytes and macrophages. Unable to phagocytose the large biomaterial, macrophages fuse together to form a foreign body giant cell (FBGC) and release signals recruiting and activating fibroblasts. Fibroblasts secrete collagen resulting in a dense collagenous capsule isolating the biomaterial from the body. Reproduced with permission of [70].

1.5.1 Low-fouling hydrogels

To mitigate the FBR to hydrogels, low-fouling interfaces can be utilized to prevent non-specific protein adsorption and ultimately macrophage recruitment.

1.5.1.1 Poly(oligo(ethylene glycol) methyl ether methacrylate) (P(EG)$_x$MA)

PEG is one of the most widely used polymers in biomedical applications.[71] Due to its hydrophilicity, PEG materials have purported non-fouling, stealth properties, reducing non-specific adsorption and immunogenicity. However, a growing body of literature indicates that PEG materials are recognized by the immune system.[17,72–78] There is an increasing prevalence of

anti-PEG antibodies in the general population (estimates range from ~20 – 40%),[72,73,77,78] and PEG hydrogels also exhibit a FBR after 28 d subcutaneous implantation in mice.[17,76] Therefore, alternative materials for drug delivery are needed that are less immunogenic.

Poly(oligo(ethylene glycol) methyl ether methacrylate) ($P(EG)_xMA$) is a synthetic comb-like PEG-analogue polymer that hydrogen-bonds to water molecules, creating a barrier against non-specific adsorption of biomolecules and cells (**Figure 1-3A**).[21] $P(EG)_xMA$-drug conjugates with three PEG repeat units did not bind to anti-PEG antibodies while those with nine PEG repeat units had significantly reduced binding compared to equivalent PEG-drug conjugates,[74] which may lead to more biocompatible degradation products. Surfaces grafted with $P(EG)_xMA$ resist protein fouling (7 ng cm^{-2})[79] and prevent platelet binding from whole blood,[80] owing both to the water layer and steric repulsion by PEG side chains creating a barrier to non-specific adsorption. $P(EG)_xMA$ hydrogels resist bovine serum albumin (BSA) and lysozyme adsorption (~20 µg cm^{-2}) and reduce the adsorption of human serum albumin and fibrinogen from blood plasma.[81] Moreover, the in vivo response to subcutaneously injected hydrazone-crosslinked $P(EG)_xMA$ hydrogels showed a minimal inflammatory response after 30 d, dependent on the hydrophilicity of the hydrogel (**Figure 1-3B-G**).[22] Furthermore, unlike PEG, which is only chain-end functionalizable, $P(EG)_xMA$ monomers can be copolymerized using radical polymerization with functional monomers to incorporate sites for in situ crosslinking,[82] controlled degradation,[32] and biomolecule tethering[63] throughout the polymeric backbone.

Therefore, the synthetic tunability of P(EG)$_x$MA along with its resistance to non-specific adsorption make it a promising alternative to PEG for the design of low-fouling hydrogels.

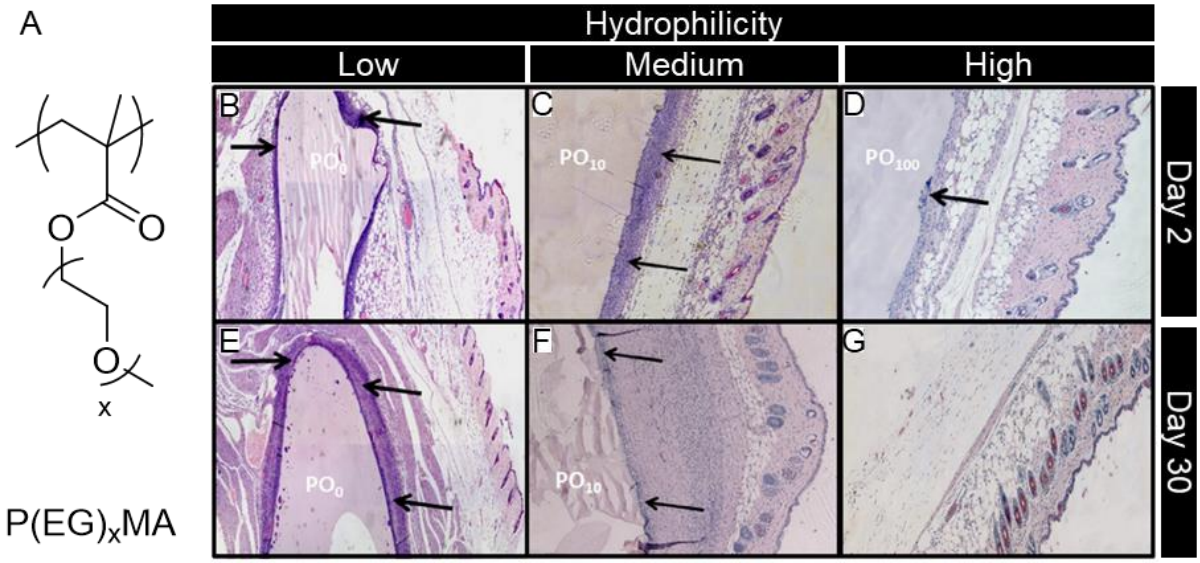

Figure 1-3. P(EG)$_x$MA structure and resistance to FBR. Chemical structure of poly(oligoethylene glycol) methyl ether methacrylate (P(EG)$_x$MA). **B-G)** In situ gelling hydrazone-crosslinked P(EG)$_x$MA hydrogels (15 wt.%) in BALB/c mice. P(EG)$_x$MA hydrogels with higher hydrophilicity (PO_{100}) elicit less leukocyte infiltration and degrade after 1 month in vivo. Hydrophobic hydrogels (PO_0) elicit more leukocyte infiltration and do not degrade. Cells were stained with eosin and hematoxylin. Arrows indicate leukocytes. Figure reproduced with permission of [22].

1.5.1.2 Poly(carboxybetaine methacrylate) (PCBMA)

Zwitterionic materials have recently garnered significant interest as a novel class of biomaterials, with steady increase in publications and exponential increase in citations over the last 10 years, according to a Web of Science search of "zwitterionic materials". Zwitterionic polymers are net neutral polymers that contain oppositely charged groups. Though most zwitterionic polymers are synthetically made, they are biomimetic in nature. The presence of charged groups in zwitterionic polymers creates a tight hydration shell providing an excellent energetic barrier to non-specific protein adsorption. As such, zwitterionic materials present an emerging class of materials for the fabrication of low-fouling hydrogels for long-term applications.

Poly(carboxybetaine) (PCB) is a zwitterionic polymer that mimics glycine betaine, a solute vital to osmotic regulation (**Figure 1-4A**).[83] PCB electrostatically interacts with water creating a strong energetic barrier against non-specific adsorption.[21] PCB coated surfaces resist non-specific protein adsorption[84] in complex and challenging media, such as undiluted aged human blood serum, with undetectable levels of protein adsorption (<5 ng cm^{-2}).[85] PCB hydrogels also resist non-specific adsorption of BSA (~20 µg cm^{-2}).[27,86–88] Moreover, a PCB hydrogel subcutaneously implanted in mice produced no FBR for three months in vivo (**Figure 1-4C**).[23] PCB's low-fouling characteristics have also been leveraged for cell delivery applications. A pure PCB hydrogel maintained stem cell phenotype and multipotency by resisting protein adsorption, which was found to affect stem cell differentiation.[89] Additionally, PCB is known to retain or enhance protein-ligand interactions;[90] cell adhesive moieties improve survival and function of encapsulated cells.[34,91] Thus, PCB represents another class of material for the design of low-fouling hydrogels for long-term drug delivery.

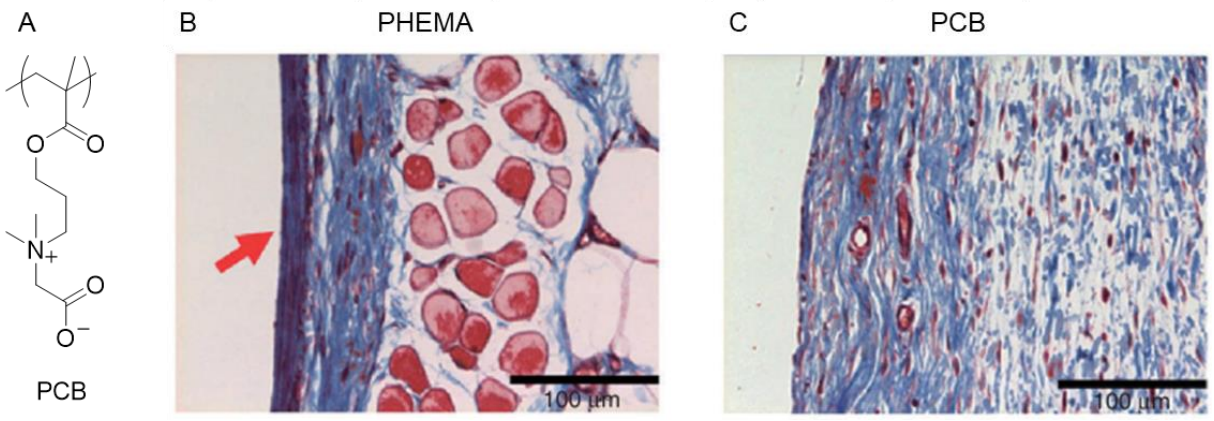

Figure 1-4. PCB structure and resistance to FBR. A) Structure of poly(carboxybetaine methacrylate) (PCB). **B-C)** Three months after subcutaneous implantation of hydrogels with 5% crosslink density in C57BL/6 mice, tissues were stained with Masson's trichrome. Hydrogels are located on the left side of images. **B)** Blue staining indicates collagen capsule surrounding poly(2-hydroxyethyl methacrylate) (PHEMA) hydrogels, indicated by the red arrow **C**). No capsule formation is observed around PCB hydrogels. Reproduced with permission from [23].

1.6 Controlled hydrogel degradation

Hydrogel degradation must be tuned to maximize therapeutic benefit from drug and cell delivery. Uncontrolled degradation of hydrogels leads to a burst release of drug, which decreases therapeutic efficacy, particularly for long-term therapies.[12] Moreover, the hydrogel should degrade into non-toxic and non-inflammatory by-products that can be excreted from the body (PEG <50 kDa can be renally excreted),[92] to avoid unwanted immune reactions or surgical removal. For cell delivery applications, hydrogel degradation can lead to large decreases in storage modulus and affect cell release. Thus, hydrogel degradation is often coordinated with tissue growth to improve tissue regeneration.[15,16] Therefore, hydrogel degradation must be optimized for each unique application to improve therapeutic efficacy.

The mechanism of hydrogel degradation depends on the polymer constituents and gelation mechanism. Hydrogels can degrade due to disulfide reduction, enzymatic degradation, or hydrolysis. Degradation rate can be modified by: 1) increasing the number of crosslinks in the hydrogels; and/or 2) modifying the rate of crosslink degradation. Ideally, degradation should be easily tuned without extensive synthetic modifications or changes to hydrogel properties. Moreover, to increase the scope of application, hydrogels should degrade predictably under different environmental conditions.

Table 1-1. Typical mechanisms to control hydrogel degradation.

Degradation mechanism	Degradation time*	Ref.
Disulfide reduction	1 d	[24]
	<1 h	[93]
	n.d.	[25, 94]
Enzymatic	~21 d	[95]
	>7 d	[96]
	10 – 14 d	[97]
	5 – 10 d	[98]
	13 d	[99]
	8 h	[100]
	14 d	[101]
	10 – 19 d	[102]
	n.d.	[103, 104]
Backbone hydrolysis	~11 d	[105]
	~7 d	[106]
	~7 d	[107]
Reversible bond hydrolysis	4 d (pH 3)	[108]
	>14 d	[109]
	25 d	[110]
	1 – 62 d	[111]
Ester hydrolysis	18 – 130 d	[112]
	5 d	[113]
	3 d	[114]
	1 – 24 d	[115]
Base-catalyzed hydrolysis	1 – 105 d	[32]

*time until complete degradation reported. n.d. = no data on complete hydrogel degradation.

1.6.1 Disulfide reduction

Dithiol-containing crosslinkers can be used to form hydrogels that are degraded by serum thiols.[116] Modifying crosslinker mole % is used to control degradation rate, which varies based on glutathione concentration. Hydrogel degradation through disulfide reduction by glutathione occurs quickly, with most hydrogels degrading within 1 d (**Table 1-1**).[24,25,93,94]

1.6.1.1 Limitations

Glutathione concentrations vary throughout the body making degradation unpredictable; extracellular glutathione concentration can vary an order of magnitude (2 – 20 μM).[117] Additionally, glutathione concentration can vary depending on the oxidative state of the tissue. Tumor tissue is more reductive than normal tissue,[118] whereas inflammatory tissue, undergoing oxidative stress, has lower glutathione concentrations.[119]

1.6.2 Enzymatic degradation

Incorporating peptide crosslinkers into hydrogels allows for local cell-secreted proteases to remodel the ECM as cells grow and differentiate.[120] In addition to modifying crosslinker concentration, the peptide sequence can be molecularly engineered to tune degradation.[95–97] For example, PEG hydrogels crosslinked using a library of protease-degradable linkers had differential degradation based on the matrix metalloproteinase (MMP) used.[98] Additionally, peptide sequences containing more aromatic or hydrophobic residues have also been shown to slow degradation rate.[104] Thus, in addition to simply increasing polymer/crosslinker concentration, the susceptibility of peptide-crosslink degradation can be tuned, resulting in a broader range of degradation times (8 h to 21 d; **Table 1-1**).[95–104]

1.6.2.1 Limitations

Due to the dynamic nature of the biological environment,[30,31] enzyme-mediated degradation is difficult to control in vivo. The concentration of specific enzymes, such as MMP[121] and hyaluronidase,[122] vary significantly based on the specific disease. Thus, hydrogel degradation rate may need to be re-optimized for each unique application.

1.6.3 Hydrolytic degradation

Hydrolytic degradation of hydrogels is a promising alternative, since pH is relatively constant throughout the body. Degradation often occurs due to hydrolysis of ester moieties in the polymer backbone or crosslinks but other degradable moieties that are pH-sensitive are also used.

1.6.3.1 Backbone degradation

Backbone degradation focuses on sandwiching a block of polyethylene glycol (PEG) polymer between blocks of poly(α-hydroxy esters), such as poly(lactic acid) (PLA), poly(glycolic acid) (PGA), or poly(lactic-*co*-glycolic acid) (PLGA), with telechelic acrylate groups that form hydrogels through bulk polymerization.[105–107] The hydrolytically labile ester groups of the poly(α-hydroxy esters) lead to hydrogel degradation, which is controlled by the concentration of polymer. This strategy to control degradation, however, limits hydrogel composition exclusively to polymers with degradable backbones and leads to short-term hydrogel degradation (~7 d; **Table 1-1**).[105–107]

1.6.3.2 Crosslink degradation

1.6.3.2.1 Reversible chemical crosslinks

Reversible chemical crosslinks (e.g. Diels-Alder cycloaddition[55,103,110] and hydrazone formation[58,108,109]) are used, wherein, the dynamic nature of the bond allows for crosslink hydrolysis over time, with reports of hydrogel degradation up to 62 d (**Table 1-1**).

1.6.3.2.2 Ester hydrolysis

One of the most common methods to control hydrogel degradation is through the incorporation of ester moieties into hydrogel crosslinks. Several factors, in addition to increasing polymer concentration,[114] have been tuned to control ester hydrolysis. By modifying the number (1 or 2) and location of labile esters, the degradation of SPAAC-crosslinked PEG hydrogels was tuned to degrade from 18 – 130 d in PBS with minimal effect on hydrogel swelling and stiffness.[112] The local hydrophobicity of the ester environment also affects degradation.[112–115] For example, increasing the number of methylene spacers between ester groups and the polymer backbone decreased hydrogel degradation rate, due to increased hydrophobicity.[113,114] Given the various parameters that can be tuned to alter ester hydrolysis, reports of hydrogel degradation through hydrolysis of ester-containing crosslinks varies over a wide range (1 – 130 d; **Table 1-1**).[112–115]

1.6.3.2.3 Base-catalyzed hydrolysis

Base-catalyzed hydrolysis of carbamate crosslinks is of particular interest due to its high tunability.[32,123] Based on the strength of EWGs, the acidity of the carbamate β-hydrogen can be controlled, the deprotonation of which is rate-determining for hydrolysis[124] (**Figure 1-5**). Instead of increasing crosslinking density, which impacts hydrogel physical properties, the strength of EWGs can be altered to extend hydrogel lifetime up to 105 d (**Table 1-1**). Moreover, as the degradable moieties are incorporated using amine-reactive NHS molecules, this method of degradation could potentially be used with other polymer types.

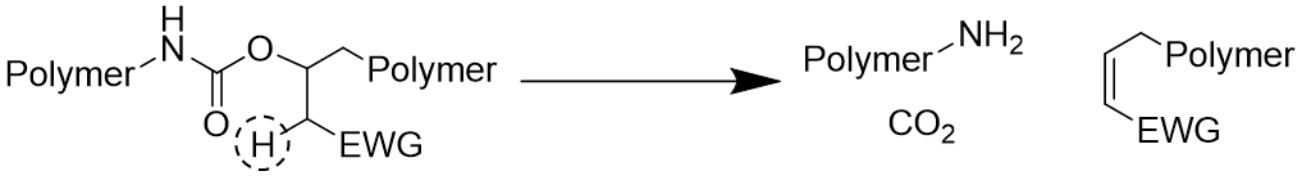

Figure 1-5. Base-catalyzed carbamate hydrolysis. By tuning the acidity of carbamate β-hydrogen (dashed circle), the rate of crosslink hydrolysis, and thus hydrogel degradation, can be controlled.

1.6.3.3 Limitations

Current methods to tune hydrogel degradation by hydrolysis require extensive synthetic modifications to achieve a wide range of degradation rates. Moreover, many of the hydrogels tested are PEG-based, and are encapsulated in vivo[30,76] severely impairing drug and cell delivery.

1.7 Bioactive hydrogels for cell delivery

In addition to minimizing non-specific interactions to prevent fibrosis of encapsulated cells[65] and coupling hydrogel degradation to tissue regeneration,[15] several studies demonstrate that incorporation of cell adhesion moieties (e.g. RGD or IKVAV) provides a anchorage site for cell attachment, guides cell differentiation, and improves their function.[10,25,34,91,125–130] The RGD density of RGD-modified alginate hydrogels was found to regulate myoblast proliferation and differentiation.[127] Human mesenchymal stem cells (hMSCs) encapsulated in RGD-modified PEG hydrogels had improved survival compared to unmodified PEG gels.[130] RGD-modified alginate hydrogels were shown to improve encapsulated human umbilical vein endothelial cell (HUVEC) survival, migration, and 3D organization.[128] A collagen-mimetic peptide incorporated into alginate hydrogels improved T cell viability and egress compared to unmodified alginate, reducing tumor relapse in mice.[34] Incorporation of cell adhesion moieties into hydrogels

improves the cell survival and function in a wide range of cell types and is thus an important design parameter that needs to be incorporated into hydrogel cell delivery vehicles.

1.8 Current limitations

Hydrogels have been developed to resist non-specific protein and cell adsorption to mitigate deleterious in vivo reactions. However, current methods to control their degradation rates are unpredictable,[24–26,28,93,94] dependent on enzymes (e.g. MMP and hyaluronidase) whose concentration varies significantly based on the specific disease. Thus, there is a great need to develop a versatile method to tune degradation rates of low-fouling hydrogels that are independent of endogenous triggers with minimal synthetic steps. To create a broadly applicable method, a library of polymers is needed to form hydrogels with degradation rates tailored for each unique application.

2 Controlled degradation of low-fouling poly(oligo(ethylene glycol)methyl ether methacrylate) hydrogels

*This chapter was published in RSC Advances

M. M. Shoaib, V. Huynh, Y. Shad, R. Ahmed, A. H. Jesmer, G. Melacini and R. G. Wylie, *RSC Adv.*, 2019, **9**, 18978–18988.

2.1 Abstract

Degradable low-fouling hydrogels are ideal vehicles for drug and cell delivery. For each application, hydrogel degradation rate must be re-optimized for maximum therapeutic benefit. We developed a method to rapidly and predictably tune degradation rates of low-fouling poly(oligo(ethylene glycol) methyl ether methacrylate) ($P(EG)_xMA$) hydrogels by modifying two interdependent variables: (1) base-catalysed crosslink degradation kinetics, dependent on crosslinker electronics (electron withdrawing groups (EWGs)); and, (2) polymer hydration, dependent on the molecular weight (MW) of poly(ethylene glycol) (PEG) pendant groups. By controlling PEG MW and EWG strength, $P(EG)_xMA$ hydrogels were tuned to degrade over 6 to 52 d. A 6-member $P(EG)_xMA$ copolymer library yielded slow and fast degrading low-fouling hydrogels suitable for short- and long-term delivery applications. The degradation mechanism was also applied to RGD-functionalized poly(carboxybetaine methacrylamide) (PCBMAA) hydrogels to achieve slow (~50 d) and fast (~13 d) degrading low-fouling, bioactive hydrogels.

2.2 Introduction

Degradable low-fouling hydrogels are being developed as implantable vehicles for drug and cell delivery to decrease the incidence rate of adverse events (e.g. foreign body response (FBR)) by minimizing non-specific protein adsorption and cell binding.[18,19] The FBR cascade impedes drug

release or cell egress from hydrogels by surrounding implants in dense fibrous capsules.[20] Due to their strong hydration shells, non-specific protein adhesion to low-fouling polymers such as poly(oligo(ethylene glycol)$_x$ methyl ether methacrylate) (P(EG)$_x$MA) and poly(carboxybetaine methacrylamide) (PCBMAA) is energetically unfavorable.[21] P(EG)$_{4\text{-}5}$MA coated surfaces resist protein fouling[79] and platelet binding.[80] Moreover, carboxybetaine surfaces have been shown to prevent non-specific protein adsorption in serum[85] and resist the FBR for up to 3 months in vivo.[23]

The degradation of low-fouling hydrogels must be tuned to match requirements for short- and long-term delivery applications. Hydrogel drug delivery applications, such as cancer therapies,[1,33,131] wound healing,[35] pain management,[36,37] and retinal degenerative disease treatments,[132,133] often require drug release profiles that span a wide-distribution of timeframes, ranging from as little as a days to several weeks. We therefore require low-fouling hydrogels with highly tunable degradation timeframes. Predictable degradation rates are particularly important for long-term drug delivery (~4 weeks) wherein uncontrolled hydrogel degradation can limit efficacy by increasing the initial burst release[40]. Thus far, degradation mechanisms for low-fouling gels have focused on endogenous triggers (e.g. reduction of disulfide bonds,[24,25,27] enzyme cleavage sites[26]), or hydrolytic bonds (e.g. esters, hydrazones).[28] In situ crosslinking P(EG)$_x$MA copolymers with aldehyde and hydrazide repeats yield hydrogels that crosslink through reversible hydrazone bonds with degradation rates proportional to pH and copolymer molecular weight (MW).[109,134] Carboxybetaine copolymers with zwitterionic thiol repeats have been developed to achieve biodegradable hydrogels in the presence of reducing agents such as glutathione.[25,27,94] A detailed description of hydrogel degradation mechanisms is provided in the referenced review.[135]

Endogenous triggered degradation is dependent on dynamic biological environments, which may result in unpredictable degradation rates, and current methods to tune hydrolysis rates require extensive synthetic modifications. To improve therapies requiring low-fouling hydrogels, there is a great need to develop a versatile method to easily tune degradation rates that are independent of endogenous triggers and don't require additional synthetic steps. To achieve an accessible library of low-fouling hydrogels with varied degradation profiles, hydrogels should be formed by simply mixing a limited number of pre-defined polymers for in situ crosslinking. The combination of low-fouling $P(EG)_xMA$ hydrogels of varying hydration levels with different crosslinkers for irreversible base-catalyzed degradation[32,123] is expected to provide a method to rapidly tune degradation over clinically relevant timeframes. Irreversible base-catalyzed crosslink degradation[32,123] is solely dependent on the pH of the implantation site, a known value, and not reliant on dynamic endogenous triggers. Furthermore, hydrogels composed of $P(EG)_xMA$ with different PEG pendant group molecular weights (MWs) will exhibit different hydration levels to further tune base-catalyzed crosslinker degradation rates.[136] By simply mixing pre-defined polymers, a library of $P(EG)_xMA$ copolymers is expected to yield low-fouling hydrogels with highly tunable degradation kinetics.

2.3 Materials and Methods

2.3.1 Materials

Triethylene glycol methyl ether methacrylate 93% ($(EG)_3MA$), poly(ethylene glycol) methyl ether methacrylate average M_n 300 ($(EG)_{4\text{-}5}MA$), poly(ethylene glycol) methyl ether methacrylate average M_n 500 ($(EG)_{8\text{-}9}MA$), 4-cyano-4-(phenylcarbonothioylthio)pentanoic acid (CTP), 4,4'-Azobis(4-cyanovaleric acid) (V-501), N-[3-(dimethylamino)propyl]-

methacrylamide (DMAPMA), *t*-Butyl bromoacetate, trifluoroacetic acid, 6-chloro-1-hexanol, sodium azide, trichloroisocyanuric acid, TEMPO, sodium bicarbonate, 1.6 M n-butyllithium in hexane, 4-(Methylsulfonyl)toluene, pyridine, triphosgene, N-hydroxysuccinimide (NHS), fluorescamine, triethylamine, picrylsulfonic acid 5% (w/v), sodium dodecyl sulfate (SDS), bovine serum albumin (BSA), and fluorescein sodium salt were purchased from Sigma-Aldrich (Oakville, ON). N-(3-Dimethylaminopropyl)-N′-ethylcarbodiimide hydrochloride was purchased from Chem-Impex International (Wood Dale, IL). 4-chlorophenyl methyl sulfone was purchased from Alfa Aesar (Ward Hill, MA). N-(3-Aminopropyl)methacrylamide hydrochloride, >98% (APMA) was purchased from Polysciences, Inc. (Warrington, PA). 1,2-Bis(2-(4,5-dihydro-1H-imidazol-2-yl)propan-2-yl)diazene dihydrochloride (VA-044) was purchased from Toronto Research Chemicals (Toronto, ON). CGRGDS >95% was purchased from GenScript (Piscataway, NJ). Calcein AM fluorescent dye was purchased from Corning, New York, USA. PrestoBlue™ cell viability reagent, Hoescht 33342, HyClone™ bovine calf serum (CBS) and DME/F-12 1:1 (1x) were purchased from Thermo Fisher Scientific (Whitby, ON). Methylcellulose (MC; METOLOSE® SM-4000) was purchased from Shin-Etsu Corp (Tokyo, Japan). Solvents were reagent grade and obtained from Caledon Laboratories (Georgetown, ON) and Thermo Fisher Scientific (Whitby, ON). Dibenzylcyclooctyne-NHS ester (DBCO-NHS) was gifted by Prof. Alex Adronov at McMaster University (Hamilton, ON).

2.3.2 Synthesis and characterization of P(EG)$_x$MA copolymers

2.3.2.1 Synthesis of P(EG)$_x$MA-APMA

Inhibitors were removed from (EG)$_x$MA monomers using an aluminum oxide column. For P(EG)$_3$MA-APMA, (EG)$_3$MA (2 g, 8.6 mmol), APMA (81.0 mg, 0.44 mmol), CTP (5.8 mg, 21 µmol), and VA-044 (1.35 mg, 4.18 µmol) were dissolved in 2:1 water:dioxane (7 mL). For

$P(EG)_{4\text{-}5}MA$-APMA, $(EG)_{4\text{-}5}MA$ (1 g, 3.3 mmol), APMA (48 mg, 0.27 µmol), CTP (5.8 mg, 21 µmol) and VA-044 (1.35 mg, 4.2 µmol) were dissolved in 2:1 water:dioxane (2.5 mL). For $P(EG)_{8\text{-}9}MA$-APMA, $(EG)_{8\text{-}9}MA$ (1 g, 2 mmol) APMA (29 mg, 0.16 mmol), CTP (5.8 mg, 21 µmol) and VA-044 (1.35 mg, 4.2 µmol) were dissolved in 2:1 water:dioxane (1.1 mL). All reaction solutions were freeze-pump-thawed (3 times) followed by a nitrogen backfill, and acidified to pH ~3.5 using 0.1 M HCl prior to polymerization at 40°C for ~16 h. Polymers were purified by dialysis (MWCO 12 -14k) against pH 3 water and lyophilized to yield a pink paste ($P(EG)_3MA$-APMA: 1.325; $P(EG)_{4\text{-}5}MA$-APMA: 0.904; $P(EG)_{8\text{-}9}MA$-APMA: 0.948 g).

2.3.2.2 Characterization of $P(EG)_xMA$-APMA copolymers

Polymer number average molecular weight (M_n) and dispersity (Đ) were determined using an Agilent 1260 Infinity II gel permeation chromatography (GPC) system equipped with an Agilent 1260 Infinity refractive index detector and GE healthcare Superose^{TM} 6 Increase 10/30 GL with 10 mM PBS running buffer. The column was calibrated using polyethylene glycol/polyethylene oxide (PEG/PEO) standards (M_n of 3 to 60 kDa). ^{1}H NMR (600 MHz, D_2O, 128 scans) of $P(EG)_xMA$-APMA copolymers was used to quantify polymer composition by comparing the methylene peak adjacent to the ester (4 – 4.4 ppm) to that of the methylene group adjacent to the amino group (~3 ppm).

2.3.2.3 Synthesis of $P(EG)_xMA$-azide ($P(EG)_xMA$-AZ) and $P(EG)_xMA$-DBCO copolymers

NHS-AZ derivatives were synthesized as previously described,[123] see appendix for detailed protocols. $P(EG)_xMA$-APMA polymers were dissolved at 100 mg mL^{-1} in dry DMSO and NHS-AZ derivatives (1.2 eq. relative to amines) and triethylamine (3 eq.) overnight at room temperature. Complete reaction of amines was confirmed by disappearance of the APMA-associated ^{1}H NMR (Figure S 4 – Figure S 15) and a fluorescence-based detection using a

fluorescamine assay. The reaction mixture was diluted to 0.5 mg mL^{-1} and reacted with 3 mM fluorescamine (100 µL total volume) and incubated at room temperature for 1 h. Reduction of fluorescence to that of $P(EG)_xMA$ homopolymer controls indicated complete consumption of amines. Polymers were purified by dialysis (MWCO 12 -14k) against water at pH ~3 for 3 d and lyophilized to yield pink pastes. As seen in Scheme 2-1, three different $P(EG)_xMA$-AZ copolymers were prepared that contained a non-degradable (R1; H), slow-degrading (R2; 4-methylphenyl sulfone), or fast-degrading (R3; 4-chlorophenyl sulfone) adjacent to the carbamate bond for base-catalyzed crosslink degradation.

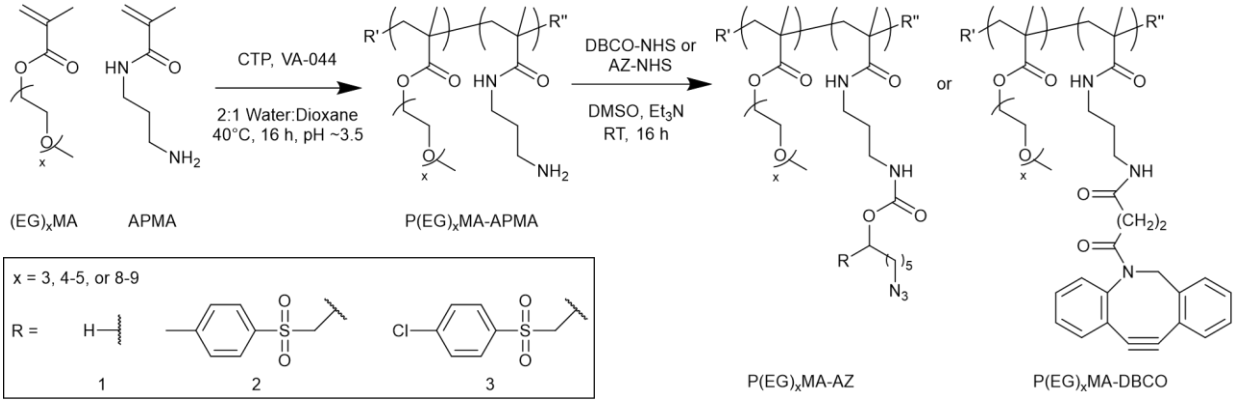

Scheme 2-1. Synthesis of $P(EG)_xMA$-AZ and $P(EG)_xMA$-DBCO copolymers for in situ crosslinking. $P(EG)_xMA$-APMA copolymers were synthesized by acidic, aqueous RAFT polymerization for subsequent derivatization with NHS-AZ derivatives or NHS-DBCO. For each PEG pendant group MW, three $P(EG)_xMA$-AZ copolymers were synthesized with a non-degradable linker (R1) and two degradable crosslinkers with EWGs (R2 = methylphenyl sulfone and R3 = 4-chlorophenyl sulfone). Copolymers were synthesized in mixed aqueous conditions due to monomer solubility and at acidic pH to limit aminolysis of chain transfer agent.[137]

2.3.2.4 Characterization of $P(EG)_xMA$-AZ and $P(EG)_xMA$-DBCO copolymers

Copolymer lower critical solution temperatures (LCSTs) was determined by following the absorbance (600 nm) of polymer solutions (25 mg mL^{-1}) in pH 7.4 PBS or pH 9.3, 0.1 M borax buffer was followed in a 96-well plate with a temperature range of 30 – 65°C and a ramp of 1°C per 10 min on a BioTek Cytation 5 plate reader. Copolymer cytotoxicity was assessed using NIH

3T3 mouse fibroblasts. Cells in DMEM-F12 media were seeded on a 96-well plate at 5000 cells per well. After 24 h, polymer solutions in PBS (sterilized using a 0.2 µm filter) were added to each well to reach a final concentration of 1 mg mL^{-1}. Cells were incubated at 37°C, 5 % CO_2 for 24 h. PrestoBlue reagent solution (22.2 µL) was then added to each well and incubated at 37°C, 5 % CO_2 for 15 min. Fluorescence was measured using a BioTek Cytation 5 plate reader (λ_{ex} = 560 nm; $\lambda_{em.}$ = 590 nm).

2.3.3 ^{1}H NMR kinetic analysis of P(EG)$_x$MA-AZ-R3 copolymer degradation

^{1}H NMR spectra were recorded at 37°C with 128 scans, 32K complex points and spectral widths of 20 ppm on a Bruker 700 MHz spectrometer equipped with a TCI cryoprobe. All spectra were processed and analyzed on TopSpin 3.2.1. The base-catalyzed degradation of the polymers was assessed through the time-dependent increase in the ^{1}H – NMR signal intensity of the nascent hydrolyzed product centred around ~ 7.8 ppm. For the purpose of comparison, the enhancement in the hydrolyzed product intensity was measured relative to the final intensity of the P(EG)$_{8-9}$MA hydrolyzed product at the end of the three-hour experimental period. The resulting experimental points were used to create the kinetic profiles shown in **Figure 2-3E**. To determine the initial hydrolysis rates of the three polymers, a linear regression was used to compute the slopes over the first 1-hour period post lag phase (0.6 h). For the purpose of comparison, the initial time point at which the three polymers began to hydrolyze was set as time 0.

2.3.4 Gelation and characterization of P(EG)$_x$MA hydrogels

Gelation time was measured via gravitational flow analysis. Hydrogels (100 µL) were made with equal volumes and concentrations (50 mg mL^{-1}) of azide and DBCO copolymers. Vials were tilted periodically until flow was no longer observed. The number of crosslinks was determined by tracking the absorbance of 100 µL hydrogels (5 wt.%) at 309 nm was monitored at room

temperature over 24 h to measure consumption of DBCO; gels were formed in a 96-well polypropylene plate. After 24 h, a 10-fold excess of sodium azide was added to react remaining DBCO groups to determine background hydrogel absorbance. After overnight gelation, hydrogel (5 wt.%) cloud points were measured using the same procedure as for copolymer LCSTs.

After overnight gelation at room temperature (~22 h), hydrogel swelling was determined by incubating 100 µL hydrogels (5 wt.%) at 37°C in pH 7.4 PBS. After selected time intervals, buffer was removed, and hydrogel surfaces were gently blotted prior to measuring their wet weight.

2.3.5 Protein adsorption and cell adhesion to P(EG)$_x$MA hydrogels

2.3.5.1 Synthesis of BSA-fluorescein and RGD-AZ

For BSA-fluorescein synthesis, EDC (1.45 mg, 7.6 µmol) and NHS (0.87 mg, 7.5 µmol) were added to a fluorescein sodium salt (3.2 mg, 8.5 µmol) solution in 1 mL DMSO and incubated in the dark at room temperature for 25 min. Separately, 100 mg of BSA was dissolved in 9 mL of pH 7.4 PBS and combined with the NHS activated fluorescein solution. The solutions were reacted for 2 h at room temperature in the dark then dialyzed (MWCO 12-14k) against PBS in the dark at 4°C. For RGD-AZ synthesis, CGRGDS (11 mg, 14 µmol) was dissolved in water (0.1 mL) with triethylamine (7.8 µL, 3 eq.). NHS-AZ (non-degradable linker; 20 mg, 4 eq.) was dissolved in methanol (0.3 mL) and added to the peptide solution. The solution was reacted overnight at room temperature. The precipitate was collected by centrifugation, washed with water, dissolved in 0.1 M HCl, and the aqueous layer was washed with DCM (3 times). The aqueous layer was lyophilized to yield a white powder (3 mg). MS (ESI) analysis determined $[M+1]^+$ peaks of 932.4 g mol^{-1} for disubstituted peptide and 763.4 g mol^{-1} for monosubstituted peptide.

2.3.5.2 BSA adsorption assay

$P(EG)_xMA$ and PCBMAA hydrogels (60 µL at 50 mg mL^{-1}) were formed in triplicate in a 96-well plate and incubated at 37°C for 5 h. PCBMAA-MC hydrogels were formed by mixing 10 wt.% PCBMAA-DBCO dissolved in PBS with 0.5 wt.% MC and 10 wt.% PCBMAA-AZ-R1 dissolved in PBS with 0.5 wt.% MC and gelled for 5 h at 37°C. After gelation, BSA-fluorescein (60 µL at 0.5 mg mL^{-1}) was pipette onto gels and incubated at 37°C for 2 h. The supernatant was removed, and gels were rinsed three times with PBS. Then, gels were immersed in 240 µL of PBS with 0.08% SDS and incubated overnight. The mixture was then sonicated for 30 min to extract residual BSA-fluorescein and the fluorescence was measured using a BioTek Cytation 5 plate reader ($\lambda_{ex.}$ = 494 nm; $\lambda_{em.}$ = 521 nm). The concentration was quantified using a BSA-fluorescein calibration curve of known concentrations.

2.3.5.3 Cell adhesion assay

Hydrogels (60 µL; 5 wt.% in pH 7.4 PBS) were formed in a 96-well plate after gelation for 5 h at 37°C. CGRDGS-AZ (60 µL, 1 mg mL^{-1} in PBS) was pipette on top of hydrogels and incubated overnight at 4°C. Gels were then immersed in PBS for 2 d at 4°C to remove unreacted CGRGDS-AZ. Then, 5000 cells per well of NIH 3T3 mouse fibroblasts were seeded on top of each of the hydrogels (with and without RGD-AZ) and incubated for 24 h at 37°C, 5% CO_2. Cells were then stained with Calcein AM and Hoescht as per the manufacturer's protocol. Hydrogels were then rinsed three times with PBS to remove non-adhered cells prior to imaging using a BioTek Cytation 5 cell imager.

2.4 Results and discussion

We developed low-fouling P(EG)$_x$MA hydrogels with tunable degradation rates by controlling two interdependent variables: (1) base-catalyzed crosslink degradation kinetics, dependent on the strength of the incorporated EWG (**Figure 2-1A**); and, (2) polymer hydration, dependent on the MW of PEG pendant groups (**Figure 2-1B**). By combining P(EG)$_x$MAs with different PEG pendant groups (x = 3, 4-5, and 8-9) with two different crosslinkers (EWG = 4-methylphenyl sulfone or 4-chlorophenyl sulfone), we developed a copolymer library to rapidly tune P(EG)$_x$MA hydrogel degradation over 6, 13, 31, or 52 d, yielding gels suitable for short- and long-term applications (**Figure 2-1C**). We also demonstrate the short- and long-term degradation of RGD functionalized low-fouling PCBMAA hydrogels over 13 and 52 d to produce bioactive, low-fouling hydrogels for cell delivery applications.[34]

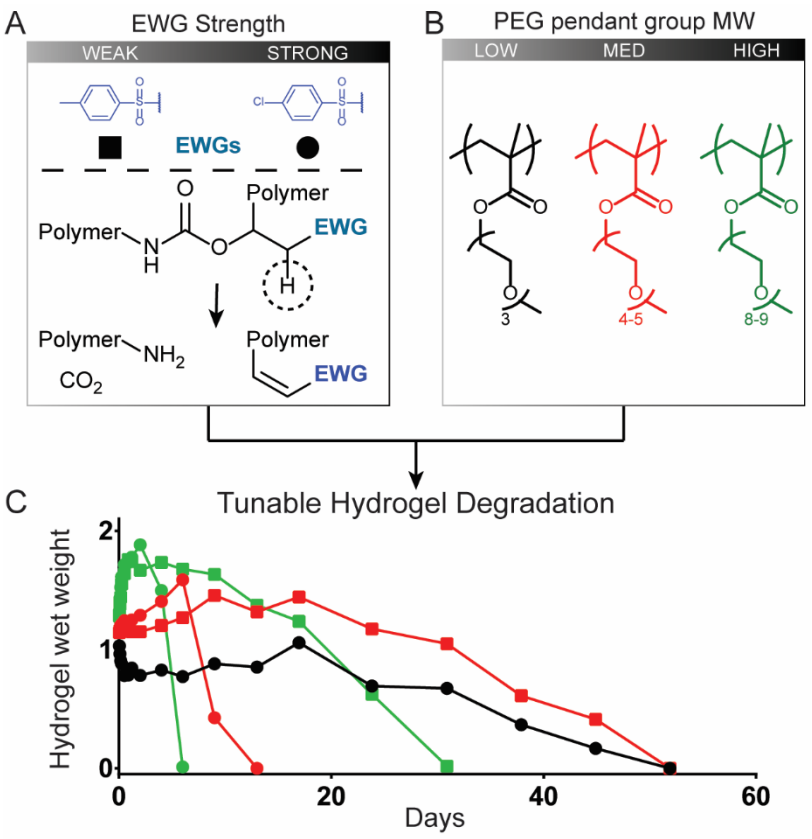

Figure 2-1. Schematic highlighting the short- and long-term degradation of low-fouling hydrogels from a P(EG)$_x$MA copolymer library. A) Irreversible base-catalyzed hydrolysis of carbamate crosslinks tuned with two different EWGs (4-methylphenyl sulfone and 4-chlorophenyl sulfone). Deprotonation site is highlighted by a dashed circle. **B)** The MW of PEG pendant groups in P(EG)$_x$MA influences hydrogel degradation rates. **C)** Tunable hydrogel degradation from 6 to 52 d achieved by creating a library consisting of three P(EG)$_x$MAs copolymers with two different EWGs. Lower PEG MW (less hydrated) P(EG)$_x$MAs and weaker EWGs produced slower degradation rates.

2.4.1 Synthesis and chemical characterization of P(EG)$_x$MA copolymers

Because P(EG)$_x$MA is synthesized by controlled radical polymerization, monomers with reactive functional groups can be polymerized into P(EG)$_x$MA copolymers for in situ crosslinking[82] and controlled degradation.[32] We first synthesized random P(EG)$_x$MA copolymers with N-(3-aminopropyl)methacrylamide (APMA) using reversible addition-fragmentation chain-transfer (RAFT) polymerization to yield P(EG)$_x$MA-APMA with MWs and dispersities (Đ) between 30-

40 kDa and 1.06 to 1.35, respectively (**Scheme 2-1; Table 2-1**). P(EG)$_x$MA-APMA copolymers with different PEG pendant groups (x = 3, 4-5, and 8-9), were prepared to determine the influence of polymer hydration on hydrogel degradation.

The (EG)$_x$MA to APMA composition in copolymers was optimized to ensure similar crosslink densities (crosslinks per g of polymer) in all P(EG)$_x$MA hydrogels, which allowed for the comparison of polymer hydration on degradation rates. To this end, P(EG)$_3$MA-APMA, P(EG)$_{4\text{-}5}$MA-APMA, and P(EG)$_{8\text{-}9}$MA-APMA were synthesized with 2, 5 and 10 APMA mol%, respectively, as confirmed by ^{1}H NMR upon comparing integrations of methylene peaks in (EG)$_x$MA and APMA (**Table 2-1**; Figure S 1 – Figure S 3). Due to sterics associated with PEG pendant groups, greater crosslinker mole fractions, and thus APMA, were required for P(EG)$_x$MAs with higher PEG MWs to standardize crosslink density.

P(EG)$_x$MA-APMAs were further functionalized with NHS-AZ molecules resulting in copolymers that contained a non-degradable (R1; H, no EWG), slow-degrading (R2; 4-methylphenyl sulfone), or fast-degrading (R3; 4-chlorophenyl sulfone) carbamate bond for base-catalysed crosslink degradation. Carbamate bond half-lives have been previously reported to vary between 14 h to 437 d by substituting an adjacent EWGs for base-catalyzed degradation.[123] P(EG)$_x$MA-APMAs were also modified with NHS-DBCO to yield P(EG)$_x$MA-DBCO for in situ crosslinking with P(EG)$_x$MA-AZ copolymers. All APMA amines were fully reacted with NHS-AZ or NHS-DBCO, as confirmed by ^{1}H NMR (Figure S 4 – Figure S 15) and an amine quantification assay (fluorescamine).

Table 2-1. $P(EG)_xMA$-APMA M_n, dispersity, and composition

Polymer	M_n (kDa)*	Đ*	Mol% amine**
$P(EG)_3MA$-APMA	33.5	1.35	2
$P(EG)_{4-5}MA$-APMA	30.7	1.11	5
$P(EG)_{8-9}MA$-APMA	36.8	1.18	10

*Number average molecular weight (M_n) and dispersity determined by GPC calibrated to PEG/PEO standards. **Amine mol% determined via ^1H NMR

To compare polymer hydration through solvation, we studied the solubility of $P(EG)_3MA$ and $P(EG)_{4-5}MA$ copolymers as a function of temperature and determined LCSTs (**Figure 2-2**; Figure S 21A - B). A homopolymer (HP) of $P(EG)_3MA$ had an LCST of 45 °C (25 g L^{-1}), defined as the onset of cloudiness. In comparison to the HP, all $P(EG)_3MA$-AZ and $P(EG)_3MA$-DBCO copolymers demonstrated lower LCSTs near physiological temperature (36-37 °C) due to increased hydrophobic content. The HP of $P(EG)_{4-5}MA$ and $P(EG)_{4-5}MA$-AZ copolymers had LCSTs of 62 and 52-54 °C, respectively. Interestingly, $P(EG)_{4-5}MA$-DBCO's LCST was 2 °C lower than the $P(EG)_{4-5}MA$ HP and 6-8 °C higher than $P(EG)_{4-5}MA$-AZs. Therefore, the increased hydrophobic content from DBCO did not substantially influence $P(EG)_{4-5}MA$'s temperature-dependent solubility, indicating a DBCO composition greater than 5 mol% is required to influence $P(EG)_{4-5}MA$'s LCST. Due to larger PEG side chains, $P(EG)_{8-9}MA$ copolymers did not exhibit an aqueous LCST (Figure S 21C) when heated to 65 °C.[138] Copolymer LCSTs will also predict hydrogel fouling properties as copolymers with LCSTs near or above body temperature will maintain their low-fouling properties; hydrogels are fouling at temperatures above their LCSTs due to increased hydrophobic interactions with proteins.[139]

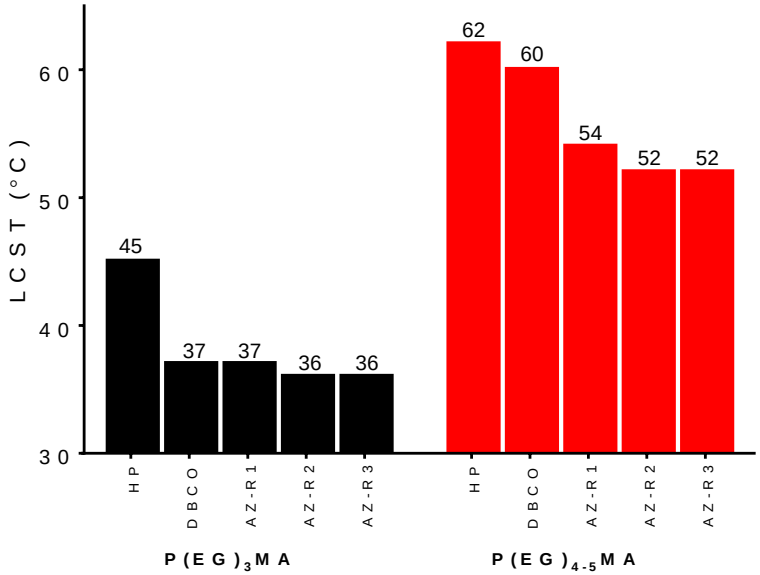

Figure 2-2. P(EG)$_3$MA and P(EG)$_{4-5}$MA copolymer LCSTs. LCSTs (cloud points) of P(EG)$_3$MA and P(EG)$_{4-5}$MA homopolymers (HP) and AZ/DBCO derivatives (25 g L^{-1} in PBS) were determined by measuring solution turbidity at 600 nm as a function of temperature. LCSTs were defined as the lowest temperature that increased turbidity. No LCST was observed for P(EG)$_{8-9}$MA HP and derivatives.

2.4.2 ^{1}H NMR kinetic analysis of P(EG)$_x$MA-AZ-R3 carbamate degradation

To probe the influence of PEG MW on carbamate degradation kinetics, ^{1}H NMR spectra of P(EG)$_x$MA-AZ copolymers with the 4-chlorophenyl sulfone EWG (P(EG)$_x$MA-AZ-R3) were acquired in real time for 3 h in borate buffer at pH 9.3, which increased reactions rates for efficient NMR analysis. Degradation was monitored by peak intensity changes of aromatic protons in 4-chlorophenyl sulfone, which is cleaved from the polymer upon hydrolysis. Over the course of the 3 h experiment, time-dependent losses in signal intensity were observed for polymer bound 4-chlorophenyl sulfone (aromatic protons, 7.8-8.1 ppm) and intensity gains for cleaved 4-chlorophenyl sulfone (aromatic protons, dashed box, sharp doublet, ⩽7.8 ppm; **Figure 2-3A-C**).

The degradation rate of P(EG)$_x$MA-AZ-R3 copolymers were dependent on the PEG MW. P(EG)$_{8-9}$MA-AZ-R3 degraded immediately due to its higher solubility (LCST > 65 °C; **Figure 2-3D**). In contrast, P(EG)$_{4-5}$MA-AZ-R3 exhibited a lag phase (~0.6 h) with no detectable degradation followed by a degradation rate similar to P(EG)$_{8-9}$MA-AZ-R3 (slopes of 0.33 and 0.35, respectively; **Figure 2-3D**). The biphasic degradation profile of P(EG)$_{4-5}$MA-AZ-R3 is a function of polymer solubility over time; the cleavage of hydrophobic 4-chlorophenyl sulfone increases P(EG)$_{4-5}$MA-AZ-R3 solubility. Only minor P(EG)$_3$MA-AZ-R3 degradation was observed over the 3 h time period (**Figure 2-3A,D**) because of its lower solubility at 37 °C, which is supported by LCST data (**Figure 2-3E** and Figure S 22A). From P(EG)$_{4-5}$MA-AZ-R3 data, we can conclude that PEG MW mainly influences initial degradation rates.

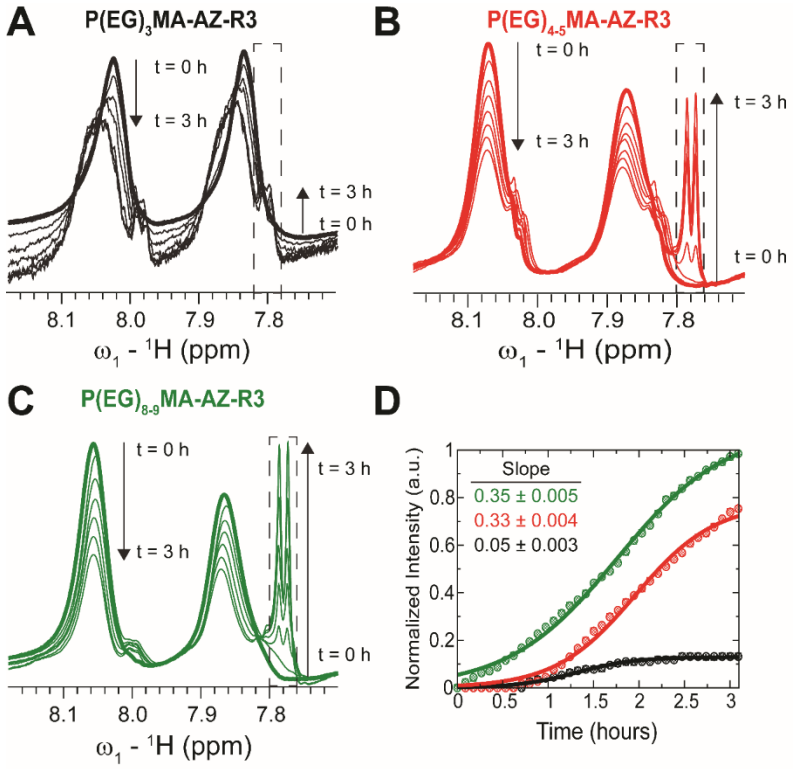

Figure 2-3. ^{1}H NMR kinetic analysis of P(EG)$_x$MA-AZ-R3 copolymer crosslinker degradation at pH 9.3 and 37°C. A) Upon base-catalysed degradation, 4-chlorophenyl sulfone is cleaved from the polymer resulting in the loss in signal intensity between 7.8-8.1 (two broad peaks) and appearance of a sharp doublet ($\leqslant$ 7.8 ppm, dashed box). The rate of **(A)** P(EG)$_3$MA-AZ-R3, **(B)** P(EG)$_{4\text{-}5}$MA-AZ-R3, and **(C)** P(EG)$_{8\text{-}9}$MA-AZ-R3 degradation was followed over 3 h. **(D)** Degradation profiles as probed by changes in intensity of 4-chlorophenyl sulfone's aromatic protons. All intensities were normalized to the intensity of the P(EG)$_{8\text{-}9}$MA decomposition signature peak (dashed box) at the end of the 3 h period. Slopes were determined by linear regression of the normalized intensities; slopes were computed from 0 to 1 h for P(EG)$_{8\text{-}9}$-AZ-R3 and from ~0.6 to 1.6 h for P(EG)$_3$MA-AZ-R3 and P(EG)$_{4\text{-}5}$MA-AZ-R3.

2.4.3 Cytotoxicity of P(EG)$_x$MA copolymers

All P(EG)$_x$MA copolymers were non-cytotoxic according to NIH 3T3 fibroblast cell viability assays (**Figure 2-4**). Cells were cultured in DMEM/F12 media with 10% calf bovine serum (CBS) in the presence of 1 mg mL^{-1} of a single copolymer. After 24 h, cell viability was determined using the PrestoBlue assay and compared to cells cultured without polymer (positive

control). All copolymer conditions were indistinguishable from the positive control, indicating copolymers are non-cytotoxic and suitable for hydrogel fabrication.

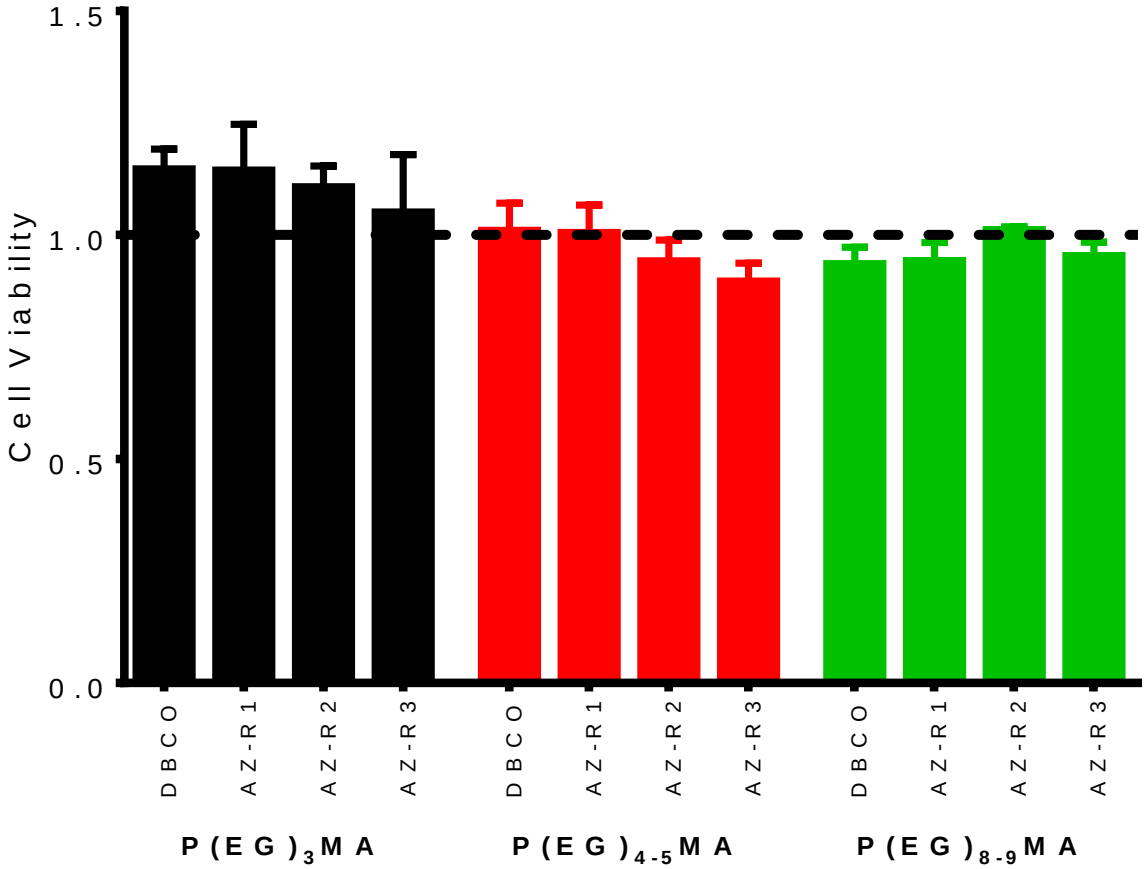

Figure 2-4. P(EG)$_x$MA copolymers are non-cytotoxic. NIH 3T3 fibroblasts were cultured in the presence of 1 mg mL^{-1} copolymer solutions for 24 h. Cell activity was measured by PrestoBlue assay fluorescence (λ_{ex} = 560 nm, λ_{em} = 590nm) and normalized to cells cultured in the absence of copolymers (positive control, dashed line). No significant difference ($p < 0.05$) from the positive control (dashed line) was observed between all copolymer conditions and the positive control (error bars represent mean + standard deviation, n = 3).

2.4.4 Hydrogel formation and characterization

Non-degradable P(EG)$_x$MA-AZ copolymers were mixed with corresponding P(EG)$_x$MA-DBCO copolymers for in situ gelation and characterization of hydrogel crosslink density, swelling and protein fouling. Hydrogels were prepared by mixing equal volumes of corresponding azide and DBCO copolymer solutions (5 wt.% in PBS) for strain-promoted alkyne-azide cycloaddition

(SPAAC) crosslinking, and gelation times were determined by gravitational flow analysis (**Figure 2-5A**); gelation time increased with larger PEGs, which limits crosslinking rates due to sterics.[22]

To study the influence of polymer hydration (PEG MW) on hydrogel degradation, all $P(EG)_xMA$ hydrogels ($P(EG)_3MA$, $P(EG)_{4-5}MA$, and $P(EG)_{8-9}MA$) required similar crosslink densities. The density of hydrogel crosslinks (μmol per g of polymer) was determined by quantifying DBCO consumption after SPAAC crosslinking (**Table 2-2**); unreacted DBCO absorbs light at 309 nm with an extinction coefficient of 12000 M^{-1} cm^{-1}.[140] To achieve $P(EG)_xMA$ hydrogels with similar crosslink densities, copolymer precursors with different AZ and DBCO mole fractions were required due to unique crosslinking kinetics. $P(EG)_3MA$, $P(EG)_{4-5}MA$, and $P(EG)_{8-9}MA$ required crosslinker mole fractions of 2, 5, and 10 mol%, respectively, to yield hydrogels with similar crosslink densities (47 - 52 μmol of crosslinks per g of polymer). Crosslink densities were determined by measuring unreacted DBCO concentrations (absorbance at 309 nm) after an overnight incubation to ensure maximum crosslinking. To calculate hydrogel background absorbance, all gels were subsequently exposed to excess sodium azide to consume remaining DBCOs[141].

To compare hydration of $P(EG)_xMA$ hydrogels, hydrogel cloud points and swelling ratios were determined. The cloud points of non-degradable (R1) and degradable (R2, **Figure 2-5B** and Figure S 23A – B) $P(EG)_3MA$ and $P(EG)_{4-5}MA$ hydrogels were similar to their corresponding $P(EG)_xMA$-AZ and $P(EG)_xMA$-DBCO copolymers; $P(EG)_3MA$ and $P(EG)_{4-5}MA$ hydrogels had cloud points of 36 and 54 °C, respectively. As expected from $P(EG)_{8-9}MA$ copolymer LCSTs, $P(EG)_{8-9}MA$ gels did not exhibit a cloud point (Figure S 23C). In agreement with hydrogel cloud points, the equilibrium swelling ratio of $P(EG)_xMA$ hydrogels increased with greater PEG MW

(**Figure 2-5C**). P(EG)$_3$MA gels incubated at 37 °C shrunk by expelling ~40% of their initial water content, due to the promotion of polymer-polymer interactions at temperatures near its cloud point (36 °C). P(EG)$_{4-5}$MA (cloud point 54 °C) and P(EG)$_{8-9}$MA hydrogels swelled to ~160 and 200%, respectively, of their initial wet weight.

To ensure P(EG)$_x$MA retained their low-fouling properties, we quantified the non-specific adsorption of fluorescent BSA to hydrogel surfaces. Non-degradable hydrogels were incubated in 0.5 mg mL^{-1} fluorescent BSA solutions for 2 h and rinsed with PBS. Adsorbed fluorescent BSA was extracted from the hydrogels with a sodium dodecyl sulfate (SDS) solution for quantification.[28] All gels bound between 5 and 10 μg cm^{-2} of fluorescent BSA, similar to other low-fouling hydrogels[28] (**Figure 2-5D**). PCBMAA hydrogels with 6 mol% AZ/DBCO content and PCBMAA gels with 0.5 wt.% methylcellulose (PCBMAA-MC) were included as controls; PCBMAA gels remain non-fouling with AZ/DBCO content below 10 mol%[88] and PCBMAA-MC gels non-specifically absorbed BSA due to MC hydrophobic interactions. PCBMAA and PCBMAA-MC non-specifically bound ~5 and 60 μg cm^{-2} of BSA, respectively. Therefore, all P(EG)$_x$MA gels remained non-fouling towards BSA.

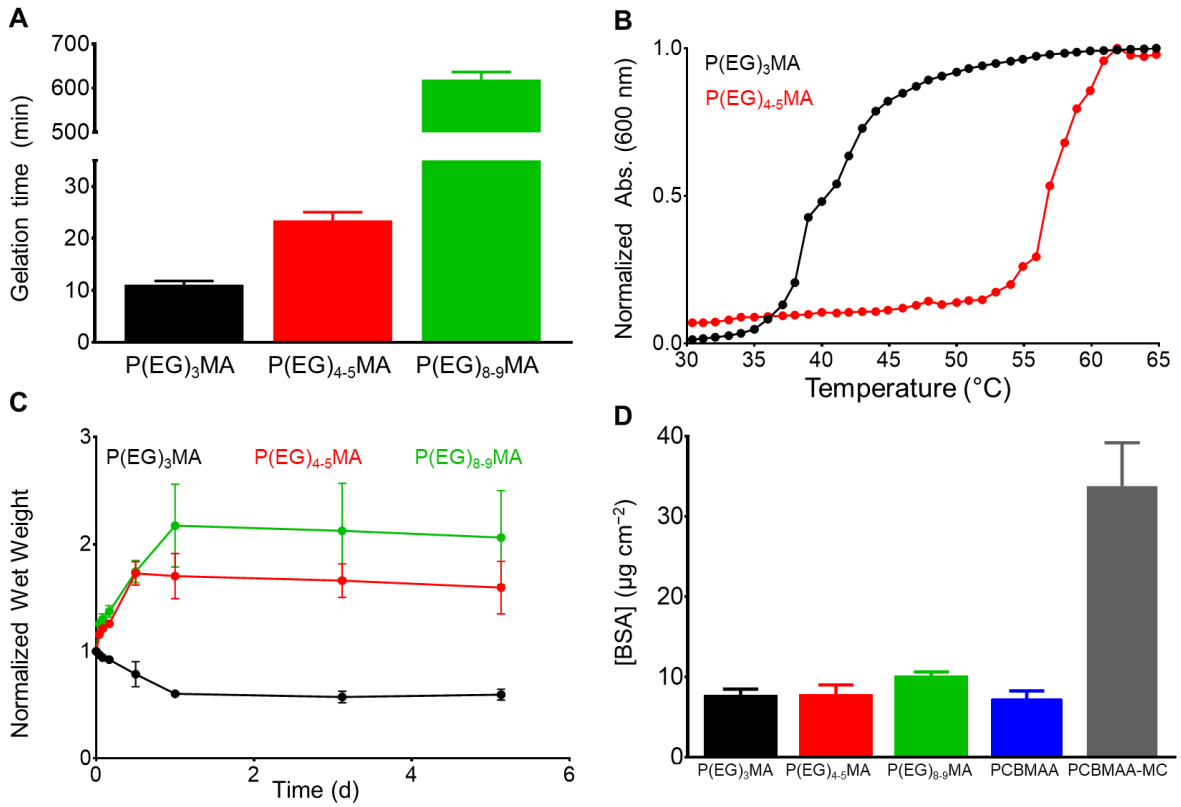

Figure 2-5. Characterization of non-degradable P(EG)$_x$MA hydrogels: gelation time, hydration, and protein fouling. A) Hydrogel (5 wt.%) gelation time, determined by gravitational flow analysis (mean + standard deviation, n = 6). **B)** Cloud point of P(EG)$_3$MA and P(EG)$_{4\text{-}5}$MA nondegradable hydrogels (5 wt.% in PBS) defined as the onset of turbidity (600 nm). No cloud point was observed for P(EG)$_{8\text{-}9}$MA hydrogels. **C)** Equilibrium swelling of non-degradable hydrogels (5 wt.%). After overnight gelation, hydrogels were submerged in PBS and their wet weight was determined at specified time points (mean ± standard deviation, n =3). **D)** Adsorbed fluorescent BSA (μg cm^{-2}) on hydrogel surfaces compared to low-fouling PCBMAA (6 mol% AZ/DBCO) and fouling PCBMAA-MC hydrogels (mean + standard deviation, n =3).

Table 2-2. Hydrogel crosslink density.

Hydrogel (5 wt.%)	μmol crosslinks/ g polymer*
P(EG)$_3$MA	52
P(EG)$_{4\text{-}5}$MA	47
P(EG)$_{8\text{-}9}$MA	48

*Determined 22 h after copolymer mixing by DBCO absorbance (309 nm).

2.4.5 Tunable degradation of P(EG)$_x$MA hydrogels

By developing a library of P(EG)$_x$MA-AZ and P(EG)$_x$MA-DBCO copolymers with R2 and R3 crosslinkers, we were able to easily achieve hydrogel degradation over 6 to 52 d (**Figure 2-6**). Degradation rates were controlled by polymer hydration (P(EG)$_3$MA, P(EG)$_{4-5}$MA, and P(EG)$_{8-9}$MA) and the acidity of the crosslinker's β-hydrogen by exchanging EWG groups (4-methylphenyl sulfone or 4-chlorophenyl sulfone). Because PEG MW influenced degradation rates (**Figure 2-3**), each crosslinker (R2 or R3) yielded three different hydrogel degradation profiles. Hydrogels with higher PEG MWs degraded faster due to greater polymer solvation and initial degradation rates, as demonstrated by hydrogel swelling (**Figure 2-5C**) and ^{1}H NMR kinetic studies (**Figure 2-3**). For example, P(EG)$_3$MA-R3, P(EG)$_{4-5}$MA-R3 and P(EG)$_{8-9}$MA-R3 gels degraded over 52, 13 and 6 d, respectively (**Figure 2-6**). As expected, P(EG)$_x$MA hydrogels degraded faster with crosslinks containing the stronger EWG (4-chlorophenyl sulfone, R3).

P(EG)$_3$MA hydrogels, which shrunk over time (**Figure 2-5C**), produced the slowest degradation profiles (**Figure 2-6A and D**). P(EG)$_3$MA-R3 gels degraded over 52 d, 4-fold slower than P(EG)$_{4-5}$MA-R3 gels. Therefore, PEG MW has a significant impact on hydrogel degradation timeframes. Interestingly, P(EG)$_3$MA-R2 gels remained intact for >120 d. We expect P(EG)$_3$MA-R2 gels to eventually degrade because P(EG)$_3$MA-R3 gels degraded, which indicates that crosslink deprotonation and cleavage occur in P(EG)$_3$MA gels. Therefore, the design of P(EG)$_3$MA gels that degrade over 6 to >120 d may be possible using the developed copolymer library. Because P(EG)$_3$MA-R3 and P(EG)$_{4-5}$MA-R2 gels both degraded over 52 d, low-fouling P(EG)$_X$MA hydrogels can be tuned to degrade over 6, 13, 31 or 52 d from a library of 6 P(EG)$_x$MA copolymers: 1) P(EG)$_{4-5}$MA-AZ-R2; 2) P(EG)$_{4-5}$MA-AZ-R3; 3) P(EG)$_{4-5}$MA-DBCO; 4) P(EG)$_{8-9}$MA-AZ-R2; 5) P(EG)$_{8-9}$MA-AZ-R3; and, 6) P(EG)$_{8-9}$MA-DBCO.

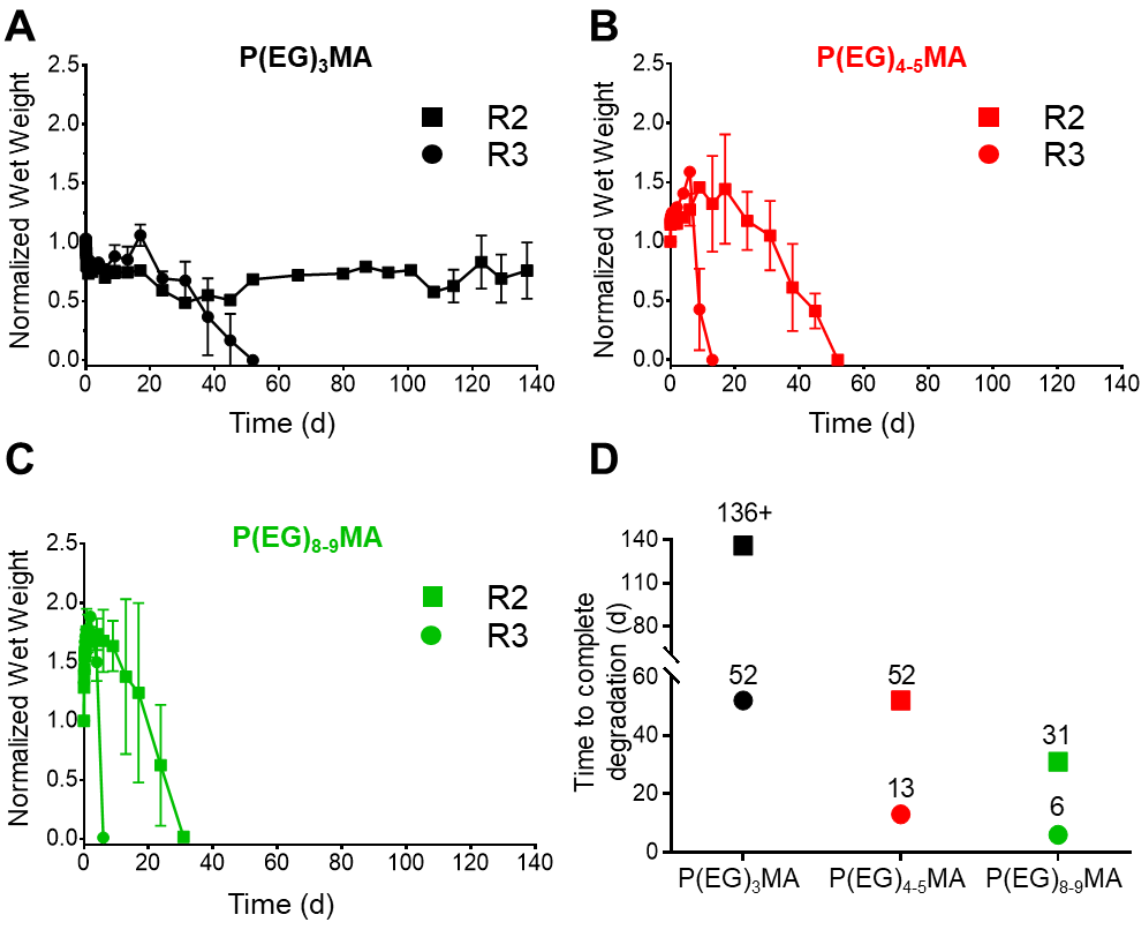

Figure 2-6. Tunable degradation of P(EG)$_x$MA hydrogels at pH 7.4. The combination of different P(EG)$_x$MA copolymers with R2 or R3 crosslinkers yields low-fouling hydrogels that degrade over 6 to 52 d. The degradation of **A)** P(EG)$_3$MA **B)** P(EG)$_{4\text{-}5}$MA and **C)** P(EG)$_{8\text{-}9}$MA hydrogels (100 µL,5 wt.%) with R2 (methylphenyl sulfone) or R3 (4-chlorophenyl sulfone) crosslinkers was followed over time in pH 7.4 PBS at 37°C (mean ± standard deviation, n =3). **D)** Illustration summarizing time required for complete degradation of each hydrogel.

2.4.6 P(EG)$_x$MA hydrogels are non-cell adhesive

Non-specific binding of cells to hydrogels can impede drug and cell delivery. To demonstrate P(EG)$_x$MA gels are resistant to non-specific cell adhesion, non-degradable P(EG)$_X$MA gels were exposed to fibroblasts in 10% CBS in DMEM/F12 media. After 24 h, gel surfaces were gently washed with PBS to remove non-adhered cells. After staining with Calcein AM and Hoechst, micrographs of cells on gel surfaces were collected. No adhered cells were detected on any

P(EG)$_x$MA gel (**Figure 2-7A**), indicating the gels are low-fouling towards cells. PCBMAA gels formed through in situ PCBMAA-AZ and PCBMAA-DBCO (6 mol% AZ/DBCO) crosslinking were included as controls; PCBMAA gels are known to resist non-specific cell binding[88] (**Figure 2-7A**).

P(EG)$_x$MA gels modified with RGD cell adhesion peptides demonstrated limited cell adhesion, indicating P(EG)$_x$MA gels also hindered integrin mediated adhesion. Excess DBCO groups in P(EG)$_x$MA gels were modified with an RGD-AZ peptide; the reaction was monitored by decreasing DBCO absorbance (309 nm; data not shown). Fibroblasts were seeded on hydrogel surfaces and incubated for 24 h. Cells were then stained with Calcein AM and Hoechst gels, gently washed with PBS to remove non-adhered cells, and gel surfaces were imaged. Only small cell clusters were observed on RGD modified P(EG)$_x$MA gels, indicating weak RGD mediated cell-hydrogel interactions (**Figure 2-7B**). In contrast, cells adhered to RGD modified PCBMAA gels (**Figure 2-7B**) with morphologies similar to cells on tissue culture plastic (TCP; Figure S 24). PCBMAA polymers are known to promote protein-ligand interactions[90], whereas the PEG pendant groups in P(EG)$_x$MA may hinder protein-ligand complexation; PEG polymers are known to decrease enzymatic activity[90]. Because all hydrogels contained a large excess of DBCO groups (>100 nmol cm^{-2} on the surface) for RGD immobilization, all hydrogel surfaces had sufficient RGD for cell adhesion (>1 fmol cm^{-2}).[142] Therefore, P(EG)$_x$MA gels are ideal for applications that require minimal protein and cell binding.

For some stem cell delivery applications, degradable hydrogels functionalized with adhesive peptide have been shown to improve cell survival.[91] Therefore, we incorporated the two crosslinkers (R2 and R3) into PCBMAA hydrogels (Scheme S 1), which degraded over 13 and 52 d (Figure S 25C). Due to the high solubility of PCBMAA copolymers, the rate of PCBMAA

hydrogel degradation was expected to be similar to P(EG)$_{8-9}$MA gels, which degraded over 6 and 31 d. The slower degradation rate was attributed to PCBMAA's greater crosslink density than P(EG)$_{8-9}$MA gels (128 vs 48 µmol g of polymer). Therefore, the PCBMAA hydrogel can be used for short- and long-term applications that require bioactive hydrogels.

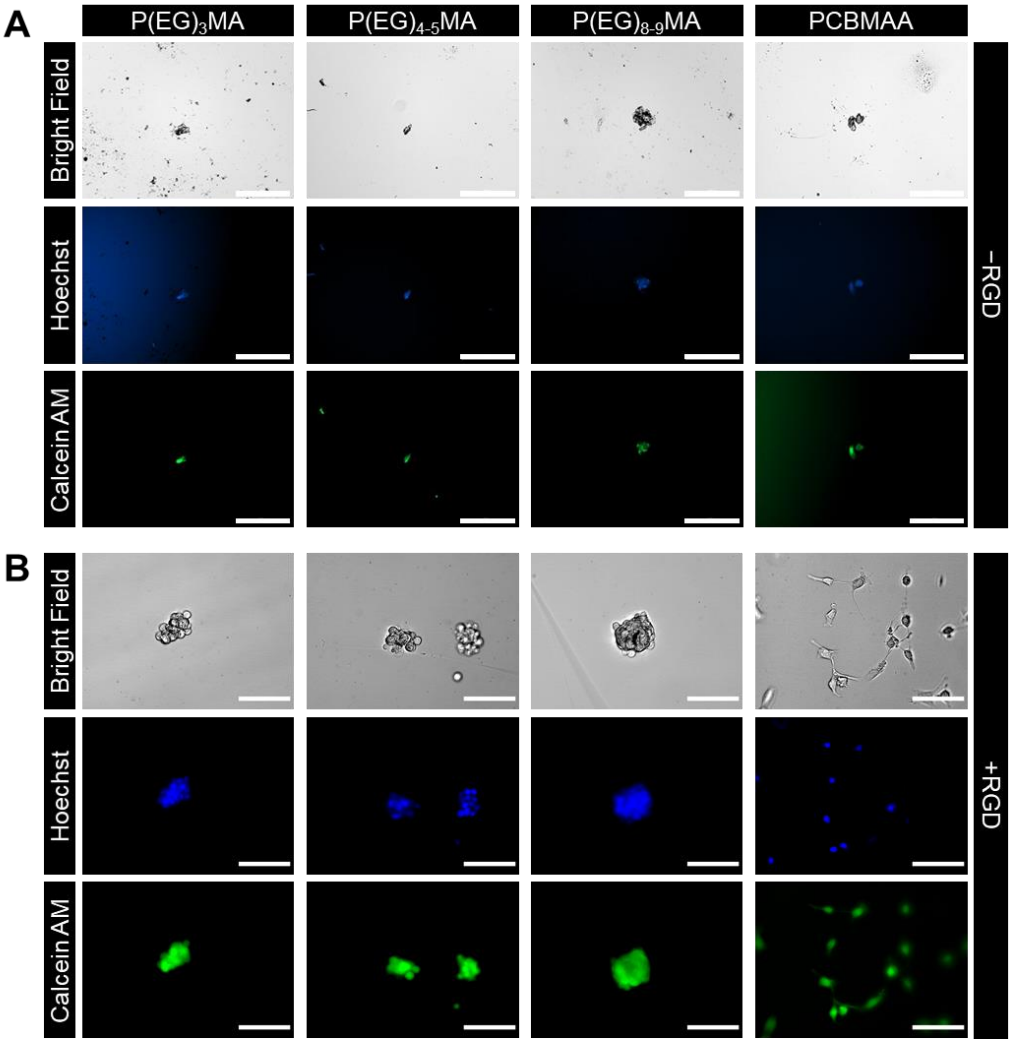

Figure 2-7. Cell adhesion to P(EG)$_x$MA and PCBMAA hydrogels with and without immobilized RGD. Fibroblasts were seeded on hydrogel surfaces, incubated for 24 h, and washed to remove non-adhered cells prior to staining with Calcein AM and Hoescht. **A)** No cell adhesion observed on P(EG)$_x$MA and PCBMAA hydrogel surfaces without RGD. Scale bars are 200 µm. **B)** Few cell clusters observed on the surface of RGD modified P(EG)$_x$MA hydrogels. In contrast, cell attachment and spreading observed on the surface of RGD modified PCBMAA hydrogels similar to TCP control (Figure S 24). Scale bars are 100 µm. Micrographs are representative samples of three independent replicates.

3 Discussion

The developed degradation mechanism for low-fouling P(EG)$_x$MA hydrogels tunes the deprotonation rate of the carbamate crosslinker, independently from endogenous triggers, by changing adjacent EWGs and PEG pendant group MW, which provides a method to reliably achieve different hydrogel degradation timeframes. The linkers have been incorporated into low-fouling SPAAC-crosslinked P(EG)$_x$MA and PCBMAA hydrogels in this study, demonstrating their synthetic versatility with potential to be incorporated into other SPAAC-crosslinked hydrogels as well. Copolymers containing amine groups, which can readily be incorporated using amine-containing monomers via RAFT polymerization,[143–146] can react with degradable NHS-AZ molecules for SPAAC crosslinking. Hence, the β-eliminative linkers could be incorporated into other SPAAC-crosslinked hydrogels through reaction of amine with NHS-AZs.

The EWGs investigated only represent a subset of possible EWGs known to tune carbamate degradation. In the current study, hydrogels contained 4-methylphenyl sulfone and 4-chlorophenyl sulfone EWGs with linker half-lives of 36 and 150 h, respectively.[123] Weaker EWGs, which significantly prolong hydrogel degradation, have yet to be investigated. For example, the weakest EWG previously reported (–CN) can prolong hydrogel degradation ~70× that of the 4-chlorophenyl sulfone EWG.[32] Furthermore, depending on the local acidity of the delivery site the hydrogel lifetime could be further extended, as the pH has a near linear dependence on degradation rate. For example, the tumor microenvironment is often more acidic (pH ~ 5.7)[147] than its surrounding environment. Thus, the hydrogel degradation times presented here are a lower bound of possible degradation times with much room to extend hydrogel degradation (e.g. >1 year) simply by reducing the strength of the EWG.

The P(EG)$_x$MA hydrogels displayed several characteristics that can help mitigate deleterious in vivo responses. SPAAC crosslinking, used to form hydrogels, is non-cytotoxic.[148] For cell delivery applications, we demonstrated that encapsulated fibroblasts in P(EG)$_x$MA gels retained high viability (Figure S 26). Once degraded, all components, except for released CO_2, remain covalently bound to degraded non-cytotoxic copolymers. Moreover, all degradation timeframes (6, 13, 31, and 52 d) can be achieved from highly soluble P(EG)$_{4\text{-}5}$MA and P(EG)$_{8\text{-}9}$MA copolymers (LCSTs > physiological temperature) that will remain soluble after hydrogel degradation and can be renally excreted (PEG <50 kDa can be renally excreted),[92] further improving biocompatibility. Therefore, we expect minimal in vivo toxicity for future applications.

For cell applications, hydrogels were functionalized with RGD, which improves encapsulated cell survival and function.[130] RGD-functionalized P(EG)$_x$MA hydrogels could not, however, be made bioactive while RGD-functionalized PCBMAA could. This is due to steric hindrance caused by pendant PEG chains, which is a common issue with PEG-based materials. PEG chains not only sterically hinder PEGylation of drugs,[149] but also sterically hinder drug-protein interactions of these PEGylated therapeutics.[74,90,150] Moreover, PEG linkers have been shown to sterically block integrin binding in bioactive hydrogels.[151–153] For example, endothelial cells showed decreased adhesion to a collagen mimetic peptide incorporated into PEG hydrogels when PEG linkers on the peptide were at high density[151] or in close proximity to the integrin binding domain.[153] Specifically for RGD-functionalized P(EG)$_x$MA hydrogels, fibroblast adhesion did not occur after 24 h incubation.[29] Therefore, it is plausible that the lack of fibroblast adhesion to P(EG)$_x$MA hydrogels in this study is due to the steric hindrance caused by PEG side chains. Furthermore, unlike PCBMAA, which promotes protein-ligand interactions, the

amphiphilicity of PEG chains reduce binding affinity by reducing the hydrophobic-hydrophobic driving force of substrate binding.[90] To improve the ability of P(EG)$_x$MA hydrogels to selectively adhere cells, a spacer could be introduced to distance the cell binding moiety from PEG side chains in the polymer backbone. Studies on RGD-modified alginate[154] and PEG[130] hydrogels indicate that by adding glycine spacers (e.g. CGGGGGGGGRGDSG)[130] the RGD moiety can be extended out from the material surface decreasing the steric hindrance of integrin-ligand interaction.[130,154]

The degradation rate of P(EG)xMA gels will influence both drug and cell delivery. For the developed P(EG)$_x$MA gels, cells seeded on the surface of RGD modified hydrogels did not migrate into the gel, indicating hydrogel pore sizes are sub-micron and prevent cell migration. Therefore, the degradation rate of the P(EG)$_x$MA gels will be the main determinant for cell delivery rates. However, hydrogel degradation will not be required for drug efflux because P(EG)$_x$MA gels with similar and higher crosslink densities have previously been demonstrated to release proteins for drug delivery applications.[155] Although, faster degradation rates will increase rates of drug release.

Controlled degradation of hydrogels is important for drug and cell delivery. For example, the sustained release of antibody checkpoint inhibitors for ~1 week from degradable poly(vinyl alcohol) hydrogels improved survival in a melanoma mouse model by 50% over intravenous injections.[156] Adoptive cell therapies are improved by creating a local cell depot with injectable hydrogels that degrade to allow for cell egress. Hydrogels have been shown to improve transplantation efficiency of neural stem cells[157] and T cell infiltration[34] into tumors for cancer immunotherapies. The ability to control hydrogel degradation will improve adoptive cell therapies by controlling the rate of cell egress from the hydrogel into surrounding tissue. To

avoid unwanted adverse events (e.g. FBR), low-fouling hydrogels that degrade over several days to weeks are required, such as those developed here.

4 Conclusion

The developed 6-member P(EG)$_x$MA copolymer library allows for the rapid fabrication of low-fouling hydrogels that degrade over 6 to 52 d, which will be useful for short- and long-term drug and cell delivery applications. Furthermore, P(EG)$_3$MA-R2 may result in hydrogels that degrade over >130 d. The combination of tunable base-catalyzed crosslink degradation and P(EG)$_x$MA hydration provides a simple method to rapidly tune degradation rates. Given that the non-cytotoxic P(EG)$_x$MA gels remained low-fouling towards proteins and cells, it is expected that they will help mitigate adverse immune responses (e.g. FBR) upon implantation. Interestingly, P(EG)$_x$MA gels modified with RGD remained non-cell adhesive by preventing integrin mediated adhesion. However, PCBMAA gels modified with RGD were cell adhesive. Thus, the establishment of a low-fouling P(EG)$_x$MA hydrogel library to easily achieve different degradation timeframes will expedite the establishment of drug delivery whereas PCBMAA hydrogels could be used for cell delivery therapies.

5 Recommendations for future work

5.1 Prolonging hydrogel degradation

For chronic diseases or those requiring lifetime treatment, hydrogel lifetime may need to be extended. To further broaden the range of degradation times accessible, the local hydration of degradable carbamate linkers or the crosslink density of hydrogels could be modified to expand the library of polymers developed in this study.

5.1.1 Changing local crosslink hydration

Polymer hydration affected the rate of hydrogel degradation and was dependent on the length of PEG pendant groups. The P(EG)$_x$MA hydrogels in this study were formed from copolymers containing only a single PEG side chain length. However, incorporating (EG)$_x$MA monomers with different PEG pendant group MW at varying ratios into a single copolymer (i.e. making a terpolymer) could be used to further fine tune hydration-dependent degradation; varying the ratio of (EG)$_2$MA to (EG)$_{8\text{-}9}$MA monomers can produce copolymers with LCSTs between that of their respective HPs.[138,158] For example, combining the strategy of using weaker EWGs with varying the ratio of (EG)$_x$MA monomers could be used to form hydrogels that degrade within 2 – 4 months. Specifically, the methylsulfone EWG could be used, which degrades over 10× slower than the 4-chlorophenyl sulfone EWG,[32] to form P(EG)$_{8\text{-}9}$MA and P(EG)$_{4\text{-}5}$MA hydrogels that would degrade in 60 or 130 d, respectively, assuming similar crosslink density. Then to achieve intermediate hydrogel degradation times (i.e. between 60 – 130 d), a terpolymer of APMA, (EG)$_{4\text{-}5}$MA, and (EG)$_{8\text{-}9}$MA could be made at desired ratios to fine tune polymer hydration. Therefore, by modifying the ratio of (EG)$_x$MA monomers with different PEG side chain lengths, the degradation of P(EG)$_x$MA hydrogels could be precisely tuned to achieve intermediate hydrogel degradation times.

5.1.2 Crosslink density

An important feature of the β-eliminative linkers used here is that they allow control of hydrogel degradation without changing crosslink density, which impacts not only degradation but other hydrogel properties important for drug and cell delivery (i.e. mesh size, mechanical properties, and fouling of hydrogels).[40,159] However, for some applications, greater crosslink densities may be required to control mesh size, dictating drug release, or increase hydrogel stiffness to match that of desired tissues.[40] Therefore, crosslink density is important to tailor hydrogel degradation for different applications.

Based on previous studies, the crosslink density of $P(EG)_xMA$ hydrogels may be increased but there may be more restriction of doing so for PCBMAA hydrogels due to electrostatic interactions between zwitterionic groups. Injectable hydrazone-crosslinked $P(EG)_xMA$ hydrogels with over 20 mol% crosslinker have shown minimal inflammation in vivo.[22] Thus, there is potential to increase the crosslinker mol% to prolong degradation of SPAAC-crosslinked $P(EG)_xMA$ hydrogels used in this study. For PCBMAA hydrogels however, increased crosslinking may increase fouling. Lightly crosslinked PCBMA hydrogels (0.1%) showed less fibrinogen adsorption than highly crosslinked ones (10%).[159] Furthermore, there is an upper limit to the crosslink density of PCBMAA hydrogels while maintaining their low-fouling character. At higher crosslink density, electrostatic associations of zwitterionic groups in proximity causes hydrogel deswelling and increased nonspecific adsorption of BSA and cells; PCBMAA hydrogels (10 wt.%) with 11 mol% crosslinker led to noticeable cell fouling.[88] Therefore, it is

important to investigate the extent to which hydrogel crosslink density can be increased while maintaining low-fouling characteristics for long-term delivery applications.

5.2 FBR to P(EG)$_x$MA and PCBMAA hydrogels

With the goal of in vivo applications, more challenging fouling conditions should be screened in vitro. Media containing more than one protein (e.g. serum) would give a better indication of the ability of hydrogels to resist non-specific protein adsorption in vivo. Moreover, as macrophages are necessary for the FBR,[68] macrophage adhesion to hydrogels should be determined to provide better indication of their ability to resist the FBR in vivo. If in vitro results are promising, hydrogels should be implanted in immunocompetent mice (e.g. C57BL/6), which produce FBRs like those observed in humans,[64] to test the ability of the hydrogels to resist collagenous encapsulation.

6 References

1. Norouzi, M., Nazari, B. & Miller, D. W. Injectable hydrogel-based drug delivery systems for local cancer therapy. *Drug Discov. Today* **21**, 1835–1849 (2016).
2. Wolinsky, J. B., Colson, Y. L. & Grinstaff, M. W. Local drug delivery strategies for cancer treatment: Gels, nanoparticles, polymeric films, rods, and wafers. *J. Control. Release* **159**, 14–26 (2012).
3. Li, K. W. *et al.* Polilactofate microspheres for paclitaxel delivery to central nervous system malignancies. *Clin. Cancer Res.* **9**, 3441–3447 (2003).
4. Nastruzzi, C. & Gambari, R. Advancing the field of drug delivery:Taking aim at cancer. *Cancer Cell* **4**, 337–341 (2003).
5. Parisi-Amon, A., Mulyasasmita, W., Chung, C. & Heilshorn, S. C. Protein-Engineered Injectable Hydrogel to Improve Retention of Transplanted Adipose-Derived Stem Cells. *Adv. Healthc. Mater.* **2**, 428–432 (2013).
6. Roche, E. T. *et al.* Comparison of biomaterial delivery vehicles for improving acute retention of stem cells in the infarcted heart. *Biomaterials* **35**, 6850–6858 (2014).
7. Levit, R. D. *et al.* Cellular encapsulation enhances cardiac repair. *J. Am. Heart Assoc.* **2**, (2013).
8. Lam, J., Lowry, W. E., Carmichael, S. T. & Segura, T. Delivery of iPS-NPCs to the stroke cavity within a hyaluronic acid matrix promotes the differentiation of transplanted cells. *Adv. Funct. Mater.* **24**, 7053–7062 (2014).
9. Aguado, B. A., Mulyasasmita, W., Su, J., Lampe, K. J. & Heilshorn, S. C. Improving viability of stem cells during syringe needle flow through the design of hydrogel cell carriers. *Tissue Eng. Part A* **18**, 806–15 (2012).
10. Su, J., Hu, B. H., Lowe, W. L., Kaufman, D. B. & Messersmith, P. B. Anti-inflammatory peptide-functionalized hydrogels for insulin-secreting cell encapsulation. *Biomaterials* **31**, 308–314 (2010).
11. Guvendiren, M. & Burdick, J. A. Engineering synthetic hydrogel microenvironments to instruct stem cells. *Curr. Opin. Biotechnol.* **24**, 841–846 (2013).
12. Huang, X. & Brazel, C. S. On the importance and mechanisms of burst release in matrix-controlled drug delivery systems. *J. Control. Release* **73**, 121–136 (2001).
13. Engler, A. J., Sen, S., Sweeney, H. L. & Discher, D. E. Matrix elasticity directs stem cell lineage specification. *Cell* **126**, 677–89 (2006).
14. Shin, J. W. & Mooney, D. J. Improving Stem Cell Therapeutics with Mechanobiology. *Cell Stem Cell* **18**, 16–19 (2016).
15. Alsberg, E. *et al.* Regulating Bone Formation via Controlled Scaffold Degradation. *J. Dent. Res.* **82**, 903–908 (2003).
16. Stevens, K. R., Miller, J. S., Blakely, B. L., Chen, C. S. & Bhatia, S. N. Degradable hydrogels derived from PEG-diacrylamide for hepatic tissue engineering. *J. Biomed. Mater. Res. - Part A* **103**, 3331–3338 (2015).
17. Swartzlander, M. D. *et al.* Linking the foreign body response and protein adsorption to PEG-based hydrogels using proteomics. *Biomaterials* **41**, 26–36 (2015).
18. Anderson, J. M., Rodriguez, A. & Chang, D. T. Foreign body reaction to biomaterials. *Semin. Immunol.* **20**, 86–100 (2008).
19. Klopfleisch, R. & Jung, F. The pathology of the foreign body reaction against

biomaterials. *J. Biomed. Mater. Res. - Part A* **105**, 927–940 (2017).
20. Chen, W., Yung, B. C., Qian, Z. & Chen, X. Improving long-term subcutaneous drug delivery by regulating material-bioenvironment interaction. *Adv. Drug Deliv. Rev.* **127**, 20–34 (2018).
21. Leng, C., Sun, S., Zhang, K., Jiang, S. & Chen, Z. Molecular level studies on interfacial hydration of zwitterionic and other antifouling polymers in situ. *Acta Biomater.* **40**, 6–15 (2016).
22. Smeets, N. M. B., Bakaic, E., Patenaude, M. & Hoare, T. Injectable poly(oligoethylene glycol methacrylate)-based hydrogels with tunable phase transition behaviours: Physicochemical and biological responses. *Acta Biomater.* **10**, 4143–4155 (2014).
23. Zhang, L. *et al.* Zwitterionic hydrogels implanted in mice resist the foreign-body reaction. *Nat. Biotechnol.* **31**, 553–556 (2013).
24. Zhang, L. *et al.* Multifunctional and degradable zwitterionic nanogels for targeted delivery, enhanced MR imaging, reduction-sensitive drug release, and renal clearance. *Biomaterials* **32**, 4604–4608 (2011).
25. Chien, H. W., Xu, X., Ella-Menye, J. R., Tsai, W. B. & Jiang, S. High viability of cells encapsulated in degradable poly(carboxybetaine) hydrogels. *Langmuir* **28**, 17778–17784 (2012).
26. Wu, H., Wang, H., Cheng, F., Xu, F. & Cheng, G. Synthesis and characterization of an enzyme-degradable zwitterionic dextran hydrogel. *RSC Adv.* **6**, 30862–30866 (2016).
27. Jain, P. *et al.* Zwitterionic Hydrogels Based on a Degradable Disulfide Carboxybetaine Cross-Linker. *Langmuir* **35**, 1864–1871 (2019).
28. Dong, D. *et al.* In Situ 'clickable' Zwitterionic Starch-Based Hydrogel for 3D Cell Encapsulation. *ACS Appl. Mater. Interfaces* **8**, 4442–4455 (2016).
29. Smeets, N. M. B., Bakaic, E., Patenaude, M. & Hoare, T. Injectable and tunable poly(ethylene glycol) analogue hydrogels based on poly(oligoethylene glycol methacrylate). *Chem. Commun.* **50**, 3306–3309 (2014).
30. Reid, B. *et al.* PEG hydrogel degradation and the role of the surrounding tissue environment. *J. Tissue Eng. Regen. Med.* **9**, 315–318 (2015).
31. Artzi, N. *et al.* In vivo and in vitro tracking of erosion in biodegradable materials using non-invasive fluorescence imaging. *Nat. Mater.* **10**, 704–709 (2011).
32. Ashley, G. W., Henise, J., Reid, R. & Santi, D. V. Hydrogel drug delivery system with predictable and tunable drug release and degradation rates. *Proc. Natl. Acad. Sci.* **110**, 2318–2323 (2013).
33. Bastiancich, C., Danhier, P., Préat, V. & Danhier, F. Anticancer drug-loaded hydrogels as drug delivery systems for the local treatment of glioblastoma. *J. Control. Release* **243**, 29–42 (2016).
34. Stephan, S. B. *et al.* Biopolymer implants enhance the efficacy of adoptive T-cell therapy. *Nat. Biotechnol.* **33**, 97–101 (2015).
35. Bharambe, S. V., Darekar, A. B. & Saudagar, R. B. Wound healing dressings and drug delivery systems: A review. *Int. J. Pharm. Technol.* **5**, 2764–2786 (2013).
36. Gerwin, N., Hops, C. & Lucke, A. Intraarticular drug delivery in osteoarthritis. *Adv. Drug Deliv. Rev.* **58**, 226–242 (2006).
37. Rai, M. F. & Pham, C. T. Intra-articular drug delivery systems for joint diseases. *Curr. Opin. Pharmacol.* **40**, 67–73 (2018).
38. Zhang, P. *et al.* Zwitterionic gel encapsulation promotes protein stability, enhances

pharmacokinetics, and reduces immunogenicity. *Proc. Natl. Acad. Sci.* **112**, 12046–12051 (2015).
39. Hoare, T. R. & Kohane, D. S. Hydrogels in drug delivery: Progress and challenges. *Polymer (Guildf).* **49**, 1993–2007 (2008).
40. Li, J. & Mooney, D. J. Designing hydrogels for controlled drug delivery. *Nat. Rev. Mater.* **1**, 16071 (2016).
41. Fu, A. S. & von Recum, H. A. Affinity-Based Drug Delivery. *Eng. Polym. Syst. Improv. Drug Deliv.* **9781118098**, 429–452 (2013).
42. Mann, B. K., Schmedlen, R. H. & West, J. L. Tethered-TGF-β increases extracellular matrix production of vascular smooth muscle cells. *Biomaterials* **22**, 439–444 (2001).
43. Shah, N. J. *et al.* Adaptive growth factor delivery from a polyelectrolyte coating promotes synergistic bone tissue repair and reconstruction. *Proc. Natl. Acad. Sci.* **111**, 12847–12852 (2014).
44. Mateen, R. & Hoare, T. Injectable, in situ gelling, cyclodextrin-dextran hydrogels for the partitioning-driven release of hydrophobic drugs. *J. Mater. Chem. B* **2**, 5157–5167 (2014).
45. Gao, W., Zhang, Y., Zhang, Q. & Zhang, L. Nanoparticle-Hydrogel: A Hybrid Biomaterial System for Localized Drug Delivery. *Ann. Biomed. Eng.* **44**, 2049–2061 (2016).
46. Calvert, P. Hydrogels for soft machines. *Adv. Mater.* **21**, 743–756 (2009).
47. Bodugoz-Senturk, H., Macias, C. E., Kung, J. H. & Muratoglu, O. K. Poly(vinyl alcohol)-acrylamide hydrogels as load-bearing cartilage substitute. *Biomaterials* **30**, 589–596 (2009).
48. Arakaki, K. *et al.* Artificial cartilage made from a novel double-network hydrogel: In vivo effects on the normal cartilage and ex vivo evaluation of the friction property. *J. Biomed. Mater. Res. - Part A* **93**, 1160–1168 (2010).
49. Li, J., Illeperuma, W. R. K., Suo, Z. & Vlassak, J. J. Hybrid hydrogels with extremely high stiffness and toughness. *ACS Macro Lett.* **3**, 520–523 (2014).
50. Yu, L. & Ding, J. Injectable hydrogels as unique biomedical materials. *Chem. Soc. Rev.* **37**, 1473–81 (2008).
51. Patenaude, M., Smeets, N. M. B. & Hoare, T. Designing injectable, covalently cross-linked hydrogels for biomedical applications. *Macromol. Rapid Commun.* **35**, 598–617 (2014).
52. Silva, E. A. & Mooney, D. J. Spatiotemporal control of vascular endothelial growth factor delivery from injectable hydrogels enhances angiogenesis. *J. Thromb. Haemost.* **5**, 590–598 (2007).
53. Hiemstra, C. *et al.* In vitro and in vivo protein delivery from in situ forming poly(ethylene glycol)-poly(lactide) hydrogels. *J. Control. Release* **119**, 320–327 (2007).
54. Harada, A., Li, J. & Kamachi, M. Double-stranded inclusion complexes of cyclodextrin threaded on poly(ethylene glycol). *Nature* **370**, 126–128 (1994).
55. Wei, H. L., Yang, Z., Zheng, L. M. & Shen, Y. M. Thermosensitive hydrogels synthesized by fast Diels-Alder reaction in water. *Polymer (Guildf).* **50**, 2836–2840 (2009).
56. Nimmo, C. M., Owen, S. C. & Shoichet, M. S. Diels-alder click cross-linked hyaluronic acid hydrogels for tissue engineering. *Biomacromolecules* **12**, 824–830 (2011).
57. Tan, H., Rubin, J. P. & Marra, K. G. Direct synthesis of biodegradable polysaccharide derivative hydrogels through aqueous Diels-Alder chemistry. *Macromol. Rapid Commun.* **32**, 905–911 (2011).

58. Luo, Y. *et al.* Injectable hyaluronic acid-dextran hydrogels and effects of implantation in ferret vocal fold. *J. Biomed. Mater. Res. - Part B Appl. Biomater.* **93**, 386–393 (2010).
59. Cao, Y. *et al.* Poly(N-isopropylacrylamide)-chitosan as thermosensitive in situ gel-forming system for ocular drug delivery. *J. Control. Release* **120**, 186–194 (2007).
60. Kim, D. Y. *et al.* Synergistic anti-tumor activity through combinational intratumoral injection of an in-situ injectable drug depot. *Biomaterials* **85**, 232–245 (2016).
61. Mather, B. D., Viswanathan, K., Miller, K. M. & Long, T. E. Michael addition reactions in macromolecular design for emerging technologies. *Prog. Polym. Sci.* **31**, 487–531 (2006).
62. Jin, R. *et al.* Synthesis and characterization of hyaluronic acid-poly(ethylene glycol) hydrogels via Michael addition: An injectable biomaterial for cartilage repair. *Acta Biomater.* **6**, 1968–1977 (2010).
63. Agard, N. J., Prescher, J. A. & Bertozzi, C. R. A Strain-Promoted [3 + 2] Azide-Alkyne Cycloaddition for Covalent Modification of Biomolecules in Living Systems. (2004). doi:10.1021/ja044996f
64. Vegas, A. J. *et al.* Combinatorial hydrogel library enables identification of materials that mitigate the foreign body response in primates. *Nat. Biotechnol.* **34**, 345–352 (2016).
65. Bochenek, M. A. *et al.* Alginate encapsulation as long-term immune protection of allogeneic pancreatic islet cells transplanted into the omental bursa of macaques. *Nat. Biomed. Eng.* **2**, 810–821 (2018).
66. Zhou, H.-X., Rivas, G. & Minton, A. P. Macromolecular crowding and confinement: biochemical, biophysical, and potential physiological consequences. *Annu. Rev. Biophys.* **37**, 375–97 (2008).
67. Anderson, J. M. & McNally, A. K. Biocompatibility of implants: Lymphocyte/macrophage interactions. *Semin. Immunopathol.* **33**, 221–233 (2011).
68. Doloo, J. C. *et al.* Colony stimulating factor-1 receptor is a central component of the foreign body response to biomaterial implants in rodents and non-human primates. (2017). doi:10.1038/NMAT4866
69. Franz, S., Rammelt, S., Scharnweber, D. & Simon, J. C. Immune responses to implants - A review of the implications for the design of immunomodulatory biomaterials. *Biomaterials* **32**, 6692–6709 (2011).
70. Grainger, D. W. All charged up about implanted biomaterials. *Nat. Biotechnol.* **31**, 507–509 (2013).
71. Lin, C. C. & Anseth, K. S. PEG hydrogels for the controlled release of biomolecules in regenerative medicine. *Pharm. Res.* **26**, 631–643 (2009).
72. Pelegri-Oday, E. M., Lin, E. W. & Maynard, H. D. Therapeutic protein-polymer conjugates: Advancing beyond pegylation. *J. Am. Chem. Soc.* **136**, 14323–14332 (2014).
73. Zhang, P., Sun, F., Liu, S. & Jiang, S. Anti-PEG antibodies in the clinic: Current issues and beyond PEGylation. *J. Control. Release* **244**, 184–193 (2016).
74. Qi, Y. *et al.* A brush-polymer/exendin-4 conjugate reduces blood glucose levels for up to five days and eliminates poly(ethylene glycol) antigenicity. *Nat. Biomed. Eng.* **1**, 0002 (2017).
75. Schöttler, S. *et al.* Protein adsorption is required for stealth effect of poly(ethylene glycol)- and poly(phosphoester)-coated nanocarriers. *Nat. Nanotechnol.* **11**, 372–377 (2016).
76. Lynn, A. D., Kyriakides, T. R. & Bryant, S. J. Characterization of the in vitro macrophage response and in vivo host response to poly(ethylene glycol)-based hydrogels. *J. Biomed.*

Mater. Res. - Part A **93**, 941–953 (2010).
77. Garay, R. P., El-Gewely, R., Armstrong, J. K., Garratty, G. & Richette, P. Antibodies against polyethylene glycol in healthy subjects and in patients treated with PEG-conjugated agents. *Expert Opin. Drug Deliv.* **9**, 1319–1323 (2012).
78. Yang, Q. & Lai, S. K. Anti-PEG immunity: Emergence, characteristics, and unaddressed questions. *Wiley Interdiscip. Rev. Nanomedicine Nanobiotechnology* **7**, 655–677 (2015).
79. Feng, W., Zhu, S., Ishihara, K. & Brash, J. L. Protein resistant surfaces: Comparison of acrylate graft polymers bearing oligo-ethylene oxide and phosphorylcholine side chains. *Biointerphases* **1**, 50–60 (2006).
80. Feng, W. *et al.* Methacrylate polymer layers bearing poly(ethylene oxide) and phosphorylcholine side chains as non-fouling surfaces: In vitro interactions with plasma proteins and platelets. *Acta Biomater.* **7**, 3692–3699 (2011).
81. Yeh, C. C., Venault, A. & Chang, Y. Structural effect of poly(ethylene glycol) segmental length on biofouling and hemocompatibility. *Polym. J.* **48**, 551–558 (2016).
82. Hodgson, S. M., Bakaic, E., Stewart, S. A., Hoare, T. & Adronov, A. Properties of Poly(ethylene glycol) Hydrogels Cross-Linked via Strain-Promoted Alkyne-Azide Cycloaddition (SPAAC). *Biomacromolecules* **17**, 1093–1100 (2016).
83. PH, Y., ME, C., SC, H., RD, B. & GN, S. *Living with water stress: evolution of osmolyte systems. Science* **217**, (1982).
84. Jiang, S. & Cao, Z. Ultralow-fouling, functionalizable, and hydrolyzable zwitterionic materials and their derivatives for biological applications. *Adv. Mater.* **22**, 920–932 (2010).
85. Yang, W., Xue, H., Li, W., And, J. Z. & Jiang, S. Pursuing ‘zero’ protein adsorption of poly(carboxybetaine) from undiluted blood serum and plasma. *Langmuir* **25**, 11911–11916 (2009).
86. Carr, L. R., Xue, H. & Jiang, S. Functionalizable and nonfouling zwitterionic carboxybetaine hydrogels with a carboxybetaine dimethacrylate crosslinker. *Biomaterials* **32**, 961–968 (2011).
87. Huynh, V., D’Angelo, A. D. & Wylie, R. Tunable degradation of low-fouling carboxybetaine-hyaluronic acid hydrogels for applications in cell encapsulation. *Biomed. Mater.* (2019). doi:10.1088/1748-605X/ab2bde
88. Huynh, V., Jesmer, A. H., Shoaib, M. M. & Wylie, R. G. Influence of Hydrophobic Cross-Linkers on Carboxybetaine Copolymer Stimuli Response and Hydrogel Biological Properties. *Langmuir* **35**, 1631–1641 (2019).
89. Bai, T. *et al.* Restraint of the differentiation of mesenchymal stem cells by a nonfouling zwitterionic hydrogel. *Angew. Chemie - Int. Ed.* **53**, 12729–12734 (2014).
90. Keefe, A. J. & Jiang, S. Poly(zwitterionic)protein conjugates offer increased stability without sacrificing binding affinity or bioactivity. *Nat. Chem.* **4**, 59–63 (2012).
91. Ho, S. S., Murphy, K. C., Binder, B. Y. K., Vissers, C. B. & Leach, J. K. Increased Survival and Function of Mesenchymal Stem Cell Spheroids Entrapped in Instructive Alginate Hydrogels. *Stem Cells Transl. Med.* **5**, 773–81 (2016).
92. Yamaoka, T., Tabata, Y. & Ikada, Y. Distribution and tissue uptake of poly(ethylene glycol) with different molecular weights after intravenous administration to mice. *J. Pharm. Sci.* **83**, 601–606 (1994).
93. Jain, P. *et al.* Zwitterionic Hydrogels Based on a Degradable Disulfide Carboxybetaine Cross-Linker. *Langmuir* **35**, 1864–1871 (2019).

94. Chien, H. W., Tsai, W. B. & Jiang, S. Direct cell encapsulation in biodegradable and functionalizable carboxybetaine hydrogels. *Biomaterials* **33**, 5706–5712 (2012).
95. West, J. L. & Hubbell, J. A. Polymeric biomaterials with degradation sites for proteases involved in cell migration. *Macromolecules* **32**, 241–244 (1999).
96. Seliktar, D., Zisch, A. H., Lutolf, M. P., Wrana, J. L. & Hubbel, J. A. MMP-2 sensitive, VEGF-bearing bioactive hydrogels for promotion of vascular healing. *J. Biomed. Mater. Res. - Part A* **68**, 704–716 (2004).
97. Halstenberg, S., Panitch, A., Rizzi, S., Hall, H. & Hubbell, J. A. Biologically engineered protein-graft-poly(ethylene glycol) hydrogels: A cell adhesive and plasmin-degradable biosynthetic material for tissue repair. *Biomacromolecules* **3**, 710–723 (2002).
98. Patterson, J. & Hubbell, J. A. Enhanced proteolytic degradation of molecularly engineered PEG hydrogels in response to MMP-1 and MMP-2. *Biomaterials* **31**, 7836–7845 (2010).
99. Kim, S. & Healy, K. E. Synthesis and characterization of injectable poly(N-isopropylacrylamide-co-acrylic acid) hydrogels with proteolytically degradable cross-links. *Biomacromolecules* **4**, 1214–1223 (2003).
100. Miller, J. S. *et al.* Bioactive hydrogels made from step-growth derived PEG-peptide macromers. *Biomaterials* **31**, 3736–3743 (2010).
101. Chen, G., Taghavi, S., Marecak, D. & Amsden, B. G. Tough and Enzyme-Degradable Hydrogels. *Macromol. Mater. Eng.* **303**, 1700162 (2018).
102. Brandl, F. P., Seitz, A. K., Teßmar, J. K. V., Blunk, T. & Göpferich, A. M. Enzymatically degradable poly(ethylene glycol) based hydrogels for adipose tissue engineering. *Biomaterials* **31**, 3957–3966 (2010).
103. Alge, D. L., Azagarsamy, M. A., Donohue, D. F. & Anseth, K. S. Synthetically tractable click hydrogels for three-dimensional cell culture formed using tetrazine-norbornene chemistry. *Biomacromolecules* **14**, 949–953 (2013).
104. Shih, H. & Lin, C. C. Cross-linking and degradation of step-growth hydrogels formed by thiol-ene photoclick chemistry. *Biomacromolecules* **13**, 2003–2012 (2012).
105. Mahoney, M. J. & Anseth, K. S. Three-dimensional growth and function of neural tissue in degradable polyethylene glycol hydrogels. *Biomaterials* **27**, 2265–2274 (2006).
106. Metters, A. T., Anseth, K. S. & Bowman, C. N. Fundamental studies of a novel, biodegradable PEG-b-PLA hydrogel. *Polymer (Guildf).* **41**, 3993–4004 (2000).
107. Anseth, K. S. *et al.* In situ forming degradable networks and their application in tissue engineering and drug delivery. *J. Control. Release* **78**, 199–209 (2002).
108. Bakaic, E. *et al.* Injectable and Degradable Poly(Oligoethylene glycol methacrylate) Hydrogels with Tunable Charge Densities as Adhesive Peptide-Free Cell Scaffolds. *ACS Biomater. Sci. Eng.* **4**, 3713–3725 (2018).
109. Urosev, I., Bakaic, E., Alsop, R. J., Rheinstädter, M. C. & Hoare, T. Tuning the properties of injectable poly(oligoethylene glycol methacrylate) hydrogels by controlling precursor polymer molecular weight. *J. Mater. Chem. B* **4**, 6541–6551 (2016).
110. Kirchhof, S. *et al.* New insights into the cross-linking and degradation mechanism of Diels-Alder hydrogels. *J. Mater. Chem. B* **3**, 449–457 (2015).
111. Kirchhof, S., Brandl, F. P., Hammer, N. & Goepferich, A. M. Investigation of the Diels-Alder reaction as a cross-linking mechanism for degradable poly(ethylene glycol) based hydrogels. *J. Mater. Chem. B* **1**, 4855–4864 (2013).
112. Xu, J., Feng, E. & Song, J. Bioorthogonally cross-linked hydrogel network with precisely controlled disintegration time over a broad range. *J. Am. Chem. Soc.* **136**, 4105–4108

(2014).
113. Zustiak, S. P. & Leach, J. B. Hydrolytically degradable poly(ethylene glycol) hydrogel scaffolds with tunable degradation and mechanical properties. *Biomacromolecules* **11**, 1348–1357 (2010).
114. Zustiak, S. P. & Leach, J. B. Characterization of protein release from hydrolytically degradable poly(ethylene glycol) hydrogels. *Biotechnol. Bioeng.* **108**, 197–206 (2011).
115. Truong, V., Blakey, I. & Whittaker, A. K. Hydrophilic and amphiphilic polyethylene glycol-based hydrogels with tunable degradability prepared by 'click' chemistry. *Biomacromolecules* **13**, 4012–4021 (2012).
116. Shu, X. Z., Liu, Y., Luo, Y., Roberts, M. C. & Prestwich, G. D. Disulfide cross-linked hyaluronan hydrogels. *Biomacromolecules* **3**, 1304–1311 (2002).
117. Wu, G., Fang, Y.-Z., Yang, S., Lupton, J. R. & Turner, N. D. *Glutathione Metabolism and Its Implications for Health*. *The Journal of Nutrition* **134**, (2004).
118. Kuppusamy, P. *et al. Noninvasive imaging of tumor redox status and its modification by tissue glutathione levels*. *Cancer Research* **62**, (2002).
119. Usal, A. *et al. Decreased Glutathione Levels in Acute Myocardial Infarction. Japanese Heart Journal* **37**, (1996).
120. Sternlicht, M. D. & Werb, Z. How Matrix Metalloproteinases Regulate Cell Behavior. *Annu. Rev. Cell Dev. Biol.* **17**, 463–516 (2002).
121. Lu, Y., Aimetti, A. A., Langer, R. & Gu, Z. Bioresponsive materials. *Nat. Rev. Mater.* **2**, 16075 (2016).
122. Tan, J. X. *et al.* HYAL1 overexpression is correlated with the malignant behavior of human breast cancer. *Int. J. Cancer* **128**, 1303–1315 (2011).
123. Santi, D. V., Reid, R., Schneider, E. L., Ashley, G. W. & Robinson, L. Predictable and tunable half-life extension of therapeutic agents by controlled chemical release from macromolecular conjugates. *Proc. Natl. Acad. Sci.* **109**, 6211–6216 (2012).
124. Fontaine, S. D. *et al.* Primary deuterium kinetic isotope effects prolong drug release and polymer biodegradation in a drug delivery system. *J. Control. Release* **278**, 74–79 (2018).
125. Lam, J., Carmichael, S. T., Lowry, W. E. & Segura, T. Hydrogel design of experiments methodology to optimize hydrogel for iPSC-NPC culture. *Adv. Healthc. Mater.* **4**, 534–539 (2015).
126. Cheng, T.-Y., Chen, M.-H., Chang, W.-H., Huang, M.-Y. & Wang, T.-W. Neural stem cells encapsulated in a functionalized self-assembling peptide hydrogel for brain tissue engineering. *Biomaterials* **34**, 2005–2016 (2013).
127. Rowley, J. A. & Mooney, D. J. Alginate type and RGD density control myoblast phenotype. *J. Biomed. Mater. Res.* **60**, 217–223 (2002).
128. Bidarra, S. J. *et al.* Injectable in situ crosslinkable RGD-modified alginate matrix for endothelial cells delivery. *Biomaterials* **32**, 7897–7904 (2011).
129. Burdick, J. A. & Anseth, K. S. *Photoencapsulation of osteoblasts in injectable RGD-modified PEG hydrogels for bone tissue engineering. Biomaterials* **23**, (2002).
130. Salinas, C. N. & Anseth, K. S. The influence of the RGD peptide motif and its contextual presentation in PEG gels on human mesenchymal stem cell viability. *J. Tissue Eng. Regen. Med.* **2**, 296–304 (2008).
131. Singh, A. & Peppas, N. A. Hydrogels and scaffolds for immunomodulation. *Adv. Mater.* **26**, 6530–6541 (2014).
132. Schwartz, S. G., Scott, I. U., Flynn, H. W. & Stewart, M. W. Drug delivery techniques for

treating age-related macular degeneration. *Expert Opin. Drug Deliv.* **11**, 61–68 (2013).
133. Huynh, V. & Wylie, R. G. Competitive Affinity Release for Long-Term Delivery of Antibodies from Hydrogels. *Angew. Chemie Int. Ed.* **57**, 3406–3410 (2018).
134. Bakaic, E. *et al.* Injectable and Degradable Poly(Oligoethylene glycol methacrylate) Hydrogels with Tunable Charge Densities as Adhesive Peptide-Free Cell Scaffolds. *ACS Biomater. Sci. Eng.* **4**, 3713–3725 (2018).
135. Leijten, J. *et al.* Spatially and temporally controlled hydrogels for tissue engineering. *Mater. Sci. Eng. R Reports* **119**, 1–35 (2017).
136. Ieong, N. S. *et al.* Polymers with molecular weight dependent LCSTs are essential for cooperative behaviour. *Polym. Chem.* **3**, 794 (2012).
137. Thomas, D. B., Convertine, A. J., Hester, R. D., Lowe, A. B. & McCormick, C. L. Hydrolytic Susceptibility of Dithioester Chain Transfer Agents and Implications in Aqueous RAFT Polymerizations. *Macromolecules* **37**, 1735–1741 (2004).
138. Lutz, J. F. Polymerization of oligo(ethylene glycol) (meth)acrylates: Toward new generations of smart biocompatible materials. *J. Polym. Sci. Part A Polym. Chem.* **46**, 3459–3470 (2008).
139. Yang, B. *et al.* A thermoresponsive poly(N-vinylcaprolactam-co-sulfobetaine methacrylate) zwitterionic hydrogel exhibiting switchable anti-biofouling and cytocompatibility. *Polym. Chem* **6**, 3431 (2015).
140. Kotagiri, N. *et al.* Antibody Quantum Dot Conjugates Developed via Copper-Free Click Chemistry for Rapid Analysis of Biological Samples Using a Microfluidic Microsphere Array System. *Bioconjug. Chem.* **25**, 1272–1281 (2014).
141. Bjerknes, M., Cheng, H., McNitt, C. D. & Popik, V. V. Facile Quenching and Spatial Patterning of Cylooctynes via Strain-Promoted Alkyne-Azide Cycloaddition of Inorganic Azides. *Bioconjug. Chem.* **28**, 1560–1565 (2017).
142. Massia, S. P. and Hubbell, J. A. An RGD spacing of 440 nm is sufficient for integrin alpha V beta 3- mediated fibroblast spreading and 140 nm for focal contact and stress fiber formation. *J. Cell Biol.* **114**, 1089–1100 (1991).
143. Lihong, H., Read, E. S., Armes, S. P. & Adams, D. J. Direct synthesis of controlled-structure primary amine-based methacrylic polymers by living radical polymerization. *Macromolecules* **40**, 4429–4438 (2007).
144. Deng, Z. *et al.* Facile synthesis of controlled-structure primary amine-based methacrylamide polymers via the reversible addition-fragmentation chain transfer process. *J. Polym. Sci. Part A Polym. Chem.* **46**, 4984–4996 (2008).
145. Alidedeoglu, A. H., York, A. W., McCormick, C. L. & Morgan, S. E. Aqueous RAFT polymerization of 2-aminoethyl methacrylate to produce well-defined, primary amine functional homo- And copolymers. *J. Polym. Sci. Part A Polym. Chem.* **47**, 5405–5415 (2009).
146. Yildirim, T. *et al.* RAFT made methacrylate copolymers for reversible pH-responsive nanoparticles. *J. Polym. Sci. Part A Polym. Chem.* **53**, 2711–2721 (2015).
147. Chen, L. Q. & Pagel, M. D. Evaluating pH in the Extracellular Tumor Microenvironment Using CEST MRI and Other Imaging Methods. *Adv. Radiol.* **2015**, 1–25 (2015).
148. Han, S. S. *et al.* In situ cross-linkable hyaluronic acid hydrogels using copper free click chemistry for cartilage tissue engineering. *Polym. Chem.* **9**, 20–27 (2018).
149. Youn, Y. S., Na, D. H. & Lee, K. C. High-yield production of biologically active mono-PEGylated salmon calcitonin by site-specific PEGylation. *J. Control. Release* **117**, 371–

379 (2007).
150. Pasut, G. & Veronese, F. M. Polymer-drug conjugation, recent achievements and general strategies. *Prog. Polym. Sci.* **32**, 933–961 (2007).
151. Browning, M. B., Russell, B., Rivera, J., Höök, M. & Cosgriff-Hernandez, E. M. Bioactive hydrogels with enhanced initial and sustained cell interactions. *Biomacromolecules* **14**, 2225–2233 (2013).
152. Browning, M. B. *et al.* Endothelial Cell Response to Chemical, Biological, and Physical Cues in Bioactive Hydrogels. *Tissue Eng. Part A* **20**, 3130–3141 (2014).
153. Cereceres, S. *et al.* Chronic Wound Dressings Based on Collagen-Mimetic Proteins. *Adv. Wound Care* **4**, 444–456 (2015).
154. Lee, J. W., Park, Y. J., Lee, S. J., Lee, S. K. & Lee, K. Y. The effect of spacer arm length of an adhesion ligand coupled to an alginate gel on the control of fibroblast phenotype. *Biomaterials* **31**, 5545–5551 (2010).
155. Bakaic, E., Smeets, N. M. B. & Hoare, T. Injectable hydrogels based on poly(ethylene glycol) and derivatives as functional biomaterials. *RSC Adv.* **5**, 35469–35486 (2015).
156. Wang, C. *et al.* In situ formed reactive oxygen species-responsive scaffold with gemcitabine and checkpoint inhibitor for combination therapy. *Sci. Transl. Med.* **10**, eaan3682 (2018).
157. Nih, L. R., Carmichael, S. T. & Segura, T. Hydrogels for brain repair after stroke: An emerging treatment option. *Curr. Opin. Biotechnol.* **40**, 155–163 (2016).
158. Kobayashi, K., Oh, S. H., Yoon, C. K. & Gracias, D. H. Multitemperature Responsive Self-Folding Soft Biomimetic Structures. *Macromol. Rapid Commun.* **39**, 1700692 (2018).
159. Yang, W. *et al.* The effect of lightly crosslinked poly(carboxybetaine) hydrogel coating on the performance of sensors in whole blood. *Biomaterials* **33**, 7945–7951 (2012).
160. Cao, Z., Yu, Q., Xue, H., Cheng, G. & Jiang, S. Nanoparticles for drug delivery prepared from amphiphilic PLGA zwitterionic block copolymers with sharp contrast in polarity between two blocks. *Angew. Chemie - Int. Ed.* **49**, 3771–3776 (2010).

Appendix

Methods

CBMAA monomer synthesis

Carboxybetaine methacrylamide was synthesized according to previously established procedures.[160] Briefly, 7.75 g (46 mmol) of N-[3-(dimethylamino)propyl]- methacrylamide was dissolved in 100 mL of dry acetonitrile under N_2. *t*-Butyl bromoacetate (10 g, 51 mmol) was added, and the reaction was kept at 50 °C overnight. The reaction was cooled to room temperature, and the product was precipitated in ether (250 mL). The white precipitate was collected by vacuum filtration, washed with ether, and dried overnight in a vacuum oven at 60 °C. The *t*-butyl group was removed by reacting 12 g of the white solid with trifluoroacetic acid (10 mL, 131 mmol) for 2 h at room temperature, followed by precipitation in ether (100 mL). The precipitate was collected, washed with ether, and dried overnight in a vacuum oven at 60 °C. The product was then dissolved in water and lyophilized to yield 8 g (83% yield). ^{1}H NMR (D_2O, 600 MHz) δ: 5.63 (s, 1H), 5.34 (s, 1H), 4.10 (s, 2H), 3.53 (m, 2H), 3.28 (t, J = 6.42, 2H), 3.18 (s, 6H), 1.96 (m, 2H), 1.85 (s, 3H).

Synthesis of PCBMAA-APMA

Previously synthesized carboxybetaine monomer (2 g, 8.7 mmol) and APMA (40 mg, 0.22 mmol) were dissolved in 1 M acetate buffer pH 5.2. Separately, CTP (5.7 mg, 20 µmol) was dissolved in dioxane and added to the monomer solutions resulting in a 1 M monomer solution of 5:1 acetate buffer:dioxane. pH was adjusted between 3 to 4 using HCl and V-501 (1.15 mg, 4.1 µmol) was added. The reaction mixture was freeze-pump-thawed (3 times) with a nitrogen

backfill and reacted at 70 °C for 24 h. Polymers were purified by dialysis (MWCO 12 -14k) against water at pH ~3 for 3 d and lyophilized to yield a pink powder (2.08 g).

PCBMAA amine quantification via ^{1}H NMR

^{1}H NMR (600 MHz, D_2O, 128 scans) of PCBMAA-APMA copolymers was used to quantify polymer composition by comparing the peak of the methylene spacer between charged groups in PCBMAA-APMA (~4 ppm) to that of the methylene peak adjacent to the amino group (~3 ppm) (Figure S 16).

Synthesis of NHS-AZ derivatives

6-Azidohexanal

A mixture of 6-chloro-1-hexanol (14.4 g, 105 mmol) and sodium azide (18.7 g, 288 mmol) in 200 mL of water was heated at reflux for 20 h. After cooling to room temperature, the mixture was extracted three times with ethyl acetate. The combined extracts were washed with brine, dried with $MgSO_4$, filtered, and concentrated to yield 14.7 g (103 mmol, 98%) of 6-azidohexanol, which was used without further purification. Trichloroisocyanuric acid (11.44 g, 48.9 mmol) was added in small portions over 15 min to a vigorously stirred mixture of 6-azido-1-hexanol (14.7 g, 103 mmol), TEMPO (0.206 g, 1.32 mmol), and sodium bicarbonate (13.3 g, 158 mmol) in dichloromethane (200 mL) and water (20 mL). The mixture was stirred for an additional 30 min and filtered through Celite. The organic phase was separated and washed successively with saturated aqueous $NaHCO_3$ and brine, then dried over $MgSO_4$, filtered, and concentrated. The crude product was purified by flash column chromatography using dichloromethane:methanol with a 0 – 5% methanol gradient to yield 6-azidohexanal (8.37 g, 59.3 mmol, 58 %). ^{1}H NMR (600 MHz, $CDCl_3$): δ 9.45 (1H, t, J = 1.8 Hz), 3.01 (2H, t, J = 6.9 Hz), 2.17 (2H, dt, J = 1.1, 7.2 Hz), 1.4 – 1.3 (4H, m), 1.2 – 1.1 (2H, m).

1-(4-Chlorophenylsulfonyl)-7-azido-2-heptanol

A 1.6-M solution of n-butyllithium (~3 mL, ~4.8 mmol) in hexane was added dropwise to a stirred solution of 4-chlorophenyl methyl sulfone (952.2 mg, 4.99 mmol) in -78°C anhydrous THF (15 mL). After addition, the mixture was left to warm slowly to 0 °C in an ice bath over ~30 min. The mixture was then cooled to –78 °C, and 6-azidohexanal (0.78 g, 5.5 mmol) was added to each reaction. After 15 min of stirring, the mixture was left to warm. When the mixture became clear, 5 mL of saturated aq. NH_4Cl was added and the mixture was left to continue warming to room temperature. The mixture was diluted with ethyl acetate and washed successively with water and brine, then dried over $MgSO_4$, filtered, and evaporated to provide the crude product as an oil. Flash column chromatography on silica gel using a gradient of ethyl acetate in hexane (0% - 50 %) provided the purified product as a pale-yellow oil (757 mg, 2.29 mmol, 48%). ^{1}H-NMR (600 MHz, d6-DMSO): δ 7.90 (2H, d, *J* = 8.4 Hz), 7.70 (2H, d, *J* = 8.4 Hz), 4.83 (1H, d, *J* = 6.1 Hz), 3.86 (1H, m), 3.39 (2H, m), 3.30 (2H, t, d, *J* = 7.2 Hz), 1.5 ~ 1.2 (8H, m).

1-(4-Methylphenylsulfonyl)-7-azido-2-heptanol

Similarly synthesized and purified from 4-(Methylsulfonyl)toluene (853.8 mg, 5.02 mmol) yielding a colorless oil (391.1 mg, 1.26 mmol, 25 %). ^{1}H-NMR (600 MHz, $CDCl_3$): δ 7.80 (2H, d, *J* = 8.4 Hz), 7.38 (2H, d, *J* = 8.4 Hz), 4.13 (1H, m), 3.41 (1H, m), 3.23 (2H, t, *J* = 6.6 Hz), 3.16 (2H, m), 1.6 ~ 1.3 (8H, m).

O-(6-azidohexyl)-O'-succinimidyl carbonate

Pyridine (700 µL, 2 eq.) was added dropwise to a stirred solution of 6-azidohexanol (608 mg, 4.2 mmol) and triphosgene (2.066 g, 1.6 eq.) in 25 mL of anhydrous THF. The resulting suspension was stirred for 15 min, gravity filtered, and concentrated to provide a crude chloroformate oil.

The crude oil was dissolved in 25 mL of anhydrous THF, reacted with N-hydroxysuccinimide (1.47 g, 3 eq.), and then pyridine (1 mL, 3.1 eq.) for 15 min. The crude mixture was concentrated, dissolved in ethyl acetate, and washed successively with 0.1 M HCl, water, saturated aqueous $NaHCO_3$, water, and brine, then was dried over $MgSO_4$ and concentrated. Flash column chromatography on silica gel using a gradient of ethyl acetate in hexanes of 0 – 50% yielded a colorless oil (0.7294 g, 60%). ^{1}H NMR (600 MHz, $CDCl_3$) δ 4.33 (t, *J* = 6.5 Hz, 2H), 3.28 (t, *J* = 6.8 Hz, 2H), 2.84 (s, 4H), 1.84 – 1.69 (m, 2H), 1.68 – 1.52 (m, 2H), 1.43 (m, 4H).

O-[1-(4-chlorophenylsulfonyl)-7-azido-2-heptyl]-O'-succinimidyl carbonate

Pyridine (359 µL) was added dropwise to a stirred solution of 1-(4-chlorophenylsulfonyl)-7-azido-2-heptanol (739 mg, 2.23 mmol) and triphosgene (664 mg, 2.24 mmol) in 37 mL of anhydrous THF. The resulting suspension was stirred for 15 min, then filtered and concentrated to provide the crude chloroformate as an oil. The chloroformate was dissolved in 37 mL of dry THF and treated successively with N-hydroxysuccinimide (769 mg, 6.83 mmol) and pyridine (557 µL) for 15 min. The mixture was then concentrated, and the residue was dissolved in ethyl acetate. After washing successively with 0.1 M HCl, water, saturated aq. $NaHCO_3$, water, and brine, the solution was dried over $MgSO_4$, filtered, and evaporated. The crude succinimidyl carbonate was purified by flash column chromatography on silica gel using a gradient of ethyl acetate in hexane (0 - 50 %), providing the product as a yellow oil that crystallizes on standing (750 mg, 1.59 mmol, 72%).

O-[1-(4-methylphenylsulfonyl)-7-azido-2-heptyl]-O'-succinimidyl carbonate

Similarly synthesized and purified from 1-(4-methylphenylsulfonyl)-7-azido-2-heptanol (391.1 mg, 1.26 mmol) yielding a pink oil (367 mg, 0.81 mmol, 65 %).

PCBMAA-AZ and PCBMAA-DBCO copolymer synthesis

PCBMAA-APMA was dissolved at 30 mg mL^{-1} in dry MeOH and reacted with NHS -AZ derivatives or NHS-DBCO (1.2 eq. relative to amines) and triethylamine (3 eq.) overnight at room temperature. Complete reaction of amines was confirmed by disappearance of the APMA-associated ^{1}H NMR signals (Figure S 17 – 20) as well as monitoring absorbance of primary amines using picrylsulfonic acid. Equal volumes (50 µL) of 0.5 mg mL^{-1} reaction mixture and 0.2 wt.% picrylsulfonic acid solution in pH 9 borax buffer were mixed and the absorbance was measured at 420 nm. Reduction of absorbance to that of PCBMAA homopolymer indicated complete consumption of amines. Polymers were purified by dialysis (MWCO 12 -14k) against water at pH ~3 for 3 d and lyophilized to yield white powders.

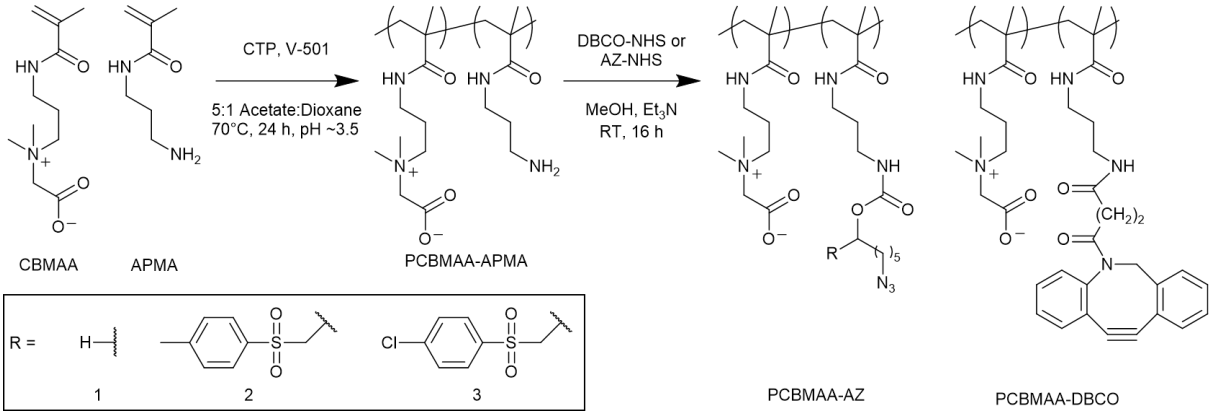

Scheme S 1. PCBMAA-AZ and PCBMAA-DBCO copolymer synthesis. PCBMAA-APMA copolymers were synthesized by acidic, aqueous RAFT polymerization and then derivatized with NHS-AZ derivatives or NHS-DBCO. Three PCBMAA-AZ copolymers were made: one with a non-degradable linker (R1) and two EWG-containing degradable linkers (R2 = methylphenyl sulfone and R3 = 4-chlorophenyl sulfone).

Cell encapsulation in $P(EG)_{4-5}MA$ hydrogels.

60 µL 5 wt.% $P(EG)_{4-5}MA$ hydrogels with 20,000 encapsulated NIH 3T3 fibroblasts were cultured in DMEM-F12 media with 10% CBS. Hydrogels were formed by mixing equal volumes

of P(EG)$_{4\text{-}5}$MA-AZ and P(EG)$_{4\text{-}5}$MA-DBCO PBS solutions that each contained 10,000 cells and incubating at 37 °C for 1 h. As a non-cytotoxic control, 20,000 cells were also encapsulated in 1 wt.% agarose hydrogels by mixing equal volumes of cell suspension with a 2 wt.% agarose solution in PBS. Agarose gels were placed at 4 °C for 15 min and incubated at 37 °C for 45 min. 200 µL of media was then added on top of each gel and incubated at 37 °C 5% CO_2. After 20 h, the media was removed from gel surfaces and replaced with media containing 10% PrestoBlue reagent. After 1 h, fluorescence was measured using a BioTek Cytation 5 plate reader (λ_{ex} = 560 nm; $\lambda_{em.}$ = 590 nm) and normalized to the non-cytotoxic agarose control.

Figures

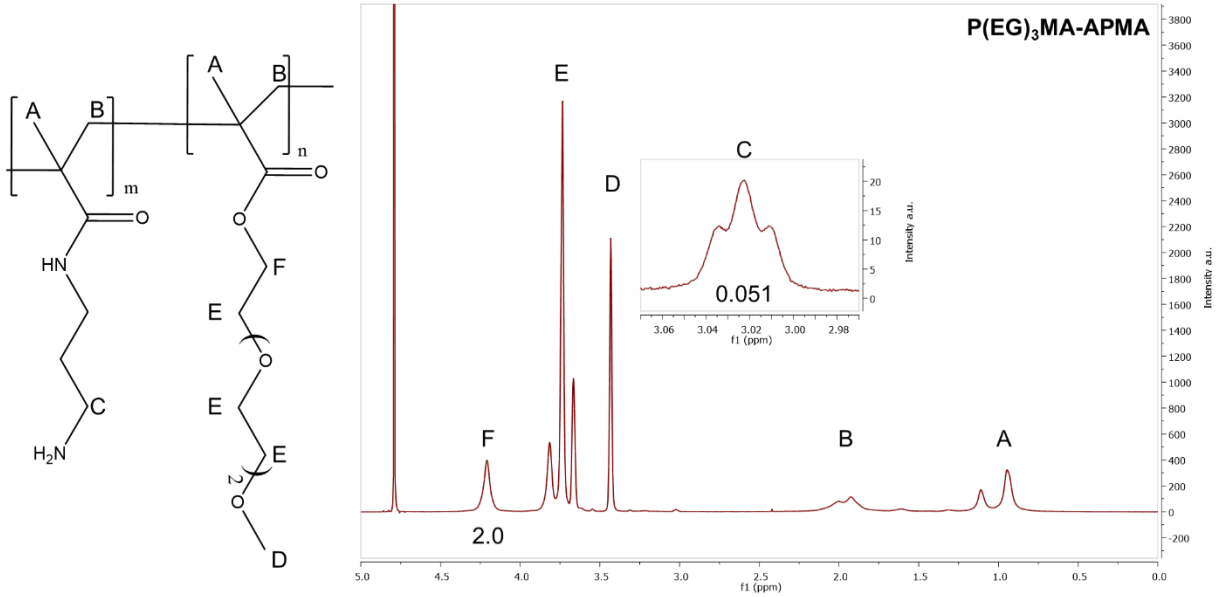

Figure S 1. ^{1}H NMR P(EG)$_3$MA-APMA in D_2O.

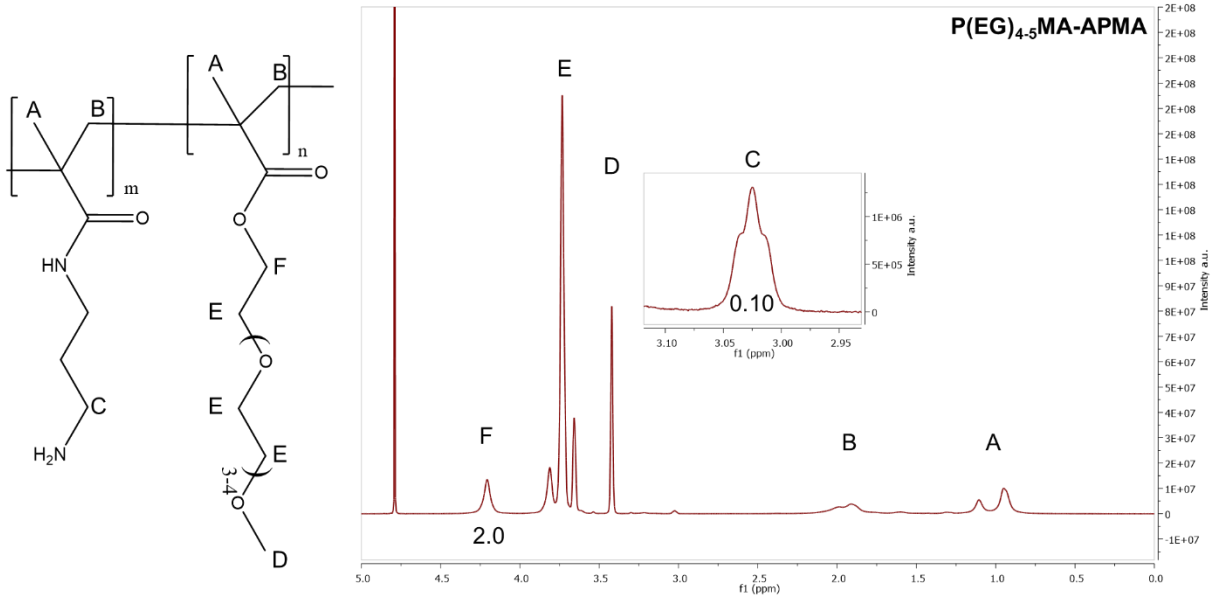

Figure S 2. ^{1}H NMR P(EG)$_{4\text{-}5}$MA-APMA in D_2O.

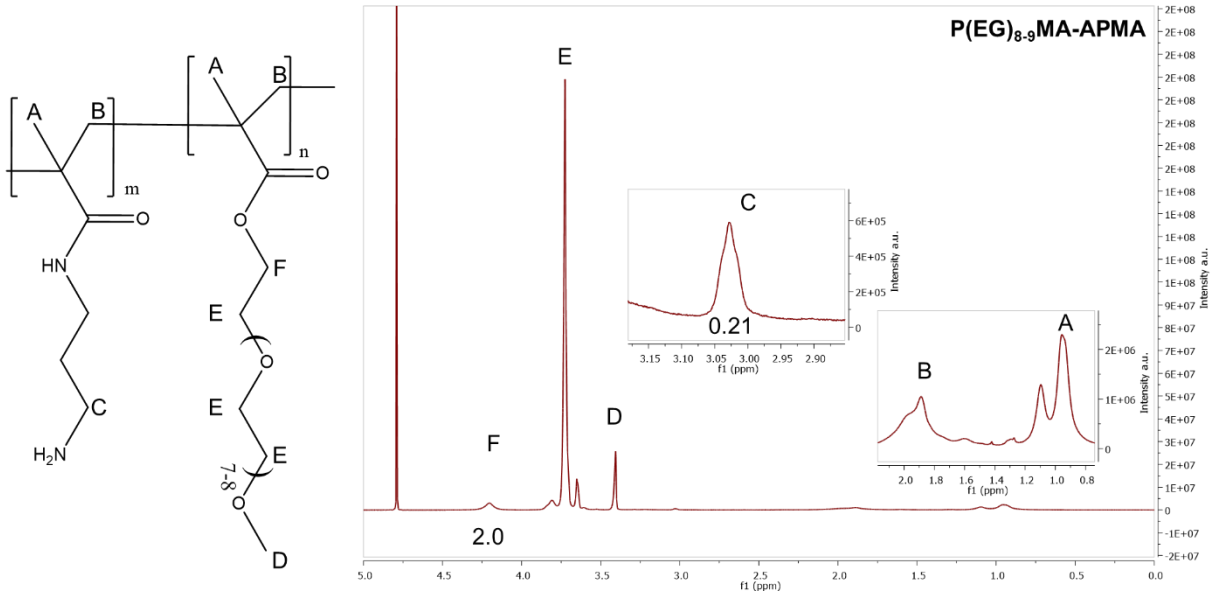

Figure S 3. ^{1}H NMR P(EG)$_{8\text{-}9}$MA-APMA in D_2O.

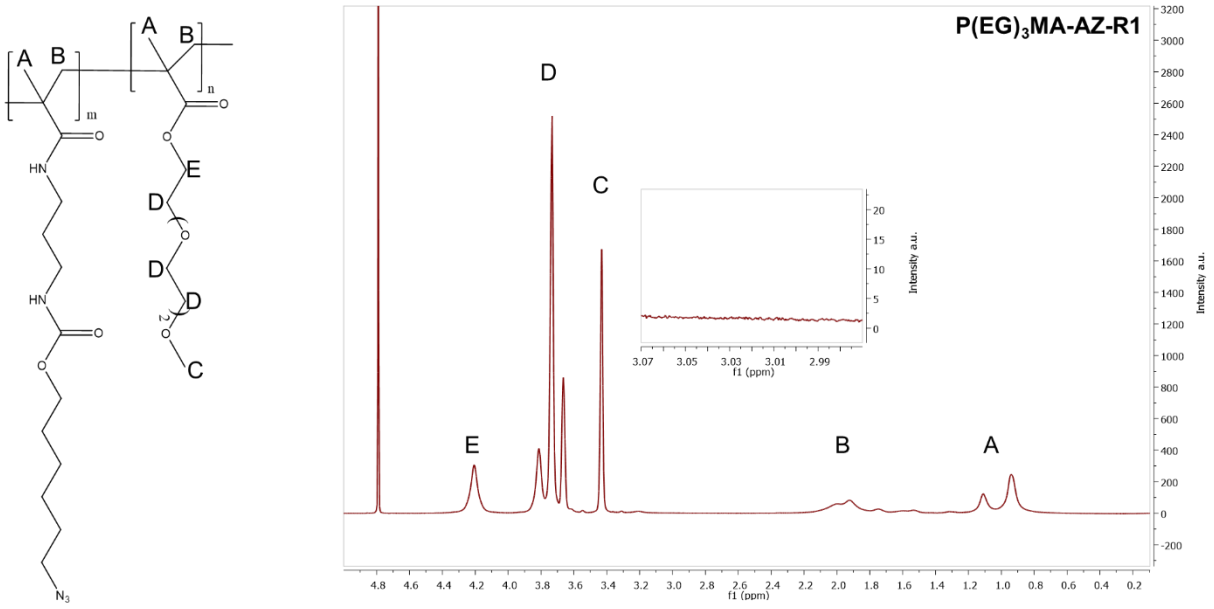

Figure S 4. ^{1}H NMR P(EG)$_3$MA-AZ-R1 in D_2O.

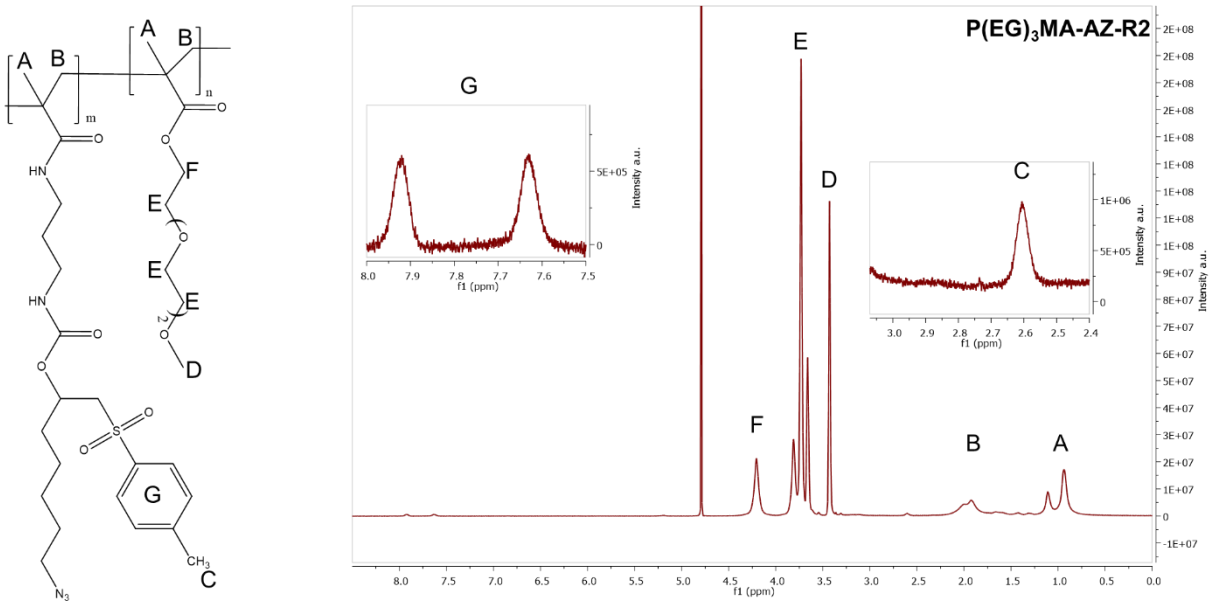

Figure S 5. ^{1}H NMR P(EG)$_3$MA-AZ-R2 in D$_2$O.

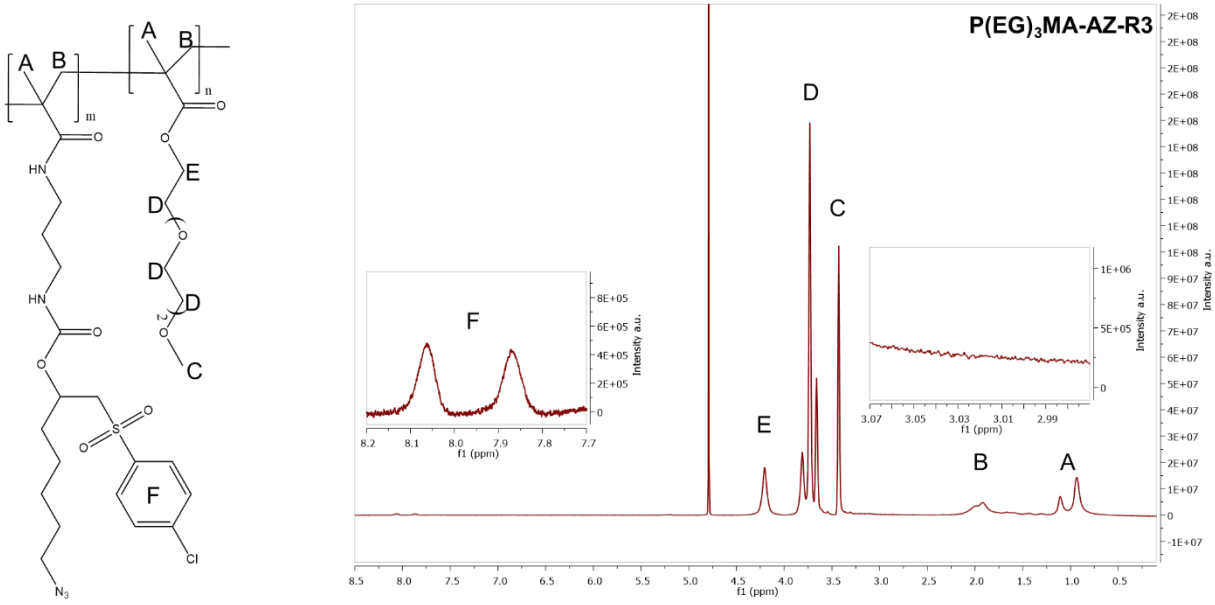

Figure S 6. ^{1}H NMR P(EG)$_3$MA-AZ-R3 in D$_2$O.

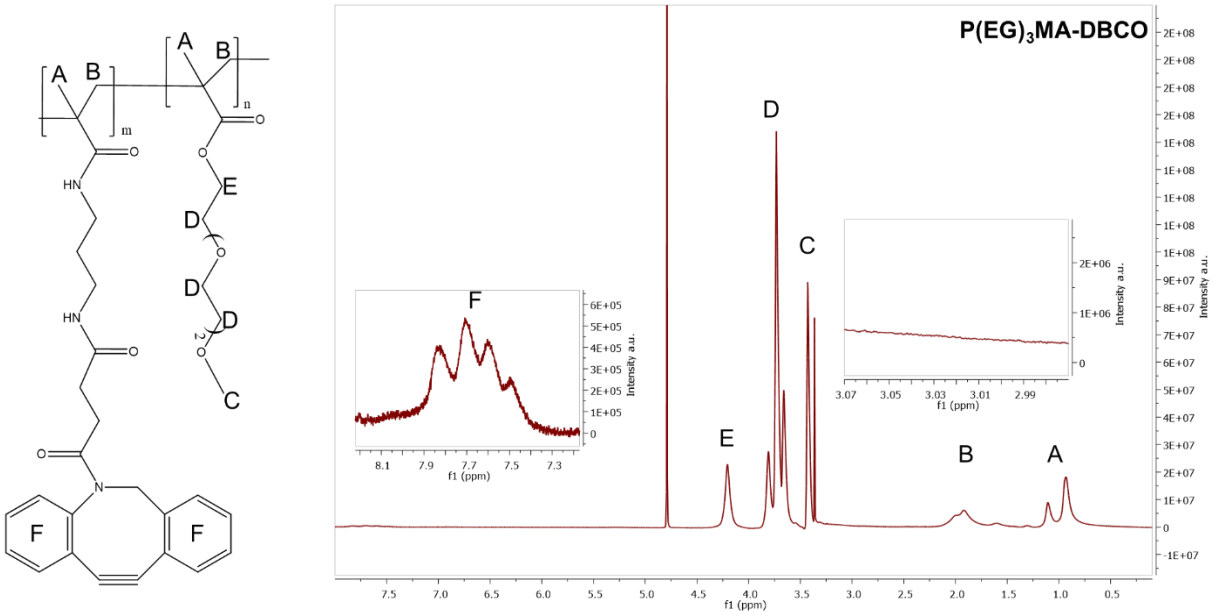

Figure S 7. ^{1}H NMR P(EG)$_3$MA-DBCO in D$_2$O.

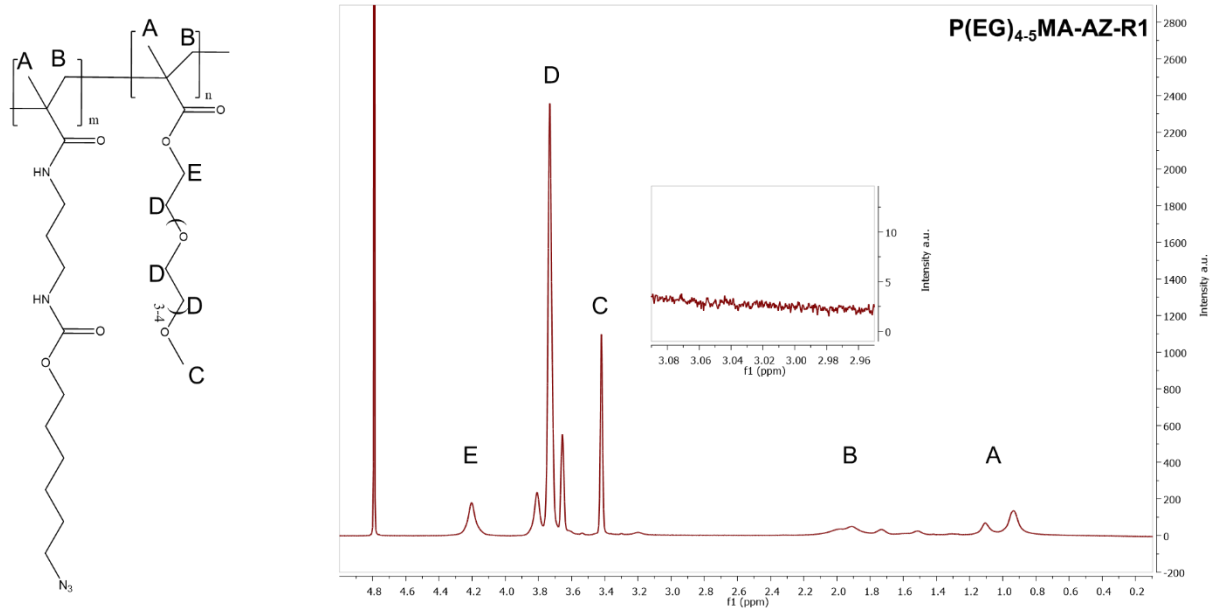

Figure S 8. ^{1}H NMR P(EG)$_{4\text{-}5}$MA-AZ-R1 in D$_2$O.

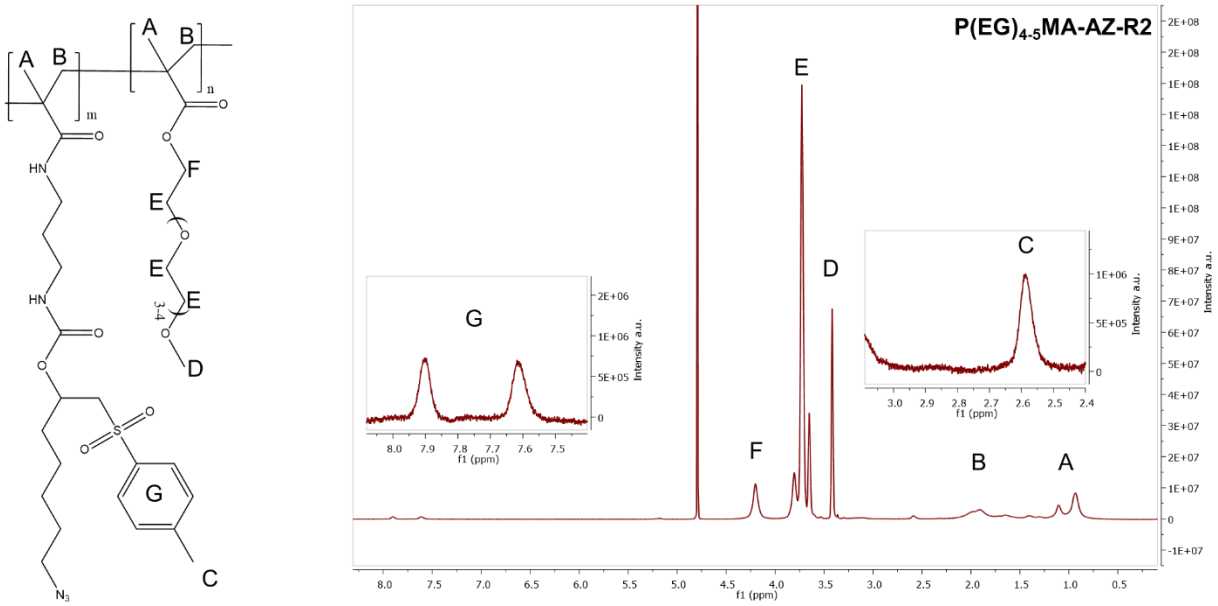

Figure S 9. ^{1}H NMR P(EG)$_{4\text{-}5}$MA-AZ-R2 in D_2O.

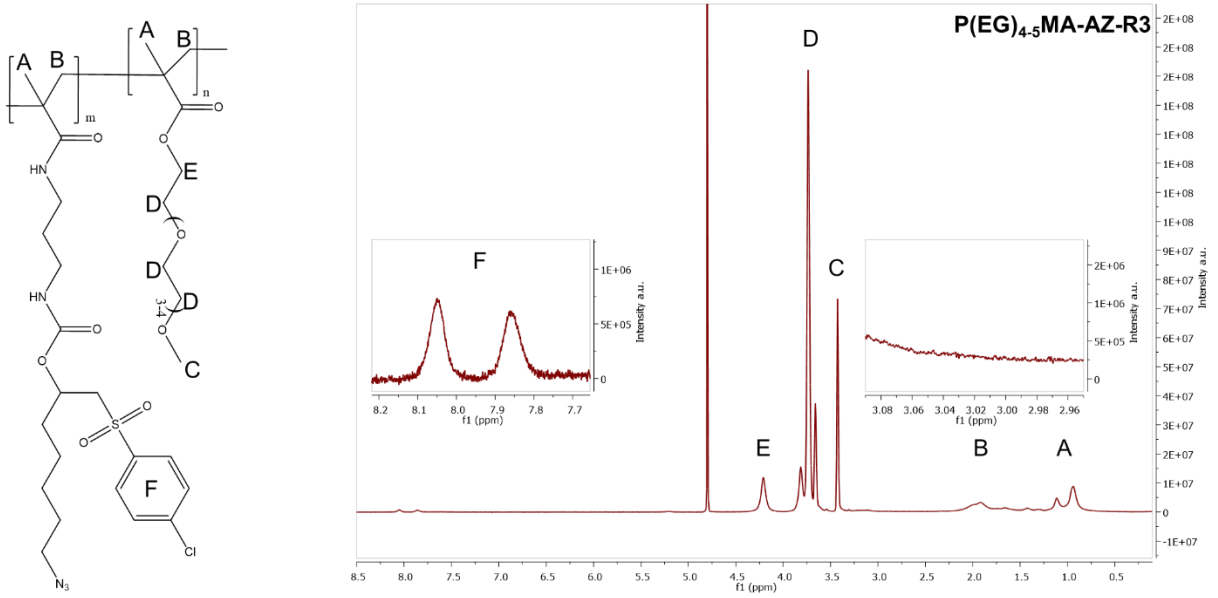

Figure S 10. ^{1}H NMR P(EG)$_{4\text{-}5}$MA-AZ-R3 in D_2O.

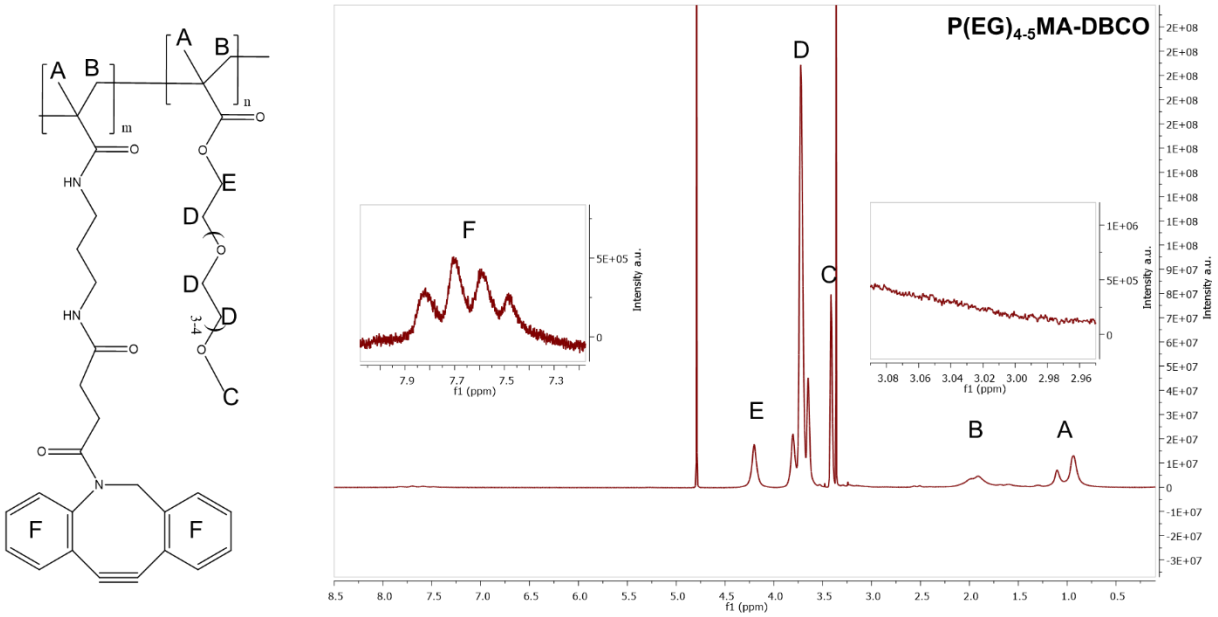

Figure S 11. ^{1}H NMR P(EG)$_{4-5}$MA-DBCO in D$_2$O. Sharp peak at ~3.4 ppm is residual MeOH solvent

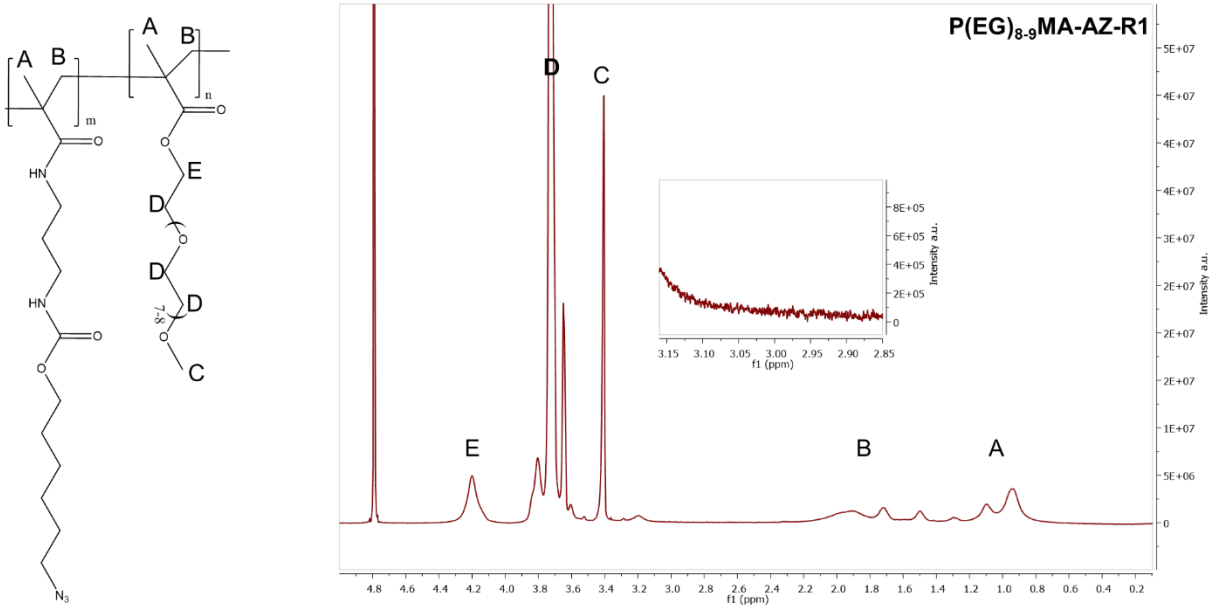

Figure S 12. ^{1}H NMR P(EG)$_{8-9}$MA-AZ-R1 in D$_2$O. Peak D set off-scale to make other peaks visible.

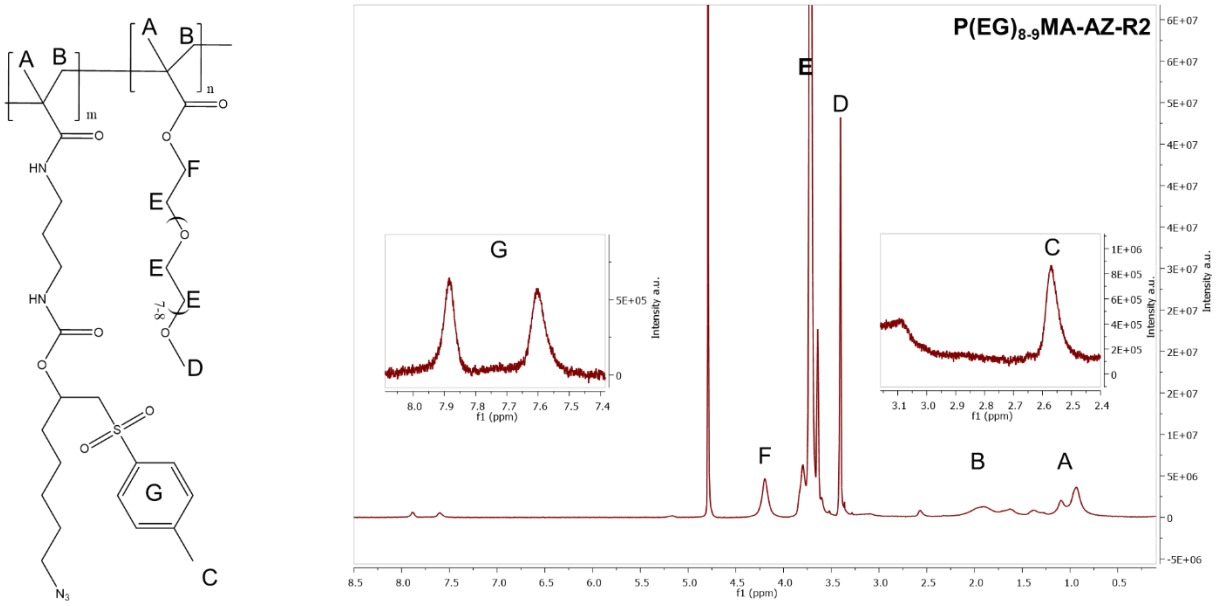

Figure S 13. ^{1}H NMR P(EG)$_{8\text{-}9}$MA-AZ-R2 in D_2O. Peak D set off-scale to make other peaks visible.

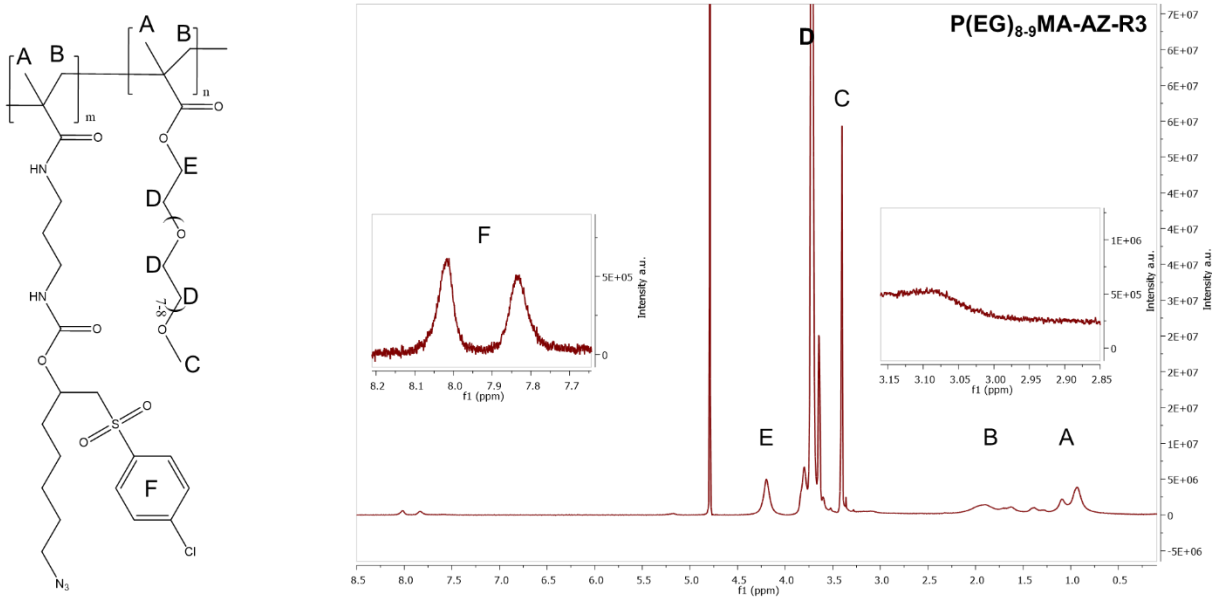

Figure S 14. ^{1}H NMR P(EG)$_{8\text{-}9}$MA-AZ-R3 in D_2O. Peak E set off-scale to make other peaks visible.

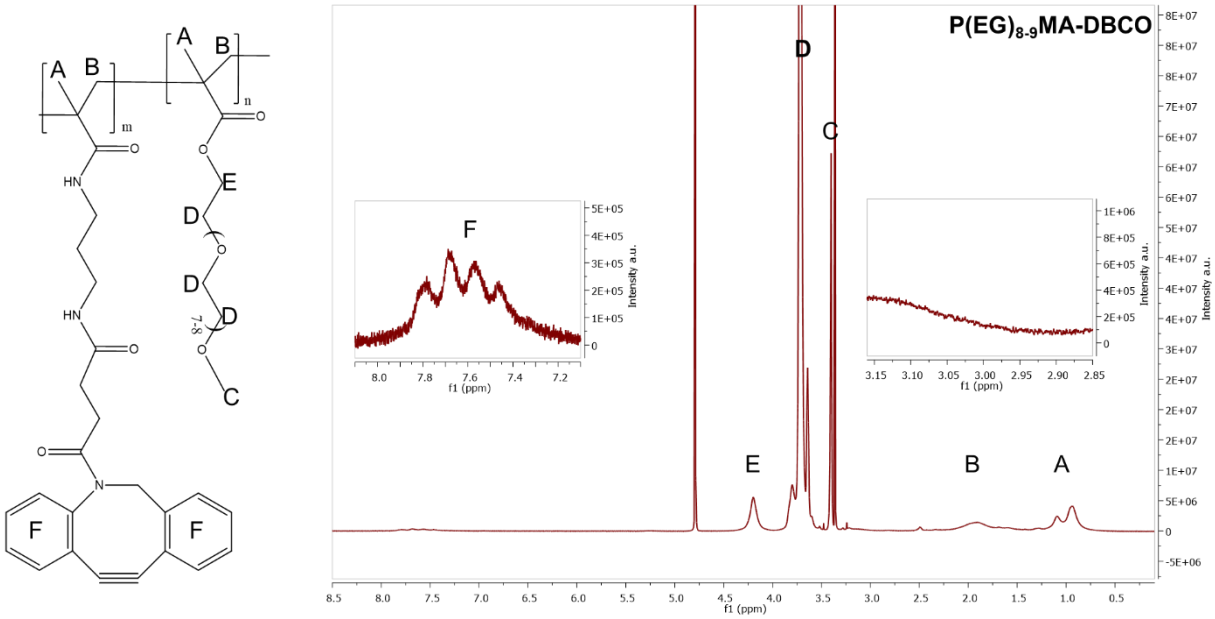

Figure S 15. ^{1}H NMR P(EG)$_{8\text{-}9}$MA-DBCO in D_2O. Peak D set off-scale to make other peaks visible.

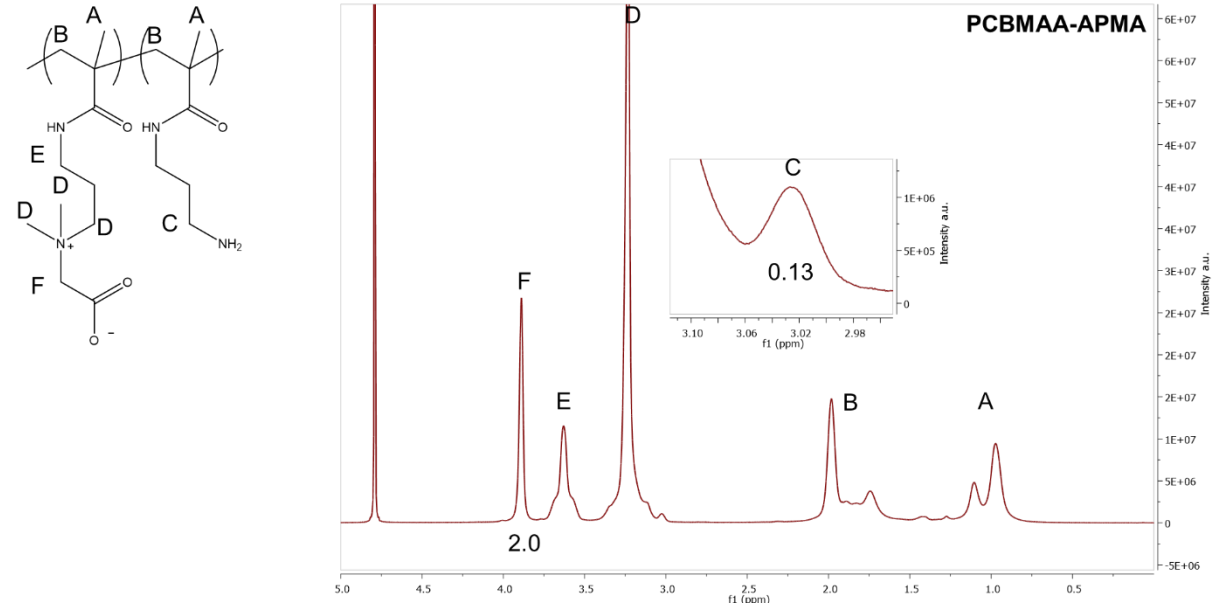

Figure S 16. ^{1}H NMR PCBMAA-APMA in D_2O.

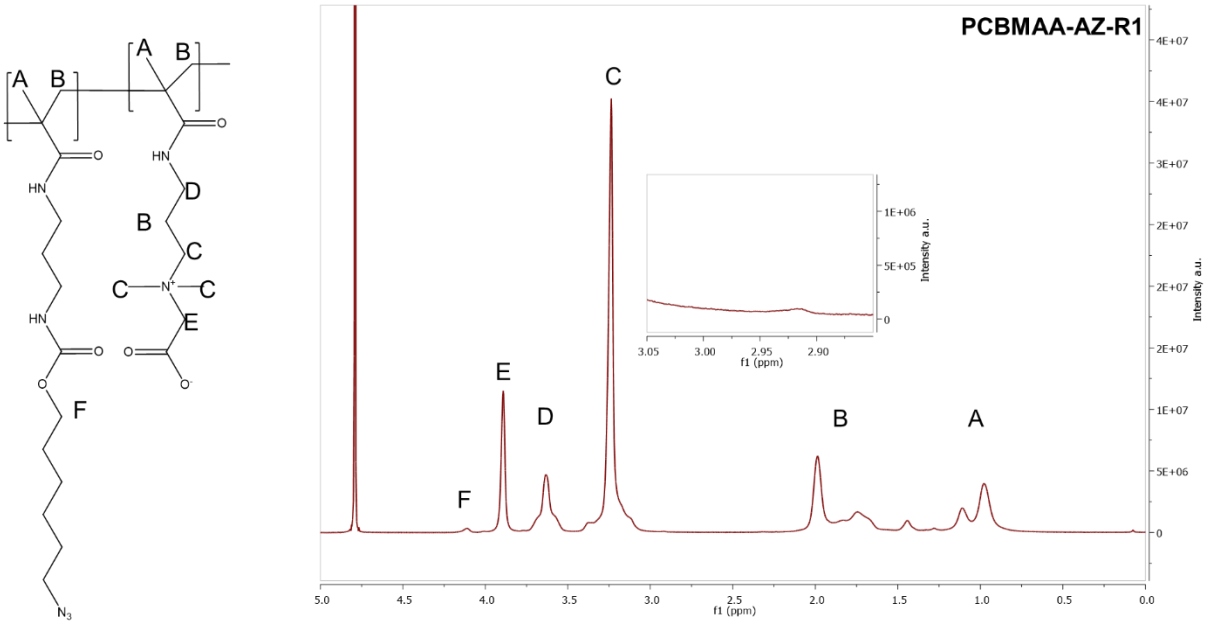

Figure S 17. ^{1}H NMR PCBMAA-AZ-R1 in D_2O.

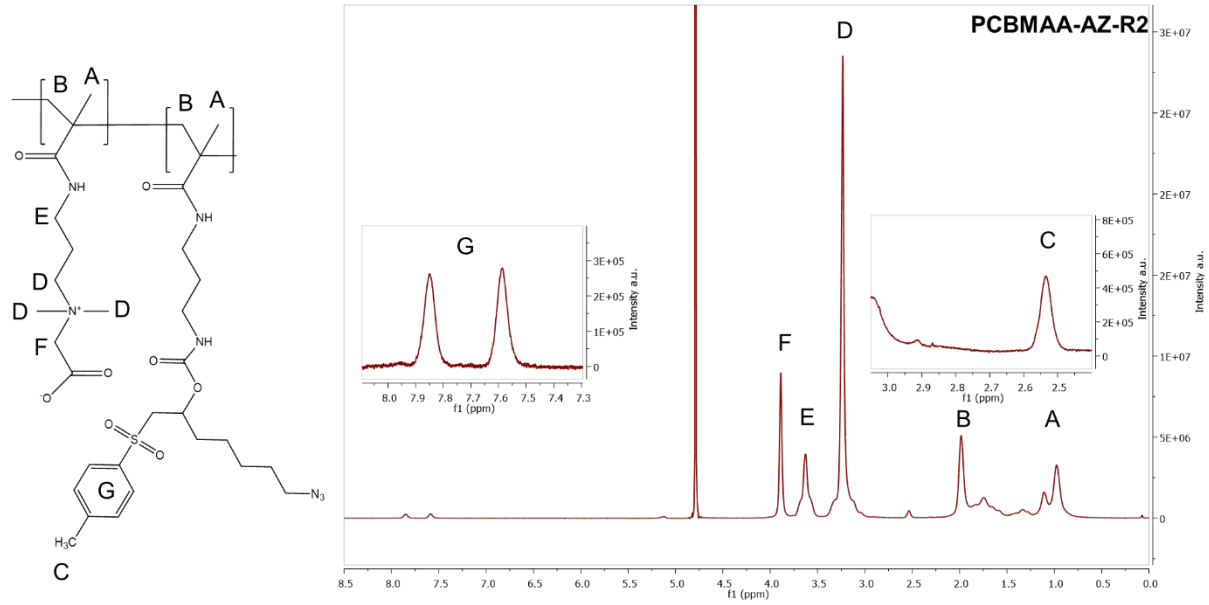

Figure S 18. ^{1}H NMR PCBMAA-AZ-R2 in D_2O.

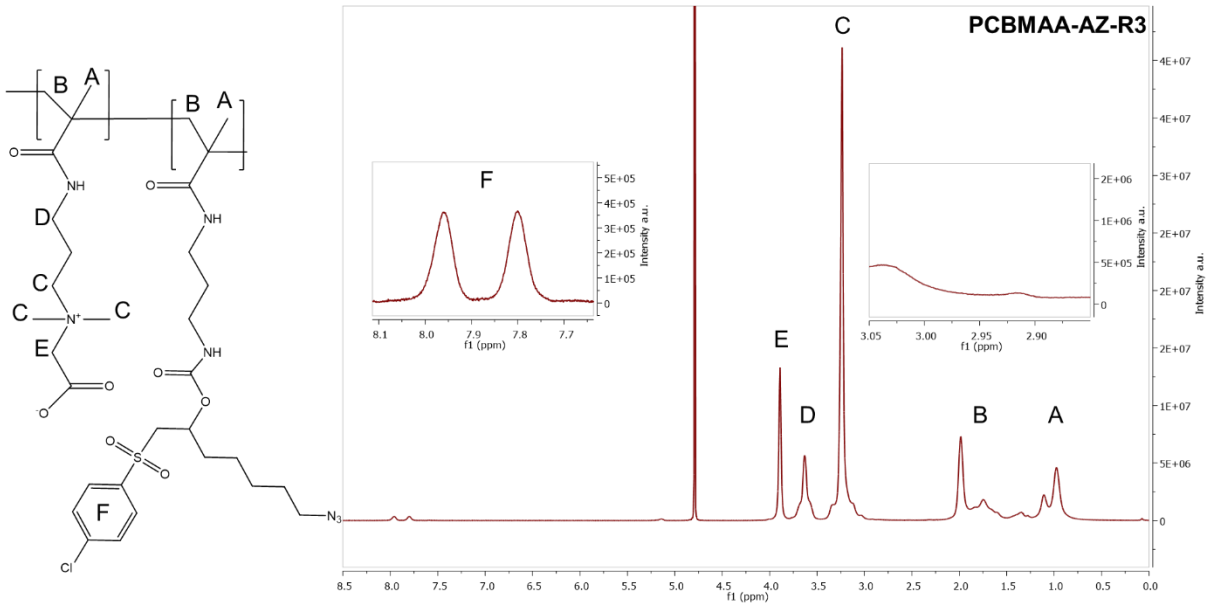

Figure S 19. ^{1}H NMR PCBMAA-AZ-R3 in D_2O.

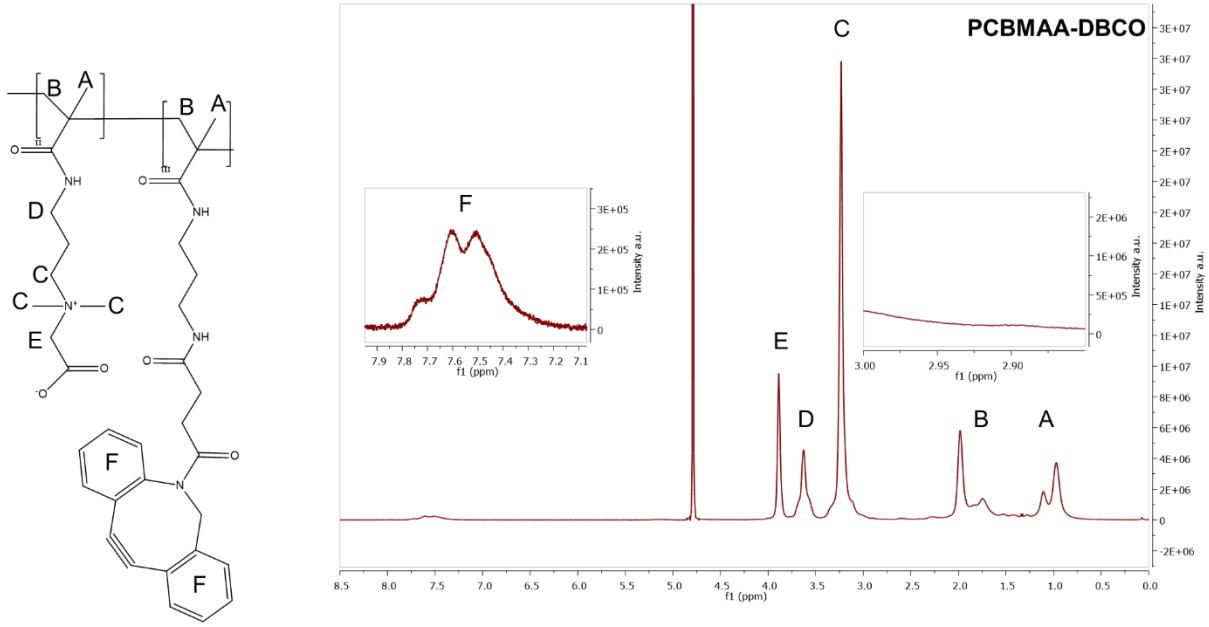

Figure S 20. ^{1}H NMR PCBMAA-DBCO in D_2O.

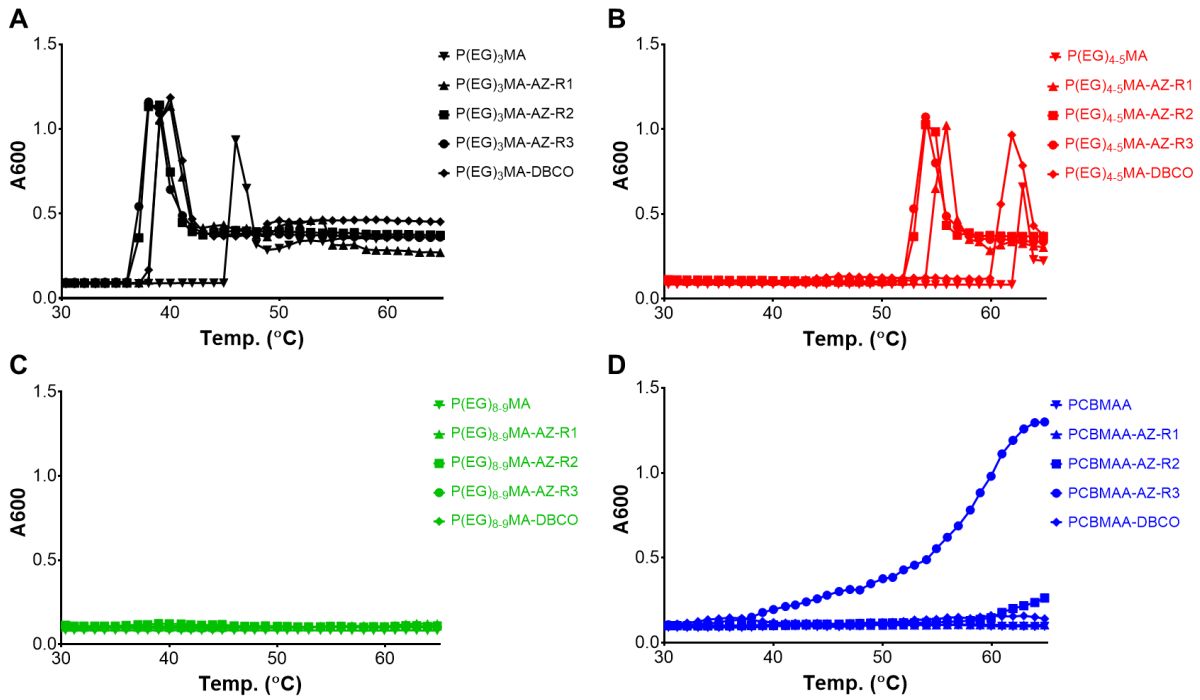

Figure S 21. LCST of P(EG)xMA and PCBMAA polymers. Turbidity (600 nm) of 25 g L^{-1} polymer solutions in PBS was measured from 30 - 65°C. Onset of turbidity was defined as the LCST. Note that the increased turbidity of PCBMAA-AZ-R3 is due to hydrolysis of the degradable linker (R3) leading to an insoluble hydrophobic by-product. For hydrogel degradation, all hydrophobic groups remain attach to a polymer, preventing insoluble product formation.

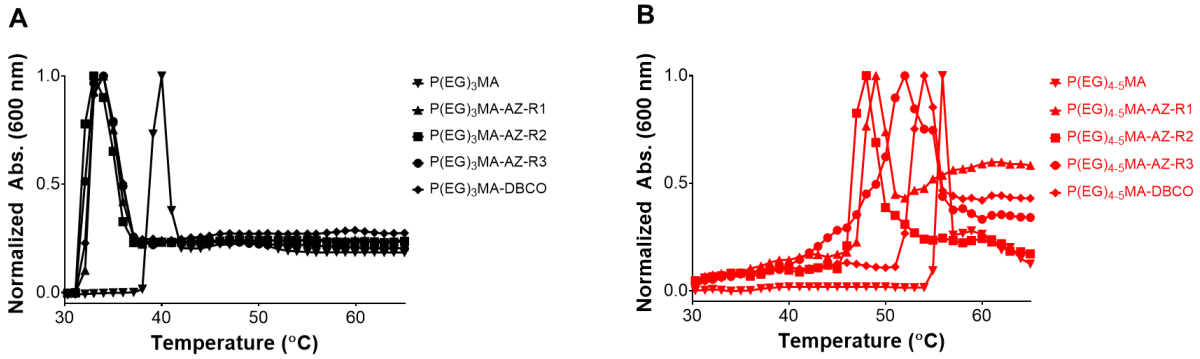

Figure S 22. LCST of P(EG)$_3$MA and P(EG)$_{4\text{-}5}$ polymers in 0.1 M borax buffer. Turbidity (600 nm) of 25 g L^{-1} polymer solutions in 0.1 M borax was measured from 30 - 65°C. Onset of turbidity defined as the LCST.

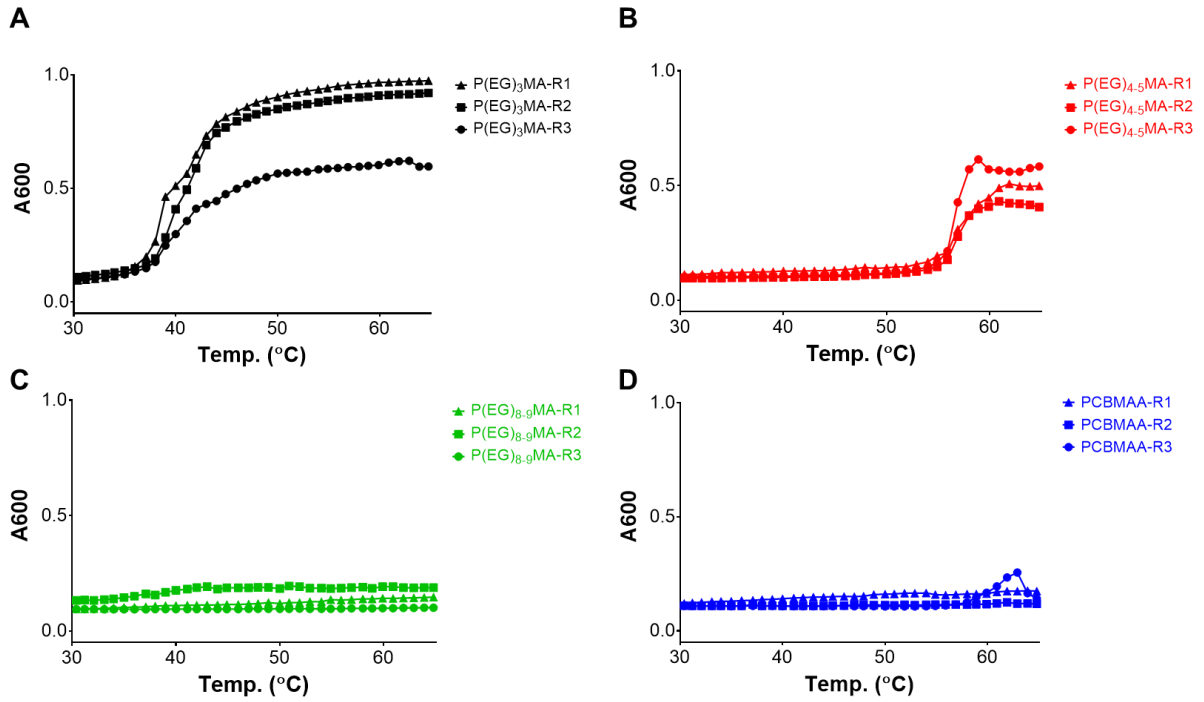

Figure S 23. Cloud point of P(EG)$_x$MA and PCBMAA hydrogels. Turbidity (600 nm) of 5 wt.% hydrogels in PBS was measured from 30 - 65°C. Onset of turbidity was defined as the cloud point.

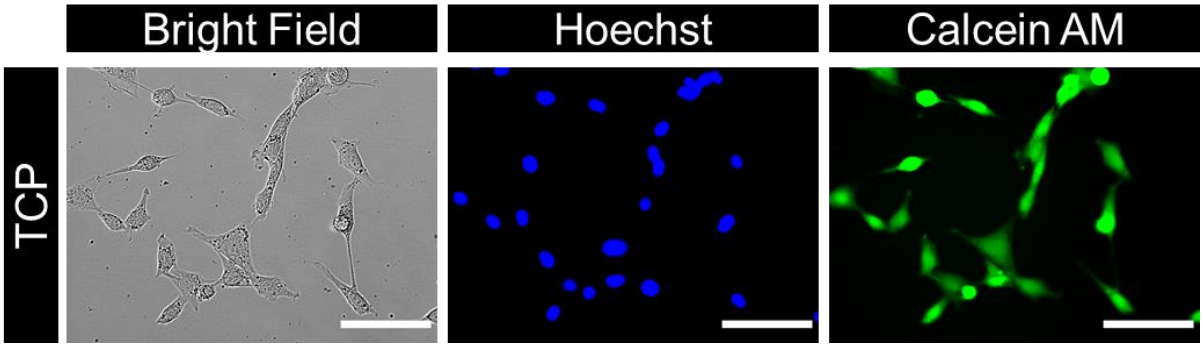

Figure S 24. Cell adhesion to tissue culture plastic (TCP). NIH 3T3 mouse fibroblasts (5000 cells per well) were seeded on TCP and incubated for 24 h in 10% calf bovine serum at 37°C. Scale bars are 100 µm.

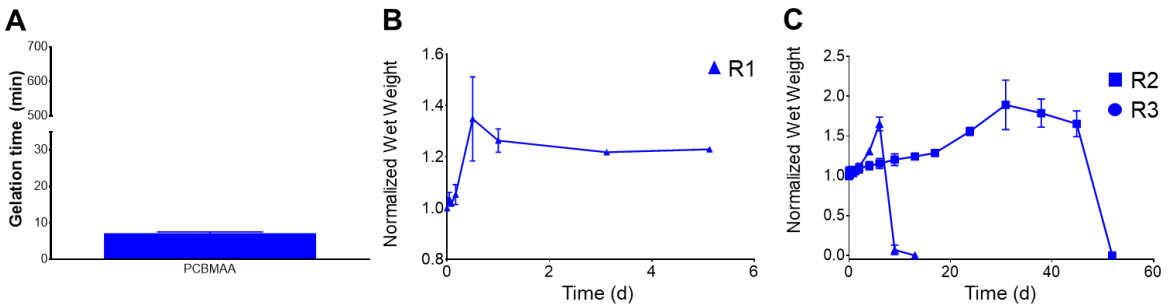

Figure S 25. PCBMAA hydrogel gelation time, swelling, and degradation. A) Gelation time of non-degradable PCBMAA-R1 hydrogels (5 wt.%) determined by gravitation flow analysis (mean ± standard deviation, n = 6). **B)** Equilibrium swelling of non-degradable PCBMAA hydrogels (5 wt.%). After overnight gelation, hydrogels were submerged in PBS and their wet weight was determined at specified time intervals (mean ± standard deviation, n =3). **C)** The wet weight of PCBMAA (100 µL,5 wt.%) with R2 (methylphenyl sulfone) or R3 (4-chlorophenyl sulfone) crosslinkers in PBS pH 7.4 overtime (mean ± standard deviation, n =3).

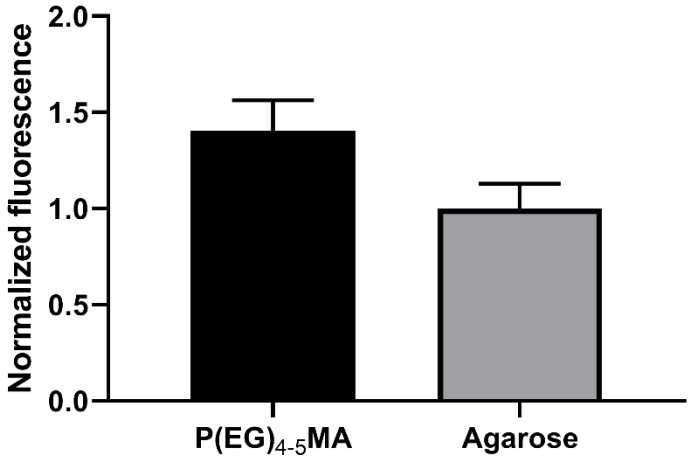

Figure S 26. Encapsulated cells remained viable in P(EG)$_{4\text{-}5}$MA gels. 20,000 NIH 3T3 fibroblasts were encapsulated in 5 wt.% P(EG)$_{4\text{-}5}$MA and non-cytotoxic 1 wt.% agarose hydrogels. After incubating for 20 h, cell viability was assessed using the fluorescent PrestoBlue assay. Cells encapsulated in P(EG)$_{4\text{-}5}$MA gels demonstrated higher viability than cells in agarose gels ($p < 0.03$; mean ± standard deviation, n =3), indicating the P(EG)$_{4\text{-}5}$MA crosslinking is non-cytotoxic.